www.csiro.au

Multiscale aquitard hydraulic conductivity characterisation and inclusion in groundwater flow models: Application to the Gunnedah Basin, New South Wales

Chris Turnadge, Lionel Esteban, Irina Emelyanova, David Nguyen , Marina Pervukhina, Tongcheng Han, Dirk Mallants

This report was commissioned by the Department of the Environment and Energy and was prepared by CSIRO.

2018

Citation

This report should be cited as:

Turnadge C, Esteban L, Emelyanova I, Nguyen D, Pervukhina M, Han T and Mallants D (2018) Multiscale aquitard hydraulic conductivity characterisation and inclusion in groundwater flow models: Application to the Gunnedah Basin, New South Wales, prepared by the Commonwealth Scientific and Industrial Research Organisation (CSIRO), Canberra.

Table of Contents

Figures

Tables

Abbreviations

Abbreviation	Description
CSG	Coal Seam Gas
CSIRO	Commonwealth Scientific and Industrial Research Organisation (Australia)
HSU	HydroStratigraphic Unit
MC	Monte Carlo (sampling methodology)
mD	milliDarcy
MPa	MegaPascals
µD	microDarcy
NSW	New South Wales
OGIA	Office of Groundwater Impact Assessment (Queensland)
PDF	Probability Density Function
Psi	Pound per square inch
Qld	Queensland

Glossary

Term	Description
Anisotropy	A term used to describe the directional dependence of given properties; for example, the hydraulic properties of an aquifer (as opposed to isotropy, which denotes identical properties in all directions)
Aquifer	Rock or sediment in a formation, group of formations or part of a formation, which is saturated and sufficiently permeable to transmit quantities of water to wells and springs
Aquitard	A saturated geological unit that is less permeable than an aquifer and incapable of transmitting useful quantities of water. Aquitards often form a confining layer over aquifers
Auto-covariance	Function that gives the covariance of the process with itself at two points in space
Coal measure	Geological strata of the Carboniferous or Permian periods usually containing sequences of coal seams
Coal seam	Individual layers containing mostly coal. Coal seams store both water and gas. Coal seams generally contain groundwater that is saltier than that in aquifers that are used for drinking water or agriculture
Coal seam gas	A form of natural gas (generally 95 to 97% pure methane, CH_4) typically extracted from permeable coal seams at depths of 300 to 1000 m. Also called coal seam methane (CSM) or coalbed methane (CBM)
Co-kriging	A form of kriging in which the distribution of a second, highly correlated variable (i.e. covariate) is used in addition to the primary variable to produce interpolated values. Co-kriging can improve interpolated estimates if the primary variable is difficult, impossible, or expensive to measure and/or if the secondary variable is sampled more intensely than the primary variable
Confined aquifer	An aquifer that is isolated from the atmosphere by an impermeable layer. Pressure in confined aquifers is generally greater than atmospheric pressure
Confining pressure	The combined hydrostatic stress and lithostatic stress; i.e. the total weight of the interstitial pore water and rock above a specified depth
Covariance	Covariance is a measure of how much two given variables vary together, as a function of either space or time
Darcy flow	Liquid flow that conforms to Darcy's law
Darcy's law	A constitutive equation that describes the flow of a fluid through a porous medium such as rock or soil
Depressurisation	The lowering of static groundwater levels through the partial extraction of available groundwater, usually by means of pumping from one or several groundwater bores or gas wells
Dewatering	The lowering of static groundwater levels through complete extraction of all readily available groundwater, usually by means of pumping from one or several groundwater bores or gas wells
Dirichlet boundary condition	Also known as a first type boundary condition, involves specification of the value that the solution of a differential equation needs to produce along the boundary of a model domain. Applicable to both numerical and analytical models

Term	Description
Effective parameters	Parameters used in ensemble-averaged equations (e.g., effective hydraulic conductivity relating the ensemble average flux to the ensemble mean gradient). They are an intrinsic property of the homogenised domain and not a function of the particular boundary conditions imposed on the domain
Effective porosity	The fraction of pores that are connected to each other and contribute to flow. Materials with low or no primary porosity can become very permeable if a small number of highly connected fractures are present
Ensemble-averaging	Formed by averaging over multiple realisations (model runs) of a spatio-temporal process.
Equivalent parameters	Equivalent parameters are derived from spatial averaging methods. They are based on numerical modelling and are therefore valid only for a specific set of imposed groundwater flow boundary conditions. Sometimes the terms block-average or volume-average are used
Gaussian (probability distribution)	A continuous function that approximates the exact binomial distribution and which represents the statistical distribution of many random variables. This can be described using only two parameters: mean (i.e. central tendency) and variance (i.e. spread). Typically visualised as a symmetrical bell-shaped graph
Groundwater	Water occurring naturally below ground level (whether in an aquifer or other low-permeability material), or water occurring at a place below ground that has been pumped, diverted or released to that place for storage. This does not include water held in underground tanks, pipes or other works
Groundwater (single phase) flow model	A numerical solution to a partial differential equation used to describe the flow of water in the subsurface. Groundwater flow models involve the flow simulation of a single fluid phase (i.e. water). Common parameters used in groundwater flow models are hydraulic conductivity, specific yield and specific storage
Hydraulic conductivity	A coefficient of proportionality describing the rate at which a fluid can move through a permeable medium
Hydraulic gradient	The difference in hydraulic head between different locations within or between hydrostratigraphic units, as indicated by water levels observed in wells constructed in those units
Hydraulic head	The potential energy contained within groundwater as a result of elevation and pressure. It is indicated by the level to which water will rise within a bore constructed at a particular location and depth. For an unconfined aquifer, it will be largely subject to the elevation of the water table at that location. For a confined aquifer, it is a reflection of the pressure that the groundwater is subject to and will typically manifest in a bore as a water level above the top of the confined aquifer, and in some cases above ground level
Hydraulic pressure	The total pressure that water exerts on the materials comprising the aquifer. Also known as pore pressure
Hydrostratigraphic unit	A formation, part of a formation, or group of formations of significant lateral extent that compose a unit of reasonably distinct (similar) hydrogeologic parameters and responses
Interburden	Material of any nature that lies between two or more bedded ore zones or coal seams
Intrinsic permeability	The permeability of a given medium independent of the type of fluid present
Inverse modelling	The process of calculating from a set of observations the causal factors that produced them. Typically involves multiple model runs or iterations, starting with an initial set of parameter values that are gradually updated during the subsequent model runs until model

Term	Description
	predictions adequately describe the observations. The final parameter set is considered to be the best-fit representation of the real parameter values at the scale of measurement
Isotropy	The condition in which the hydraulic properties of a hydrostratigraphic unit are equal in all directions
Kriging	A geostatistical method of spatial interpolation (i.e. prediction) using weighted averages of surrounding data points. The data are a set of observations with some spatial correlation present
Lithological facies	A mappable subdivision of a stratigraphic unit that can be distinguished by its facies or lithology, i.e. the texture, mineralogy, grain size, and the depositional environment that produced it
Matrix (rock matrix)	The finer grained mass of rock material in which larger grains/crystals are embedded
Monte Carlo sampling	The sampling of uncertain data for use in Monte Carlo risk analysis or simulation
Monte Carlo simulation	The use of Monte Carlo analysis techniques to estimate the most probable outcomes from a model with uncertain input data
Numerical realisation	A numerically generated sample (usually of model parameters) drawn from a probability distribution, used to run a model simulation
Permeability	The measure of the ability of a rock, soil or sediment to yield or transmit a fluid. The magnitude of permeability depends largely on the porosity and the interconnectivity of pores and spaces in the ground
Petrophysical observations	Properties that pertain to fluid behaviour within the rock, such as lithology (grain size, composition and texture), porosity, capillary pressure, permeabilities, irreducible saturations or saturations.
Porosity	The proportion of the volume of rock consisting of pores, usually expressed as a percentage of the total rock or soil mass
Probability density function	A function that describes the relative likelihood for a random variable to take on a given value
Regional-scale groundwater models	Models that encompass an entire groundwater system, geological basin or other significant area of interest that extends well beyond the measurable influence of individual bores or borefields
Relative permeability	The permeability of a medium for a specific fluid relative to the intrinsic permeability for a porous medium containing more than a single fluid phase (e.g., air and water or oil, gas, and water)
Reservoir (hydrocarbon)	Porous or fractured rock formations that contain significant reserves of hydrocarbons. Naturally-occurring hydrocarbons such as crude oil or natural gas are typically trapped in source or host rocks by overlying low permeability formations
Robustness (of model predictions)	Insensitivity of model predictions to data outliers or other small departures from assumptions required by a predictive model, including the types of parametric distributions assumed
Saturated flow	Flow through a porous medium (such as soil or rock) in which the void space within the porous medium is entirely occupied by water (as opposed to water and gas)
Single phase flow	The flow of a single phase, e.g. liquid or gas
Spatial correlation	Spatial dependency (or correlation) between samples

Term	Description
Spatial interpolation	The procedure of estimating the value of properties at unsampled sites within the area covered by existing observations
Stochastic process	Process characterised by a random probability distribution or pattern that may be analysed statistically but may not be predicted precisely
Stochastic analysis	A type of mathematical analysis that can be used to assess the uncertainty associated with models. It estimates the probability distribution of potential outcomes by allowing for random variation in one or more input parameters
Stratigraphy	An arrangement of sedimentary, metamorphic and/or igneous rocks
Transmissivity	The rate at which a fluid is transmitted through a unit width of a hydrostratigraphic unit under a hydraulic gradient
Unconfined aquifer	An aquifer in which there are no confining beds between the zone of saturation and land surface
Unconventional gas	Natural gas found in a very low permeability rock, such as coal seam gas, shale gas, and tight gas. Unconventional gas such as coal seam gas is trapped in coal beds by adsorption of the gas molecules to the internal surfaces of coal. It cannot migrate to a trap and form a conventional gas deposit. This distinguishes it from conventional gas resources, which occur as discrete accumulations in traps formed by folds and other structures in sedimentary layers
Upscaling	Upscaling is the process of transforming the detailed description of hydraulic parameters in a grid constructed at measurement scale to a coarser grid with less detailed description. It replaces a heterogeneous domain with a homogeneous one in such a way that both domains produce the same response under some upscaled boundary conditions
Variogram (also semi-variogram)	A function describing the spatial dependency (similarity) between observations of a variable. The shape of the variogram is typically a function of the distance and direction separating observations at two locations; at short distances the semi-variance is small, and typically increases with increasing separation distance. The semi-variance is defined as the variance of the difference between two variables at two locations. At zero separation distance the semivariance is called nugget (-effect). The sill is the maximum semivariance or the plateau of the semi variogram; the correlation length or spatial range is the distance over which variables are spatially correlated
Well	Borehole in which a casing (e.g. steel piping) has been placed to restrict connection to specific ground horizons/depths

Symbols

Symbol	Brief description and unit of measurement
a, b, c	regression coefficients of the porosity-confining pressure and permeability-confining pressure equation
a_1, a_2	regression coefficients in the permeability-porosity model
F	fluidity of the permeating liquid [$m^{-1}.sec^{-1}$]
G	gravitational constant [9.81 $m.sec^{-2}$]
H	dynamic viscosity [10^{-3} $kg.m^{-1}$ sec^{-1} at 20°C and 0.1 MPa for water]
K	permeability [mD or m^2]
k_h	horizontal permeability [mD or m^2]
k_v	vertical permeability [mD or m^2]
K	hydraulic conductivity [$m.day^{-1}$]
K_e	effective hydraulic conductivity [$m.day^{-1}$]
K_h	horizontal hydraulic conductivity [$m.day^{-1}$]
K_v	vertical hydraulic conductivity [$m.day^{-1}$]
m_1, m_2	regression coefficients in the two-component linear permeability-porosity models
P	lithostatic pressure or confining pressure imposed during porosity and permeability measurement [MPa]
p_1, p_2	pressure of gas (nitrogen) after sample infiltration, pressure of gas (nitrogen) before being released into the sample [MPa]
Φ	porosity [%]
Q	volumetric fluid flux [$m^3.day^{-1}$]
ρ_b	saturated rock bulk density [$kg.m^{-3}$]
ρ_f, ρ_w	fluid, water density [998.23 $kg.m^{-3}$ at 20°C and 0.1 MPa for water]
ρ_g	grain or rock density [$kg.m^{-3}$]
V	linear fluid flux [$m.day^{-1}$]
v_1, v_2	volume of nitrogen permeating rock sample, calibrated volume of nitrogen before being released into the sample [m^3]
Z	sample depth [m]

Acknowledgements

The authors would like to acknowledge the Commonwealth Department of the Environment and Energy for funding the project "Research to improve treatment of faults and aquitards in Australian regional groundwater models to improve assessment of impacts of CSG extraction". The report was subject to internal peer review processes during its development and benefitted from reviews undertaken by Dr. Ludovic Ricard (CSIRO Energy) and Dr. Karsten Michael (CSIRO Energy). We gratefully acknowledge the Department of Industry - Division of Resources and Energy (New South Wales) for providing core samples from the Gunnedah and Londonderry Drillcore libraries. Mark Dawson from Whitehaven Coal Limited facilitated sampling of cores from their Drillcore library in Boggabri. Many thanks also to Mr. Stan Smith (CSIRO Land and Water) and Dr. Eddie Banks (Flinders University of South Australia) for their support during core sampling.

Executive summary

The project "Research to improve treatment of faults and aquitards in Australian regional groundwater models to improve assessment of impacts of coal seam gas (CSG) extraction" focuses on method development to underpin the risk assessments associated with deep groundwater extraction and depressurisation from energy resource development. The project aims to develop methodologies and techniques that will improve the predictive capability of regional groundwater models used in this context, specifically with respect to the representation of faults and aquitards. The project has three components: 1) an examination of aquitards, 2) an examination of faults, and 3) an examination of the upscaling of aquitard and fault properties such that they can be adequately represented in regional groundwater flow models.

This report provides an overview of the approaches used to derive hydraulic conductivities of key aquitards in the Gunnedah Basin (New South Wales) and their subsequent upscaling into a regional groundwater flow model. Specifically this study:

- Developed a workflow to combine existing geophysical wireline logs available from coal seam gas exploration wells with laboratory measurements of porosity and permeability from which continuous porosity and permeability profiles have been generated,
- Applied the workflow to four key aquitards (Purlawaugh Formation, Napperby Formation, Watermark Formation and Porcupine Formation) within the Gunnedah Basin and generated 97 profiles of continuous permeability (or vertical hydraulic conductivity, K_v), with depths below surface of aquitards tops ranging from about 250 m to 1300 m,
- Accounted for conceptual model uncertainty in generating permeability values from porosity by developing both linear and non-linear porosity-permeability relationships,
- Upscaled the high-resolution K_v profiles into equivalent K_v values representative for large units commensurate with the typical size (i.e. vertical interval) of the numerical grid of a regional scale groundwater flow model,
- Improved the pre-existing data base on hydraulic conductivities for key aquitards in the Gunnedah basin by developing site-specific and upscaled K_v values and their statistical properties (probability density function).

The main steps of the workflow to generate high-resolution hydraulic conductivity data across the main aquitards of the selected case study area involved:

- Collation of geophysical wireline logs providing data on (neutron) bulk density. Processing (including any QA/QC) of geophysical data to convert high-resolution (0.01 m interval) bulk density values into high-resolution porosity values,
- Collect core samples from key aquitard formations and conduct porosity and permeability measurements under appropriate confining pressures. Establish regression models between porosity and permeability for each of the aquitards. Apply the regression models to convert the high-resolution porosity profiles from first step into high-resolution permeability profiles.
- Upscaling of the high-resolution permeability profiles into large-scale equivalent values using analytical procedures (i.e. harmonic averaging to derive K_v). Upscaled values are derived for each section of aquitard represented in each of the wells for which geophysical data was available. This population of upscaled values is then used to derive statistical parameters for each aquitard for future use in groundwater flow modelling.

The workflow maximises use of existing geophysical data and allows conversion to hydraulic conductivity by a minimal investment in additional site-specific data. Although developed and tested on a single case study area in NSW (Gunnedah Basin), the methodology can be readily applied in other sedimentary basins in Australia provided sufficient data is available.

Results show that all four aquitard formations display low permeability, i.e. from a few mD down to 10 nanoD in the case of the Porcupine Formation. Nearly all samples showed significant confining pressure dependency, illustrating a decreasing trend in porosity and permeability with greater depth. While all regression models, both linear and non-linear, provided a good description of the data, they were conceptually different and thus provide the opportunity to account for conceptual model uncertainty in regards to generating formation-scale hydraulic conductivities. Furthermore, the depth-dependency was incorporated in the predictive porosity-permeability models, either implicitly (via the single linear or non-linear model) or explicitly (via the multiple linear model).

In this study continuous permeability (K_v) profiles were generated for a total of 97 wells across the model area. A single equivalent K_v value for each of four aquitard units, their interburden units, and the combined aquitard-interburden unit was obtained through upscaling of the resulting high-resolution K_v profiles using harmonic averaging. Whenever the K_v profiles contained at least one of four aquitards, these profiles were used for harmonic averaging. Based on stratigraphic data availability, 62 of the 97 wells were used to upscale the permeability of the upper (i.e. Jurassic-Permian) aquitard sequence (containing the Purlawaugh and Napperby aquitard units). Likewise, 78 of the 97 wells were used to upscale the permeability of the lower (i.e. Permian) aquitard sequence (containing the Watermark and Porcupine aquitard units). Harmonic mean values provided the probability distribution of regional-scale formation-specific K_v values for subsequent use in groundwater flow modelling. Porosity-permeability relationships for some formations (i.e. Purlawaugh, Watermark and Porcupine formations) were found to be sensitive to the type of porosity-permeability model used (i.e. linear, multi-linear, or non-linear). Conversely, the porosity-permeability relationship for the Napperby Formation was found to be insensitive to the type of model selected. Finally, variability in K_v was found to be up to two times larger for the deepest formations (Watermark and Porcupine) compared to the shallower formations (Purlawaugh and Napperby).

Analysis of multiple wireline logs and permeability measurements and the derived formation-scale permeability did not provide evidence (positive or negative) that the sealing capacity of the aquitard sequences was impaired by a lack of lateral continuity of the seal. The analysis of seal properties, however, is limited in being based largely on the core-scale properties of sealing sequences. Although so-called seal bypass systems have been described in the literature for other basins, typically involving faults, intrusions, and pipes, only faults and hydrothermal pipes (dykes) have been identified in the Narrabri Gas Project Area. However, previous studies concluded that the faults present in the Project area are unlikely to provide preferential pathways for the leakage of water or hydrocarbons between strata and volcanic rocks linked to dykes are not widely detected in exploration wells. Future research could involve detailed 3-D seismic data that would enable the assessment of seal bypass structures and their permeability.

1. Introduction

1.1. Rationale

Hydrogeological properties vary naturally through space as a result of the complex geological processes through which aquifers and aquitards evolve (Kolterman and Gorelick, 1996). The key parameter of interest that varies spatially is the hydraulic conductivity (*K*), or alternatively, the transmissivity (i.e. hydraulic conductivity × formation thickness). A major complication arises when hydraulic conductivity measurements, generally determined on different, and mostly much smaller scales than the grid cells of numerical groundwater models, have to be integrated for use in modelling (Mahmud et al., 2014). Considerable progress has been made over the past few decades regarding upscaling of hydraulic conductivity values for groundwater systems, but few methods have been applied to aquitards in the context of groundwater impact assessments for coal seam gas extraction.

The extent of research into understanding the geology and fluid flow properties of low-permeability formations (variously referred to as cap rocks, seals or aquitards) undertaken in the last thirty years cannot be understated. Such research has been undertaken in various fields, including petroleum extraction (e.g. Giger et al., 2013; Dewhurst et al. 2012; TerHeege et al., 2013), geological carbon storage (e.g. Gibson-Poole et al., 2008; Green and King, 2010; Varma et al., 2013), geological disposal of radioactive waste (e.g. Gautschi, 2001; Mallants et al., 2007; Rubel et al. 2002; Yu et al., 2013) and groundwater resource assessment (e.g. Smerdon et al. 2012). The present study builds upon the combined hydrocarbon, geological carbon storage and radioactive waste disposal industry best practice and technology relevant to seal analysis, complemented with hydrogeological methodologies and practices developed for aquitard characterisation. Through integration of such methodologies an improved characterisation, conceptualisation, and representation of aquitard hydraulic properties in regional-scale hydrogeological models will be pursued.

1.2. Description

Two broad categories of determining formation-scale hydraulic conductivities will be evaluated: (i) hydraulic methods based on direct or indirect measurement of K, and (ii) inference of aquitard leakage rates through measurement of isotopes and/or geochemistry of either groundwater in adjacent aquifers or pore water and minerals in aquitards (DoE, 2014; Smith et al., 2013). Recommendations on the most effective and appropriate methods at various spatial scales will also be developed. The project will develop a workflow to represent the aquitard architecture and the distribution of its hydraulic properties for use in 3-D flow models using sedimentological and structural data. This methodology will use sequence stratigraphy methods to assign hydraulic properties to a 3-D geological model, which will form the input to the 3-D flow model. A case study will be developed by integration of information at two spatial scales: (1) the scale of the well-field where typically most calibration data are available and (ii) the wider regional scale following upscaling and interpolation of the results obtained from the well field.

The modelling of regional groundwater drawdown induced by coal seam gas (CSG) extraction poses a number of significant challenges. On the one hand, adequate representation of hydrogeological detail near extraction sites is important to provide the foundation for predicting far-scale impacts, and because individual coal layers within an extensive coal measure sequence may be of limited lateral extent, thus reducing connectivity to regional groundwater systems and limiting regional drawdown impacts. On the other hand, these models often encompass large domains and must include significant aquifers and aquitards that prevail in the large sedimentary basins wherein coal sequences are found. They must also encompass the locations where the adverse consequences of CSG extraction may be felt, which can potentially be far removed from extraction sites. Because of the computational burden, models that are built to explore the effects of coal seam gas extraction on regional groundwater systems cannot easily represent small-scale heterogeneities typical of coal measures, aquitards, and aquifers with the same level of detail as typical 3D stochastic lithofacies models. As an alternative, the entire coal measure sequence, aquitard or aquifer sequence is typically approximated using a limited number of model layers. The challenge is to determine the appropriate translation (i.e. upscaling) from the highly stratified model to a much coarser model whose “equivalent” flow properties are still able to reliably represent large-scale average groundwater flow processes (Renard and de Marsily, 1997; Sanchez-villa et al., 1996; Tran, 1996; Vistrand 2001; Wen and Gomez-Hernandez, 1996). One of the most commonly used upscaling strategies in reservoir and groundwater simulation is that whereby an upscaled model layer represents all fine-scale model layers that lie within its boundaries (this is called upscaling through lithological amalgamation, e.g. Moore et al., 2014). Hydraulic properties ascribed to each coarse model cell can be averaged over all fine-scale layers using standard averaging methods.

The simplest approach involves calculating the arithmetic, harmonic, or geometric mean of a given aquitard formation (Table 1). For flow parallel to the bedding with equal thickness z for all layers i, the equivalent hydraulic conductivity is calculated as the arithmetic mean of the hydraulic conductivities k_i (Freeze and Cherry, 1979). A thickness-weighted mean is applied to account for a variable z_i across the formation. For one-dimensional flow orthogonal to the bedding with equal thickness z for all layers i, the equivalent hydraulic conductivity is calculated as the harmonic mean of the hydraulic conductivities k_i (Freeze and Cherry, 1979). A thickness-weighted harmonic mean is applied to account for a variable z_i across the formation. The geometric mean is used as an estimator of the central value in formation that does not show distinctive layering. It represents the expected value of the mean of a lognormal distribution.

Table 1. Summary of averaging methods commonly used in the upscaling of hydraulic properties.

Averaging method	Equation
Arithmetic	$\mu = \frac{1}{n}\sum_{i=1}^{n} k_i$
Weighted arithmetic	$\mu = \frac{\sum_{i=1}^{n} z_i k_i}{\sum_{i=1}^{n} z_i}$
Harmonic	$\mu = \frac{1}{n}\sum_{i=1}^{n} \frac{1}{k_i}$
Weighted harmonic	$\mu = \frac{\sum_{i=1}^{n} z_i}{\sum_{i=1}^{n} \frac{z_i}{k_i}}$
Geometric	$\mu = \left(\prod_{i=1}^{n} k_i\right)^{1/n}$

For flow across aquitards, the upscaled vertical hydraulic conductivity (K_v) is calculated using the thickness-weighted harmonic averaging, thus preserving resistance across the layers traversed. Other strategies involve segregation of particular layers, for instance coal seams and interburden, into separate layers (this is called upscaling through lithological segregation). In other words, the multitude of discontinuous fine-scale layers (e.g. coal) that occur within the coal measure formation are migrated vertically such that they comprise a small number of coal-only layers separated by correspondingly segregated interburden-only material (Moore et al., 2014).

1.3. Methodology

1.3.1. REVIEW OF METHODS AND DATA FOR AQUITARD CHARACTERISATION

Identify and collate data and information on a range of methods used to estimate and describe vertical hydraulic conductivity of aquitards in coal-bearing sedimentary basins

As part of the project "Research to improve treatment of faults and aquitards in Australian regional groundwater models to improve assessment of impacts of coal seam gas (CSG) extraction", Turnadge et al. (2018) presented an overview of approaches to simulating the hydrological influence of aquitards and faults in regional groundwater models. This overview also included a summary of the literature relating to regional scale groundwater modelling approaches and methodologies and procedures for aquitard and fault zone characterisation and representation in regional groundwater models. In regards to aquitard characterisation methodologies, the overview by Turnadge et al. (2018) includes:

- reviews of hydraulic conductivity measurement methods across a range of spatial scales (core, bore, regional);

- examples of how soft data (mostly of a qualitative nature but plentiful in either the horizontal or vertical plane) may be used to derive improved estimates of hard (but sparse) data such as hydraulic conductivity;
- discussions on local and global upscaling methods and their advantages/disadvantages in a CSG impact assessment context; and,
- reviews of simulation-based spatial interpolation methods, including Monte Carlo sampling, two-point statistics, multi-point statistics, and transition probability geostatistics.

Building on the findings of this review, a screening of available data and opportunities for collecting additional data in selected case study areas was carried out. It was decided that the following two methods to estimate vertical hydraulic conductivity of aquitards will be evaluated: (i) hydraulic methods based on both direct or indirect measurement of K_v, (ii) inference of aquitard leakage rates through measurement of isotopes and/or geochemistry of either groundwater in adjacent aquifers, pore water in aquitards, or if the first two are not available, presence of isotopes in rock minerals such as quartz (Smith et al. 2018). Recommendations on the most effective methods at various spatial scales will be developed at a later stage following applications within a groundwater flow model (to be discussed in future reports).

Review and selection of case study area based on data and model availability

A separate assessment was undertaken as part of the larger project to discuss and decide on the most appropriate case study area. Based on availability and accessibility of data and groundwater flow models, it was decided to develop two case study areas that would each have a different focus. The first case study area focuses on improved conceptualisation, representation and parameterisation of faults in regional groundwater flow models; for this purpose the Gloucester basin (case study area #1) has been identified due to availability of sufficient pre-existing data previously compiled by gas companies and by the Bioregional Assessments Programme and (ii) accessibility to groundwater monitoring bores and surface water to carry out additional field investigations. Results for the Gloucester Basin case study will be reported in accompanying documents.

The second case study area has been selected for a focused analysis of aquitards (case study area #2). The case study area selection was based on a number of criteria:

- the availability and accessibility of a fit-for-purpose regional-scale groundwater model;
- the ability to modify (i.e. improve) the parameterisation of aquitards represented in this model and carry out sensitivity and uncertainty analyses; and,
- the opportunity to access additional pre-existing data not previously used to parameterise aquitards and combine this with new data collected within this project that would feed into a workflow for improved parameterisation of aquitard hydraulic properties.

The Gunnedah Basin is deemed appropriate to demonstrate novel characterisation techniques and/or modelling approaches that would also be relevant to improve understanding of the role of aquitards in other sedimentary coal-basins. This study will use the fit-for-purpose model previously developed for the Gunnedah Basin by CDM Smith (2014) for the Groundwater Impact Assessment component of the Environmental Impact Statement for Santos Ltd's proposed Narrabri Gas Project in NSW.

Develop a workflow to spatially represent the aquitard architecture and spatial distribution of aquitard hydraulic properties in 3D models

The representation of the spatial heterogeneity of hydraulic properties, whether for aquifers or aquitards, has received considerable attention in the literature. A typical workflow for building a reservoir or hydrogeological model with measured data, expert knowledge and statistics is that presented by Corvi et al. (1992). As Figure 1 demonstrates, several types of information underpin the development of both small-scale and large-scale geological structures (the architecture) and their properties relevant for flow modelling. Large-scale structures such as sedimentological units provide the structural framework for describing small scale variation of hydraulic properties; the latter will need to be upscaled to a coarser spatial unit for use in regional scale groundwater flow models.

A key uncertainty in forecasting aquitard performance in regional groundwater models is the prediction of lateral continuity of sealing horizons and aquifers; the next most important uncertainty is the characterisation of permeability of a given facies type or geobody. In the reservoir engineering domain the way to understand this risk is to construct multiple static geological models that consider a range of possible geometries for key aquifer and seal geobodies within the constraints of the well and seismic data. This is particularly important at the sub-basin scale where often data control is poor. Subsequently, a probability distribution of rock properties is imposed onto each of these multiple geometric realisations which are then tested in a sequence of dynamic simulations.

The spatial distribution of aquifer/aquitard facies is indeed not homogeneous, and a great amount of spatial variability exists. Heterogeneous facies distribution is an important factor constraining geological heterogeneity. Because complete three-dimensional information about (hydro)geologic properties is never obtainable, numerous methods have been developed to interpolate between data values and use of geologic, hydrogeologic, and geophysical information to create images of aquifer properties. Geostatistical simulation methods have been applied to generate realistic variability honouring the global data distribution and spatial correlation structure observed from field data. Therefore, a representative global distribution and spatial correlation that is consistent with available data are important. An essential aspect of geostatistical simulation is establishing quantitative measures of spatial correlation of regionalized variables for subsequent estimation and simulation. Several methods exist for creating images of the heterogeneous subsurface, generally classified as either structure-imitating and process-imitating (Falivene et al., 2007). The former numerically reproduce the observed spatial patterns without directly considering sedimentary processes, while the latter simulate physical processes of erosion, transport and accumulation of sediments. Statistical grid-based structure imitating methods are commonly used, such as sequential Gaussian simulation (Deutsch and Journel, 1998), multi-point geostatistics (Caers and Zhang 2004; Comunian et al. 2014; Mariethoz and Lefebre, 2014), and sequential indicator simulation (Gómez-Hernández and Srivastava, 1990).

Small-scale variability in the geological facies and their properties that influence rock porosity and permeability may be identified by applying petrophysical and other techniques, which are especially useful when calibrated with site-specific hydraulic property estimates using lab-based techniques (e.g. K_v determination from centrifuge analysis or triaxial tests) or field-based measurements (e.g. K_v determined from pumping and air-permeameter tests, hydrograph analyses, or environmental tracers). One particularly powerful approach is the estimation of high-resolution vertical profiles of K_v from wireline geophysics. Details of this method are available from Pervukhina et al. (2010).

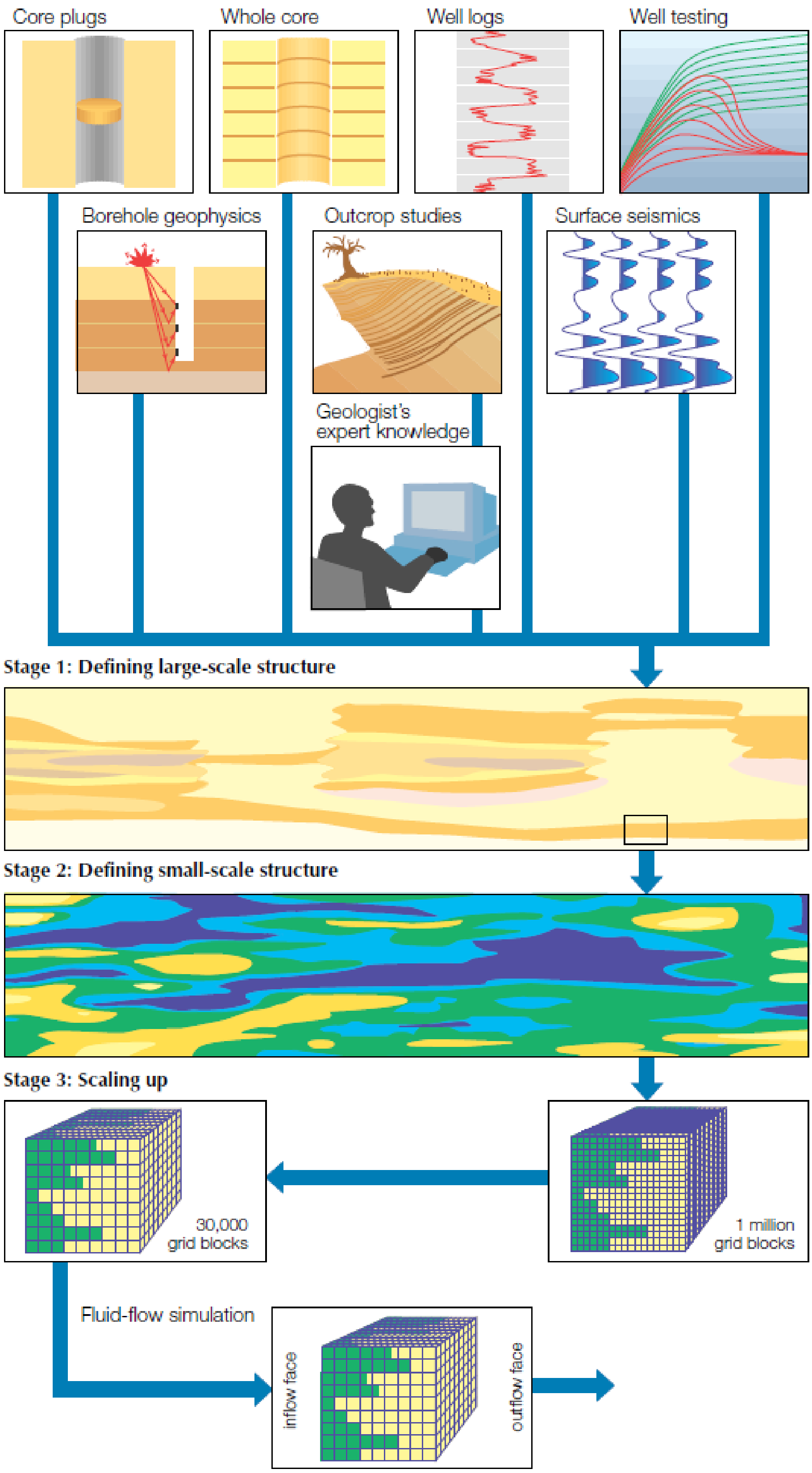

Figure 1 Example workflow for building a reservoir and hydrogeological model with measured data, expert knowledge and statistics (Source: Corvi et al. 1992).

1.4. Workflow development

A workflow was developed to generate high-resolution hydraulic conductivity data across the main aquitards of the selected case study area (see Section 1.5 for a discussion on the study area). The workflow maximises use of existing geophysical data and allows conversion to hydraulic conductivity by a minimal investment in additional site-specific data. A schematic of the workflow is presented in Figure 2. There are three steps involved to progress from the geophysical data (wireline logs) to upscaled hydraulic conductivities:

1. Collate available geophysical wireline logs that provide data on (neutron) bulk density. Process geophysical data (including QA/QC) to convert high-resolution (i.e. centimetre scale) bulk density values to porosity values.
2. Collect core samples from key aquitard formations and measure porosity and permeability values under appropriate confining pressures. Establish regression models between porosity and permeability for each of the aquitards. Apply the regression models to convert the high-resolution porosity values obtained during step 1 to permeability values. Repeat this step if different conceptual models (e.g. linear or non-linear) can be used to characterise porosity-permeability relationships.
3. Upscale high-resolution permeability values to large-scale equivalent values using analytical approaches (e.g. harmonic averaging). Upscaled values will be derived for each section of aquitard represented in each of the wells for which geophysical data was available. This population of upscaled values will then be used to derive statistical parameters (e.g. probability distribution and its parameters) for each aquitard for future use in groundwater flow modelling.

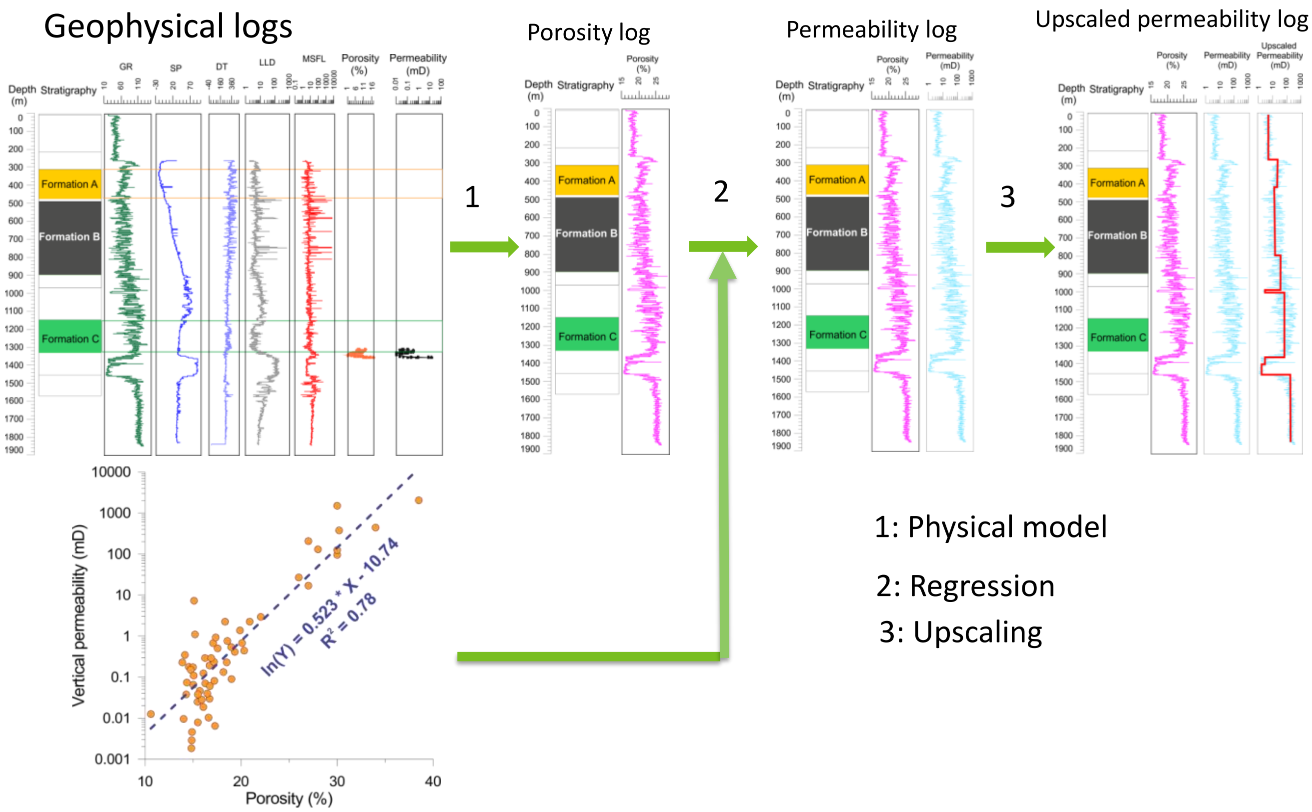

Figure 2 Workflow for generating porosity and permeability values from geophysical wireline logs and upscaling for use in cellular groundwater flow models (Source: Ricard et al., 2014).

1.5. Case study area

A regional-scale numerical groundwater flow model of the Gunnedah Basin has been developed by CDM Smith (2014) for the Groundwater Impact Assessment component of the Environmental Impact Statement for Santos Ltd's proposed Narrabri Gas Project, NSW. The Narrabri Gas Project will mainly target coal seam gas reserves associated with Early Permian coal seams of the Maules Creek Formation and secondary gas reserves associated with coal seams of the Late Permian Black Jack Group. The groundwater model was used by CDM Smith to predict the potential impacts on groundwater resources within the groundwater impact assessment study area due to water extraction from the coal seams that will be targeted for coal seam gas production.

Simulations of water extraction from the coal seams provided regional-scale predictions of depressurisation and drawdown of hydraulic head within the Gunnedah Basin and the associated induced flows between groundwater sources and hydrostratigraphic units. The same model area has been used in this study to help select exploration wells with appropriate geophysical wireline logs to generate formation-scale hydraulic conductivities for key aquitards. A total of 97 exploration wells were identified for analysis of geophysical wireline data.

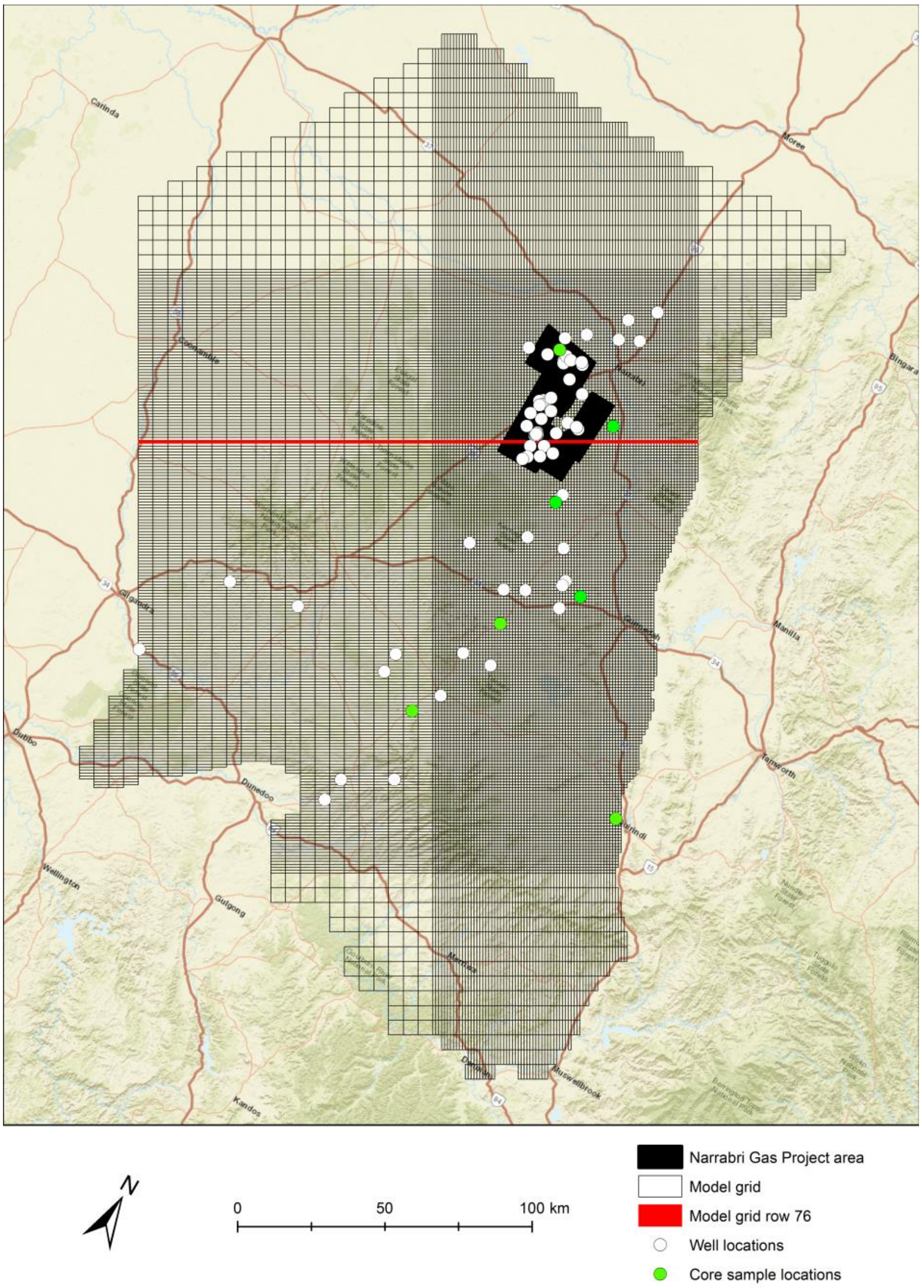

Figure 3 Groundwater model domain and Narrabri Gas Project Area with location of 97 exploration wells with geophysical wireline data. The highlighted row (red) was used to display the hydrostratigraphic cross-section shown in Figure 4.

The case study area enclosed by the groundwater model covers a total area of 53 219 km^2 (Figure 3). For this model, the aquitard sequence (referred to in Figure 4 as the Jurassic to Late Permian aquitard sequence) overlying the Hoskissons Coal represents the key aquitard that will govern the vertical propagation of hydraulic stresses to the overlying Pilliga Sandstone aquifer from coal seam gas production in the underlying coal seams (Figure 4). An important second aquitard sequence is that in between the Hoskissons Coal Formation and the Maules Creek Formation (referred to in Figure 4 as the mid to late Permian aquitard sequence). The model cross-section in Figure 4 is located along the highlighted row of the model grid (Figure 3).

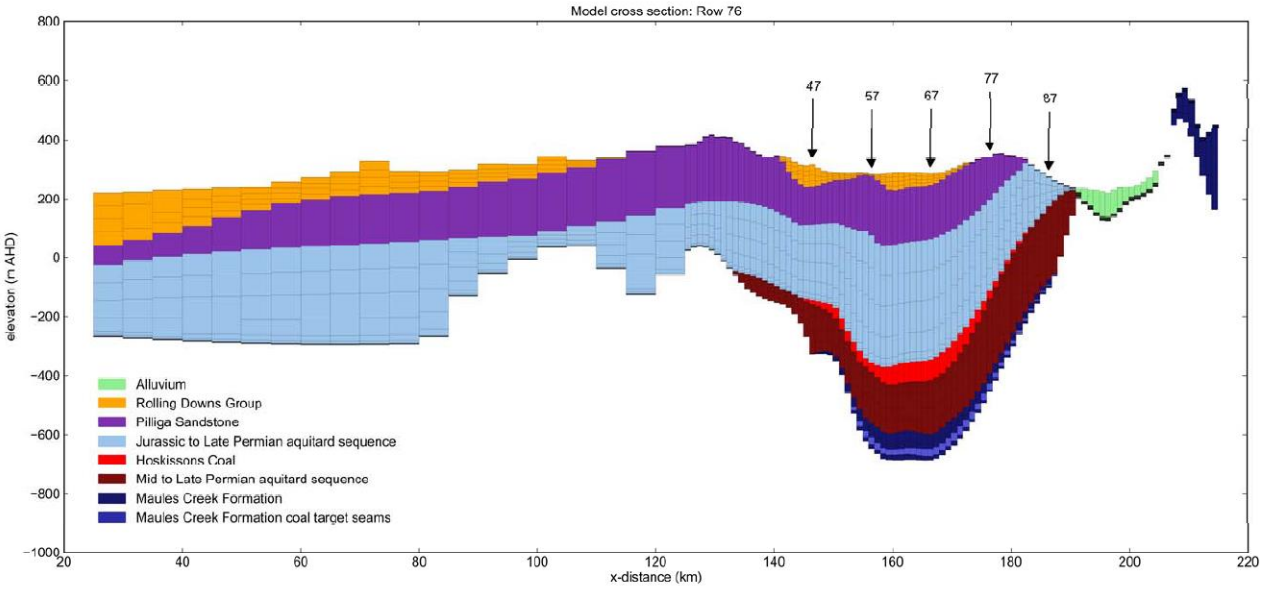

Figure 4 Approximately east-west cross-section with hydrostratigraphic units of the groundwater model for the Narrabri Gas Project Area, Gunnedah Basin (NSW).

2. Derivation of aquitard hydraulic conductivity

2.1. Sampling

In August 2015 a total of 60 core samples were collected from the following three core libraries for subsequent porosity and gas permeability measurements: the NSW Department of Industry core libraries at Gunnedah and Londonderry, and the Whitehaven Coal Limited core library at Boggabri. Core samples were of variable length (40 – 200 mm) and fixed diameter of 45 or 60 mm; all cores were transport to the CSIRO Petrophysics Laboratory in Perth for subsampling and analysis. Samples were collected from four key aquitard formations of the Gunnedah Basin (from top to bottom): Purlawaugh Formation (6 samples), Napperby Formation (14 samples), Watermark Formation (26 samples), and Porcupine Formation (13 samples). Core samples were taken from a total of 9 exploration wells; the wells were selected to provide a good spatial coverage of key aquitards across the study area. The location of these layers within the stratigraphic table shows the first two layers are part of a multi-layer aquitard that isolates the Pilliga Sandstone and Cenozoic Alluvium (Namoi alluvium) aquifers from the Hoskissons Coal Formation (secondary coal target formation, CDM Smith 2014), while the last two aquitards isolate the Maules Creek Formation (primary coal target formation, CDM Smith 2014) from the overlying aquifers (Table 2). The geological layers are model layers within the geological model that was constructed using the Leapfrog Hydro (v. 1.7) software and is based on a combination of geological datasets (CDM Smith 2014).

In the CSIRO Petrophysics laboratory all samples were sub-cored with water using a 1.5-inch or 1-inch-diameter drill bit, depending on the original core size (Figure 5). Sub-core lengths varied from 20-150 mm, depending on the length of the original core. These standardised sizes (i.e. diameter) were required to fit in a fixed core holder of 1 inch (for cores which had an original diameter of 45 mm) or 1.5 inch diameter (for cores which had an original diameter of 60 mm). After extraction of 'plugs' both top and bottom face were trimmed into flat parallel faces and stored in an oven at 105 °C to dry the samples during at least three days. After drying, the samples weight, length and diameter were measured prior to performing the porosimetry-permeametry measurements using a nitrogen gas-based setup (for details, see Section 2.2). During core preparation one sample was destroyed leaving 59 samples for analysis. Two plugs showed chipped corners and were repaired with epoxy plaster to allow proper porosity-permeability measurements under imposed confining stress.

Cores were obtained from depths ranging from 49 to 1214 meters below ground surface (Figure 6). Especially at large depths the rock material is subject to high lithostatic pressures. Measurements of porosity and permeability were undertaken at five to six confining pressures for two reasons: first, to capture the dependency of porosity and permeability on lithostatic pressure across a relevant pressure range of up to 2500 psi confining pressure to cover the maximum equivalent lithostatic pressure encountered at the maximum depth of the recovered samples assuming a rock grain density of 2.65 g/cm^3 (using a confining pressure larger than the lithostatic pressure of the samples would lead to sample breakage), and second to allow extrapolation of porosity and permeability values beyond the measurement range of the permeameter or to compute the exact porosity-permeability at a specific depth (for further details see section 2.2). The extrapolation is required for those samples whose measurement depth, and corresponding pressure, was too shallow to be within the minimum available confining pressure range. The additional advantage of having multiple porosity and permeability measurements across a range of confining pressures is that the data set is increased significantly. Although these additional data points do not capture effects of spatial variability in porosity and permeability, they do capture depth-dependency of porosity and permeability under conditions of identical rock composition and pore structure.

The confining pressures for the porosity and permeability measurements were calculated as follows. Assuming a general saturated rock bulk density ρ_b of 2500 kg.m^{-3} or 2.5 g.cm^{-3}, the lithostatic pressure was computed from the samples' depth of recovery as $P = \rho \times g_b \times z/10^6$ (Table 3), where P is the lithostatic pressure (MPa) (i.e. maximum confining pressure that will be applied on the sample during gas porosity-permeability measurement), ρ_b is the saturated rock bulk density (g.cm^{-3}), g is the gravitational constant (9.81 m.s^{-2}) and z is the sample depth (m).

Table 2. Summary of geological model layers, hydrostratigraphic units and groundwater flow model layers represented in the Santos Gunnedah Basin groundwater flow model. Core samples were taken from four aquitards (green shaded cells) (modified after CDM Smith 2014).

Geological unit	Geological model layer	Hydrostratigraphic unit	Groundwater model layer(s)
Cenozoic Alluvium	1	aquifer	1
Liverpool Range Volcanics	2		2
Wallumbilla Formation			3
Bungil Formation		aquitard	4
Mooga Sandstone	3		5
Orallo Formation			
Pilliga Sandstone	4	aquifer	6
Purlawaugh Formation	5		7
Garrawilla Volcanics	6		8
Deriah Formation	7		
Napperby Formation			9
Digby Formation	8		
Trinkey Formation			10
Wallala Formation			
Breeza Coal Member		aquitard	11
Clare Sandstone	9		
Howes Hill Coal Member			12
Benelabri Formation			
Hoskissons Coal	10	CSG reservoir	13
Brigalow Formation			14
Arkarula Formation	11		15
Melvilles Coal Member		aquitard	16
Pamboola Formation			17
Watermark Formation	12		18
Porcupine Formation			19
Maules Creek Formation (upper)		interburden	20, 21
Maules Creek Formation (coal measures)	13	CSG reservoir	22
Maules Creek Formation (lower)		interburden	23, 24

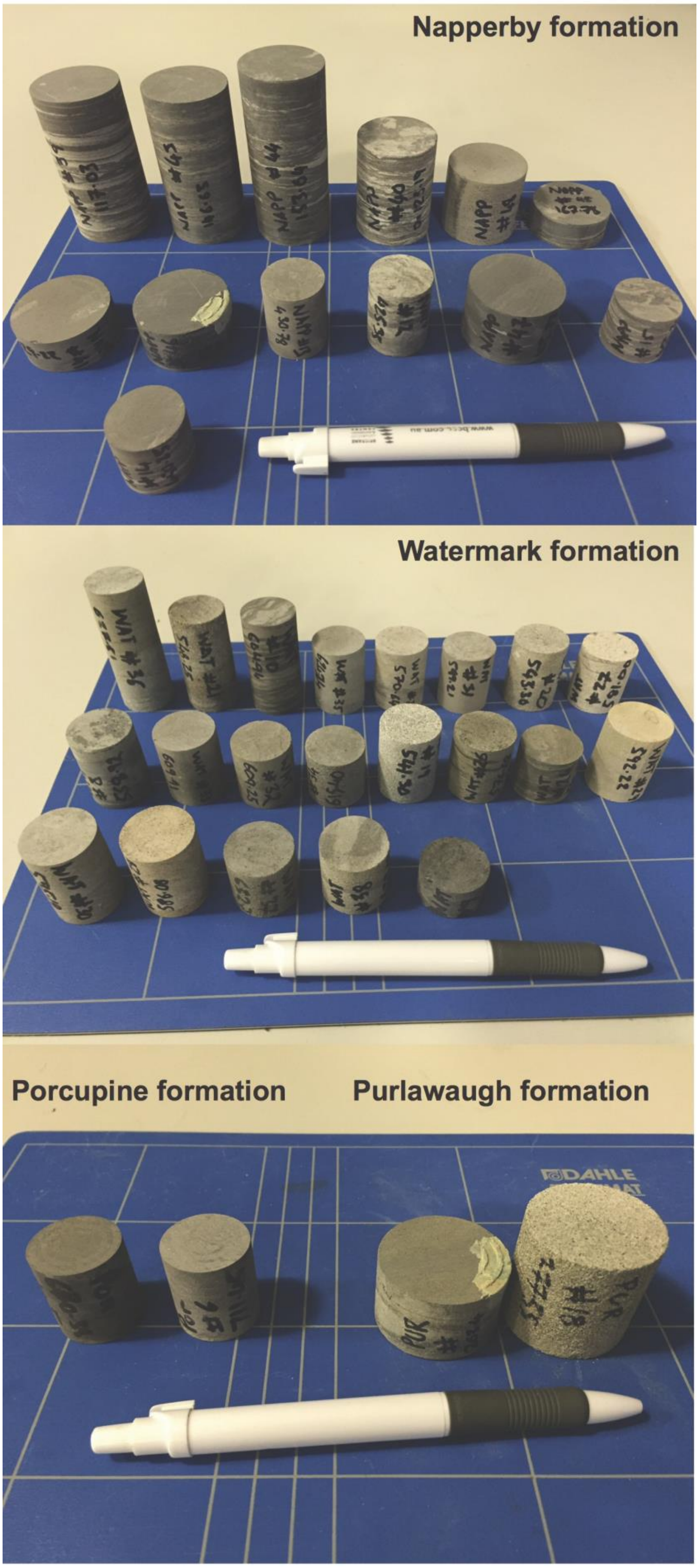

Figure 5. Picture of some of the sub-cored plugs prior to gas porosity and permeability measurement.

Table 3. Examples of computed overburden stress (lithostatic pressure) at different depths.

Depth (mBGL)	Pressure (MPa)	Pressure (psi)
200	4.9	711
400	9.8	1421
600	14.7	2132
800	19.6	2843
1000	24.5	3553

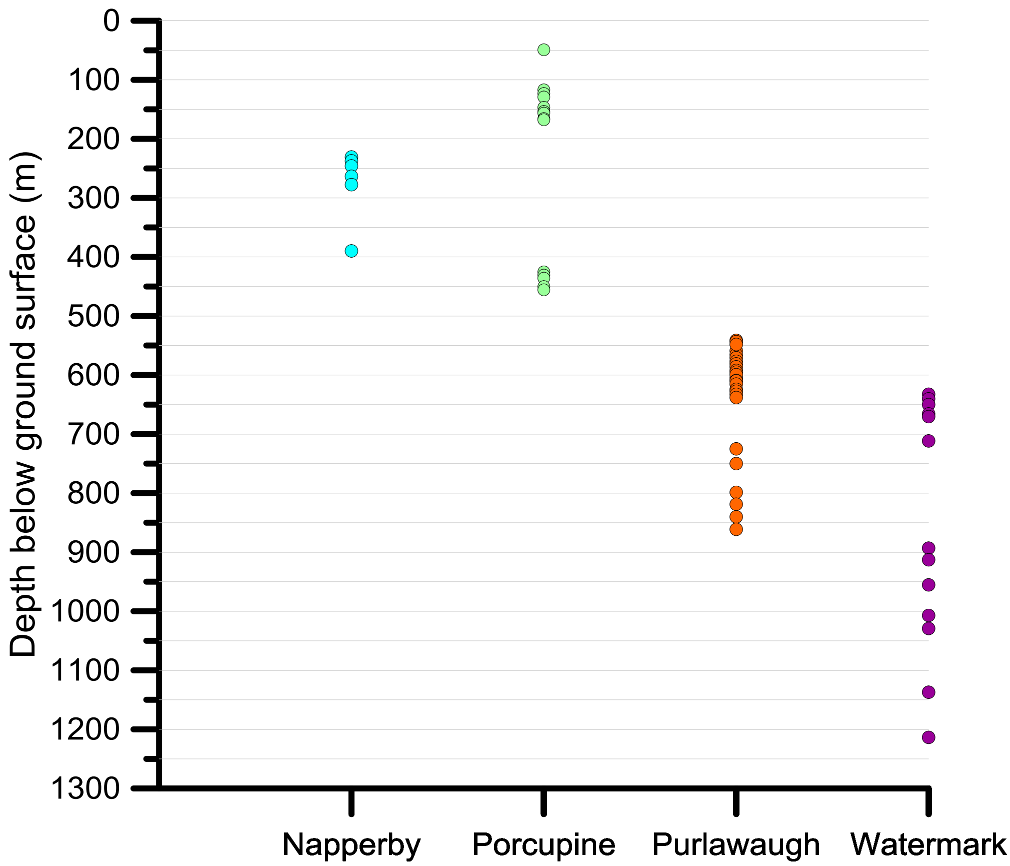

Figure 6 Sampling depths for all cores across four key aquitard formations.

2.2. Nitrogen gas porosity and permeability methodology

Each extracted plug was put in an automated AP 608 nitrogen Permeameter-Porosimeter (Coretest Inc.) (Figure 7). In a standard nitrogen gas porosity-permeability test a sample is loaded into the core holder and flooded with inert nitrogen gas. Nitrogen expansion is monitored and the pore volume (i.e. porosity) of the rock sample is calculated following Boyle's law:

$$v_1 = \frac{p_2 \cdot v_2}{p_1} \tag{1}$$

where v_1 (m^3) is the volume of nitrogen permeating rock sample, p_2 and v_2 are the pressure (MPa) and the calibrated volume (m^3) of nitrogen before being released into the sample, and p_1 (MPa) is the pressure of gas after sample infiltration. The accuracy of the porosity measurements with this apparatus is about 0.1 %.

Permeability was measured using the unsteady-state pulse decay method with a measurement range for this apparatus from 1 µD to 10 D (Jones, 1972). This method determines permeability from variations of the differential pressure at the edge of a core plug when the inlet of this plug is connected to a gas tank initially put at a given pressure. The technique is widely used in core evaluation and returns the equivalent liquid permeability (i.e. Klinkenberg corrected gas permeability), which is commonly used to estimate water flow behaviour under the assumption that no interaction between saturating fluid and solid rock frame takes place. Because all cores were sampled in the vertical direction, measured permeability represents vertical permeability (and thus vertical hydraulic conductivity, K_v).

Porosity and permeability measurements are sensitive to external pressure exerted on the porous rock. For instance, overburden pressure causes small (but noticeable) reduction of porosity due to closure of thin compliant pores and/or grain contacts (e.g., Shapiro, 2003; Pervukhina et al., 2010). As a result, permeability is expected to be also impacted by overburden pressure. Especially for deep formations both porosity and permeability need to be determined at confining pressures representative for in-situ conditions.

The porosity and permeability of each of the core plugs were measured for four to six confining pressures depending on the range of overburden stress allowed (Table 3). The maximum pressure was chosen to not exceed the overburden stresses at the depth of the plug recovery by more than 10%. The porosity and permeability of the samples were measured along the core axis (i.e. normal to bedding plane) applying gas injection from the top end of the sample toward the bottom end of the sample at a minimum confining pressure of 500 psi (to avoid gas leak between the radial surface of the sample and the sleeve) and a constant pore pressure of 250 psi: the effective pressure is therefore at a minimum of 250 psi.

Three repeat measurements were obtained at each pressure point to assess the statistical error of the measurements. The average of the repeat measurements was computed at each confining pressure stage for further analysis. The measurements at different confining pressures help to evaluate the stress sensitivity of porosity and permeability of these samples at different overburden stresses. Furthermore, doing measurements at different confining pressures allows extrapolation of porosity and permeability values from their measurement interval to higher and lower confining pressures, by first fitting the second-order polynomial curve to the measurement points (see Section 2.3.2).

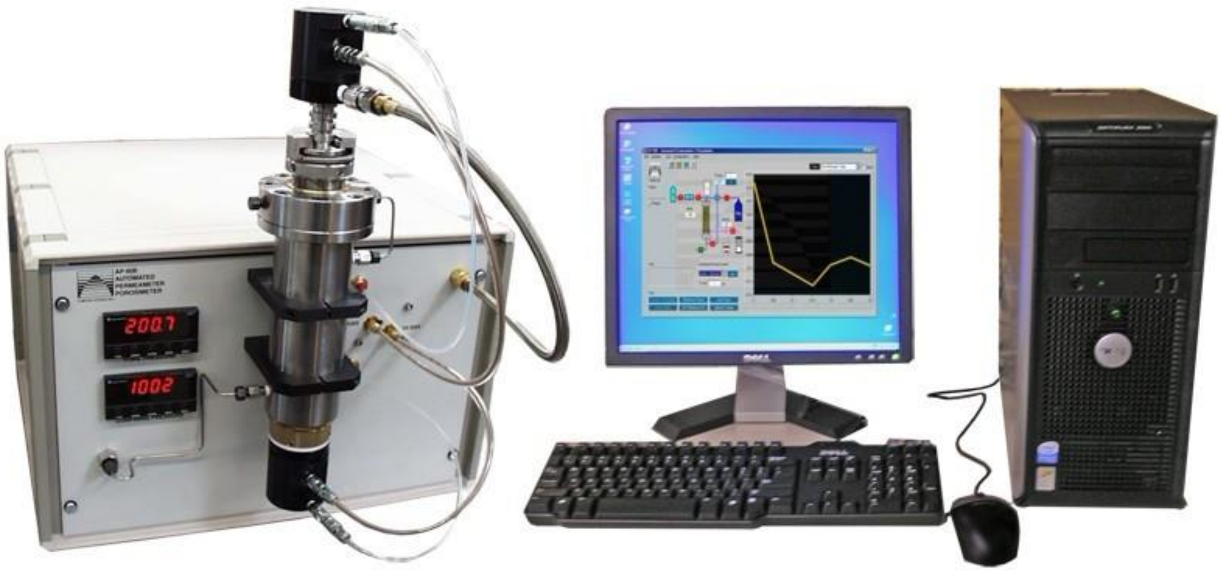

Figure 7 Gas porosimetry-permeametry device used at the CSIRO Petrophysics laboratory.

Laboratory measurements of gas permeability were corrected for the Klinkenberg effect. Klinkenberg (1941) reported variations in permeability determined by using gases as the flowing fluid compared to those obtained when using non-reactive liquids. These variations were considered to be due to slippage, a phenomenon well known with respect to gas flow in capillary tubes. The gas velocity at the walls is non-zero, and predicted gas transport is enhanced as the “gas slippage” reduces viscous drag and increases the apparent permeability (Wu et al. 1998). This phenomenon of gas slippage occurs when the diameter of the capillary pore system approaches the mean free path of the gas. The mean free path of a gas is a function of molecular size and the kinetic energy of the gas. Thus, permeability of gas depends on factors which influence the mean free path, such as temperature, pressure and the molecular size of the gas and therefore correction factors are required.

Permeability units are expressed hereafter in mD (milli Darcy). The permeability in the SI system has dimension of m^2, while in the hydrogeological literature units of $m.day^{-1}$ or $m.sec^{-1}$ are more commonly used. Conversion from mD to m^2 involves the following constant: 1 mD is approximately equal to 1×10^{-15} m^2. The saturated hydraulic conductivity, K ($m.sec^{-1}$), is related to the permeability k (m^2), as follows:

$$K = k \times f = k \frac{\rho_f \times g}{\eta} \tag{2}$$

where f ($m^{-1}.sec^{-1}$) is the fluidity of the permeating liquid, ρ_f is fluid density (998.23 kg m^{-3} at 20°C), η is dynamic viscosity (10^{-3} $kg.m^{-1}.sec^{-1}$ at 20°C), and g is gravitational constant (9.81 $m.sec^{-2}$). In other words, the conversion between K and k depends on the viscosity and density of the fluid at a given temperature. At 20°C, the fluidity f for water becomes $9.79\text{x}10^6$ $m^{-1}.sec^{-1}$. In hydrogeological studies, where the focus is on the flow of groundwater, density and viscosity of the underground water are supposed to be known. Hence, hydrogeologists use K ($m.sec^{-1}$) rather than permeability (mD), which is determined by pore space microstructure only. 1 mD is approximately equal to 10^{-8} $m.sec^{-1}$ ($8.62\text{x}10^{-9}$ $m.sec^{-1}$ to be precise) if water at 20°C is the saturating fluid.

2.3. Summary of porosity and permeability measurements

2.3.1. DATA OVERVIEW

Table 4 summarises the porosity and vertical permeability measurements at six values of the overburden stress. The highest confining pressure could not always be applied due to experimental difficulties. An overview of all porosities and permeability values at their sampling depth is provided in Figure 8, while formation-specific pressure dependencies are shown from Figure 9 to Figure 13. Some general observations are as follows:

- Being the first aquitard formation underlying the Pilliga Sandstone aquifer, the Purlawaugh Formation has porosity values from 1.35 – 14.56% with a weak stress dependency (Figure 10). Permeability measurements are from 0.00037 – 2.85 mD, also with a weak stress dependency. The Purlawaugh Formation is made up of fine to medium grained sandstone, thinly interbedded with siltstone, mudstone and thin coal seams (CDM Smith, 2014),
- Underlying the Purlawaugh Formation is the Napperby Formation, which has porosity values between 0.02 to 9.15 %, with distinct stress dependency for the higher porosities (Figure 11). The permeability ranges from 0.00006 to 0.00974 mD, with a strong stress dependency. At its top the Napperby Formation is composed of interbedded fine sandstone, claystone and siltstone, while it has shale at its base (CDM Smith, 2014),
- Considerably deeper in the stratigraphic table is the Watermark Formation, which together with the underlying Porcupine Formation, provides isolation between the Hoskissons Coal Formation and the Maules Creek Formation. The Watermark Formation has the highest maximum porosity and permeability values among the four tested formations but also the most heterogeneous. The porosity ranges from 0.09 to 18.04 %, with a distinct stress dependency (Figure 12). The permeability ranges from 0.00001 to 1.4 mD with a strong stress dependency. The Watermark Formation is a marine siltstone with shale and sandstone (CDM Smith, 2014),
- The Porcupine Formation porosity values are relatively high, i.e. from 0.22 to 15.03% with a strong stress dependency (Figure 13). Permeabilities range from 0.00006 – 1.293 mD and are clearly stress dependent. The Porcupine Formation is characterised by a fining upward sequence of conglomerate, siltstone, mudstone and coal (CDM Smith, 2014).

Because confining pressures were applied for up to six fixed values per formation (see Table 3), the confining pressures were not adjusted to match the value representative of the sampling depths. Values of porosity and permeability for confining pressures corresponding to their sampling depths were indirectly obtained by inserting the confining pressures calculated at the sampling depths into the fitted porosity-confining pressure and permeability-confining pressure relationships (see Section 2.3.2 for details).

Note that values at other confining pressures are not included in Figure 8 to allow a more focused analysis of the data at their sampling depths. Based on porosity and permeability values, the Purlawaugh Formation displays the least variation (less than two orders of magnitude) while the Watermark Formation has the largest variation (almost six orders of magnitude). Only the Watermark Formation displays a depth-dependency of the porosity and a weak depth-dependency of the permeability.

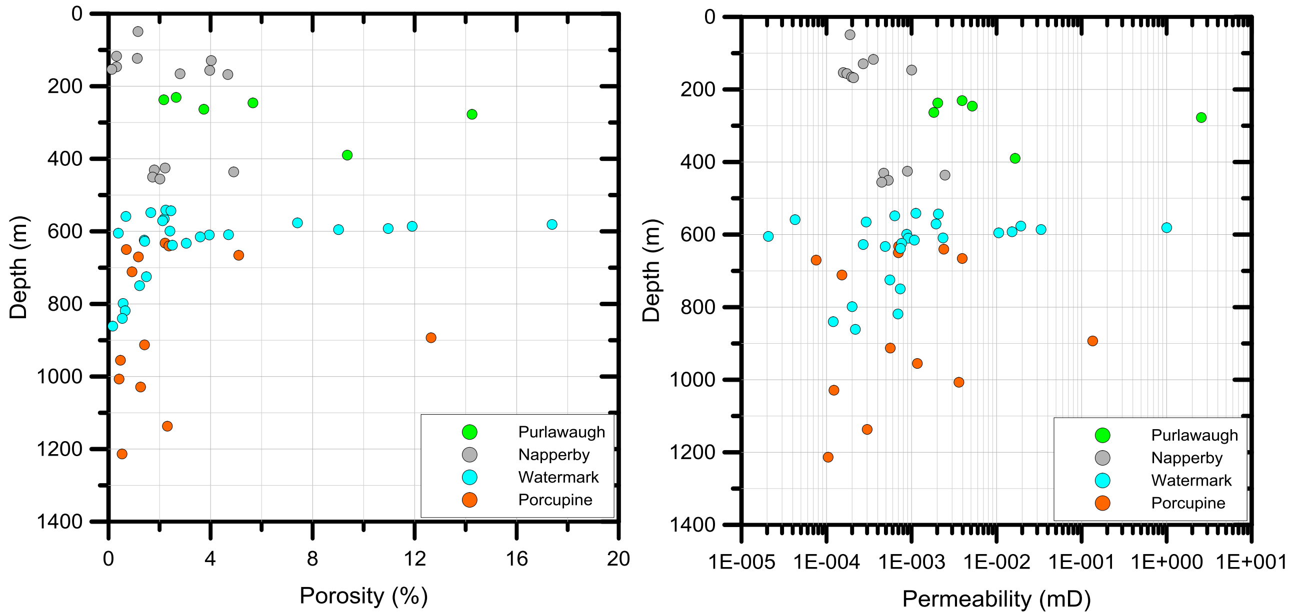

Figure 8 Porosity (left) and permeability (right) at their sampling depths (mBGL) across four aquitard formations. Values were obtained by inserting the confining pressures calculated at the sampling depths into the fitted porosity-confining pressure and permeability-confining pressure relationships (for details see Section 2.3.2).

Table 4 Summary of the porosity and permeability measurements: columns represent bore number and formation where cores were sampled from, confining pressure, porosity and permeability at six confining pressures. ND = no data.

Bore name	Formation	Sampling Depth (m)	Pconf1 (psi)	Pconf2 (psi)	Pconf3 (psi)	Pconf4 (psi)	Pconf5 (psi)	Pconf6 (psi)	Porosity1 (%)	Porosity2 (%)	Porosity3 (%)	Porosity4 (%)	Porosity5 (%)	Porosity6 (%)	K1 (mD)	K2 (mD)	K3 (mD)	K4 (mD)	K5 (mD)	K6 (mD)
ROS053C	Napperby	49.18	532.72	636.95	725.61	815.93	886.52	ND	0.84	0.89	0.83	0.74	0.69	ND	0.00013	0.00011	0.000090	0.00008	0.000070	ND
NC283C	Napperby	117.03	546.90	621.00	719.55	826.14	854.89	ND	0.23	0.28	0.38	0.28	0.31	ND	0.00073	0.00050	0.00038	0.00029	0.00025	ND
NC283C	Napperby	123.19	537.91	628.83	720.14	813.14	859.30	ND	0.52	0.58	0.52	0.54	0.48	ND	0.00023	0.00015	0.00012	0.00011	0.00010	ND
NC283C	Napperby	129.22	540.33	627.67	714.51	816.19	859.67	ND	3.12	3.62	3.49	3.52	3.20	ND	0.00048	0.00035	0.00028	0.00023	0.00022	ND
NC283C	Napperby	146.65	536.79	620.73	735.89	820.77	871.77	ND	0.11	0.25	0.38	0.33	0.29	ND	0.00043	0.00025	0.00018	0.00014	0.00012	ND
NC283C	Napperby	153.64	543.91	634.00	709.01	830.41	872.79	ND	0.02	0.12	0.13	0.14	0.12	ND	0.00039	0.00025	0.00017	0.00011	0.00010	ND
NC303C	Napperby	156.36	583.54	598.46	648.95	638.13	ND	ND	2.55	2.27	1.97	2.29	2.27	ND	0.00012	0.000060	0.000090	0.00009	0.000090	ND
NC303C	Napperby	165.72	546.98	630.83	727.12	821.56	862.52	ND	0.07	0.71	0.56	0.63	0.59	ND	0.00035	0.00028	0.00020	0.00016	0.00015	ND
NC283C	Napperby	167.78	545.11	636.66	730.37	817.90	863.76	ND	1.58	1.93	1.25	0.96	0.80	ND	0.00050	0.00032	0.00021	0.00016	0.00014	ND
Narrabri DDH02	Napperby	425.35	544.87	784.11	1029.91	1277.41	1529.71	ND	3.81	3.15	2.34	2.10	2.01	ND	0.0083	0.0030	0.0014	0.00086	0.00056	ND
Narrabri DDH02	Napperby	430.78	533.21	780.73	1031.03	1275.85	1532.29	ND	2.55	2.23	1.88	1.66	1.77	ND	0.0040	0.0015	0.00075	0.00045	0.00030	ND
Coonarah 3	Napperby	435.99	535.63	775.60	1009.28	1541.63	ND	ND	9.15	6.89	5.64	4.39	ND	ND	0.0097	0.0048	0.0033	0.00213	ND	ND
Narrabri DDH02	Napperby	450.25	548.79	798.67	1041.31	1280.38	1526.05	ND	1.96	2.18	2.02	1.53	1.18	ND	0.0061	0.0018	0.00082	0.00044	0.00027	ND
Narrabri DDH02	Napperby	455.70	532.42	769.15	1033.21	1526.98	1744.82	ND	2.54	2.59	2.22	1.51	1.73	ND	0.0048	0.0015	0.00065	0.00021	0.00013	ND
Coonarah 3	Porcupine	632.43	536.59	774.36	1019.15	1533.86	2026.92	ND	5.87	4.61	3.59	2.45	2.09	ND	0.0068	0.0028	0.0015	0.00066	0.00038	ND
Coonarah 3	Porcupine	640.28	530.38	779.22	1027.23	1519.70	2027.94	ND	6.26	5.20	3.83	2.71	2.23	ND	0.0244	0.0094	0.0059	0.00283	0.0018	ND
Coonarah 3	Porcupine	649.99	524.95	759.47	1039.13	1519.40	2013.11	ND	2.87	1.48	1.20	0.67	0.67	ND	0.0066	0.0018	0.00070	0.00019	0.000090	ND
Coonarah 3	Porcupine	665.84	376.43	619.09	864.04	1364.53	1838.87	ND	10.02	10.14	6.80	5.75	4.79	ND	0.0954	0.0126	0.0065	0.00445	0.0035	ND
Bando N1	Porcupine	670.38	531.50	771.31	1027.53	1519.38	2037.44	ND	1.42	1.89	1.12	0.76	0.79	ND	0.0029	0.0011	0.00049	0.00014	6.00E-05	ND
Bando N1	Porcupine	711.45	534.92	772.08	1033.66	1179.72	1390.37	1502.53	1.05	1.62	1.24	1.20	1.07	0.99	0.0040	0.0012	0.00054	0.0002	0.00012	0.00009
Kerawah 1	Porcupine	893.18	562.63	785.83	1023.53	1515.49	2024.34	ND	15.03	14.32	13.97	13.53	13.25	ND	1.29	0.81	0.60	0.42	0.33	ND
Kerawah 1	Porcupine	912.83	545.70	796.41	1042.91	1530.57	2035.79	ND	4.86	3.64	2.69	2.17	1.48	ND	0.0055	0.0025	0.0016	0.0008	0.00049	ND
Slacksmith 1	Porcupine	955.35	452.58	972.97	1835.92	ND	ND	ND	2.24	1.83	0.41	ND	ND	ND	0.0046	0.00048	0.00074	ND	ND	ND
Slacksmith 1	Porcupine	1007.12	525.87	782.01	1030.71	1514.13	2021.29	ND	0.49	0.39	0.53	0.44	0.22	ND	0.033	0.019	0.013	0.00672	0.0039	ND
Slacksmith 1	Porcupine	1029.11	528.37	782.78	1024.30	1519.66	2029.22	ND	1.58	1.69	1.46	1.07	0.81	ND	0.0031	0.0013	0.00071	0.00028	0.00014	ND
Slacksmith 1	Porcupine	1137.07	529.73	781.66	1013.43	1515.02	2024.06	2532.88	3.54	3.55	2.86	2.01	1.72	1.39	0.0089	0.0029	0.0014	0.00056	0.00043	0.00019
Slacksmith 1	Porcupine	1213.65	527.29	777.98	1028.84	1519.60	2025.80	2542.71	1.39	1.55	1.13	0.78	0.65	0.53	0.0084	0.0024	0.0010	0.00032	0.00014	0.00007
Dewhurst 19	Purlawaugh	230.75	497.89	840.54	985.52	ND	ND	ND	3.04	2.41	1.79	ND	ND	ND	0.0081	0.0018	0.0011	ND	ND	ND
Dewhurst 19	Purlawaugh	237.31	534.72	619.31	758.41	1018.01	ND	ND	2.62	2.32	1.96	1.35	ND	ND	0.0033	0.0025	0.00094	0.00037	ND	ND
Dewhurst 19	Purlawaugh	245.88	531.38	779.98	1027.37	ND	ND	ND	8.83	4.62	2.60	ND	ND	ND	0.011	0.0038	0.0021	ND	ND	ND
Narrabri DDH02	Purlawaugh	263.40	533.03	590.22	640.51	679.29	715.91	ND	3.74	4.23	4.03	4.03	3.79	ND	0.0027	0.0026	0.0023	0.0021	0.0020	ND
Narrabri DDH02	Purlawaugh	277.55	547.13	600.59	653.92	702.62	749.46	ND	14.56	14.43	14.44	14.39	14.27	ND	2.85	2.82	2.77	2.67	2.58	ND
Coonarah 3	Purlawaugh	389.88	540.37	765.55	1024.03	ND	ND	ND	10.43	10.06	9.49	ND	ND	ND	0.12	0.038	0.018	ND	ND	ND

Table 3 Continued

Bore name	Formation	Sampling Depth (m)	Pconf1 (psi)	Pconf2 (psi)	Pconf3 (psi)	Pconf4 (psi)	Pconf5 (psi)	Pconf6 (psi)	Porosity1 (%)	Porosity2 (%)	Porosity3 (%)	Porosity4 (%)	Porosity5 (%)	Porosity6 (%)	K1 (mD)	K2 (mD)	K3 (mD)	K4 (mD)	K5 (mD)	K6 (mD)	Depth	Pconf	Poros	Perm (mD)
Bando N1	Watermark	558.92	533.25	762.03	1037.16	1283.03	1536.34	1736.58	0.76	0.88	0.66	0.77	0.60	0.68	0.0013	0.00048	0.00017	0.000080	0.000050	0.00003	558.92	1590.49	0.680246	4.27E-05
Bando N1	Watermark	565.47	467.43	738.94	963.71	1207.32	1661.00	1925.56	4.73	4.22	2.93	2.61	2.32	1.85	0.0049	0.00077	0.00046	0.00032	0.00012	0.0001	565.47	1609.12	2.184648	0.000292
Bando N1	Watermark	604.94	559.11	709.17	1040.35	1134.08	1418.06	1580.19	0.46	0.51	0.36	0.33	0.33	0.36	0.00014	0.000050	0.000020	0.000020	0.000010	0.00001	604.94	1721.44	0.381873	2.07E-05
Slacksmith 1	Watermark	725.02	528.96	784.13	1015.16	1513.86	2038.62	ND	4.55	3.82	2.50	1.75	1.61	ND	0.012	0.0036	0.0017	0.00071	0.00040	ND	725.02	2063.15	1.483541	0.000556
Slacksmith 1	Watermark	749.78	525.68	780.18	1037.54	1523.97	2043.97	ND	4.35	3.52	2.31	1.56	1.34	ND	0.010	0.0036	0.0018	0.00078	0.00072	ND	749.78	2133.60	1.215924	0.000736
Slacksmith 1	Watermark	798.62	535.65	780.87	1035.90	1529.00	2015.92	ND	3.29	2.32	1.32	0.85	0.64	ND	0.0052	0.0017	0.00084	0.00028	0.00012	ND	798.62	2272.59	0.568488	0.0002
Slacksmith 1	Watermark	818.69	678.80	811.86	1042.37	1410.37	2025.58	ND	2.63	2.11	1.74	1.38	1.15	ND	0.0043	0.0031	0.00052	0.00071	0.00034	ND	818.69	2329.70	0.651909	0.000692
Slacksmith 1	Watermark	840.03	529.26	773.47	1015.96	1542.10	2042.81	ND	1.59	1.49	1.10	0.78	0.66	ND	0.0036	0.0011	0.00049	0.00014	0.00007	ND	840.03	2390.42	0.539079	0.00012
Kerawah 1	Watermark	861.25	527.64	771.55	1012.52	1541.39	2016.51	ND	0.26	0.21	0.15	0.11	0.09	ND	0.0024	0.0011	0.00062	0.00029	0.00019	ND	861.25	2450.81	0.164	0.000218
Narrabri DDH02	Watermark	541.30	532.88	755.07	969.43	1534.23	1732.49	ND	5.59	3.85	2.83	2.24	2.22	ND	0.0086	0.0035	0.0020	0.0010	0.00088	ND	541.30	1540.35	2.242494	0.001125
Narrabri DDH02	Watermark	543.30	460.84	689.50	991.38	1255.42	1646.17	1759.63	8.13	5.99	4.10	3.42	2.12	2.11	0.026	0.0064	0.0033	0.0023	0.0017	0.0016	543.30	1546.04	2.445731	0.002064
Narrabri DDH02	Watermark	548.25	512.64	788.52	1037.75	1284.11	1533.25	1721.06	3.07	1.94	1.77	1.70	1.56	1.70	0.0018	0.00099	0.00090	0.0012	0.00058	0.00038	548.25	1560.12	1.656316	0.000634
Narrabri DDH02	Watermark	570.64	538.15	791.92	938.69	1203.60	1443.08	1567.57	4.51	3.47	1.91	2.36	2.18	2.21	0.0041	0.0027	0.0023	0.0020	0.0019	0.0017	570.64	1623.84	2.118818	0.00194
Narrabri DDH02	Watermark	576.68	532.34	769.29	1028.98	1527.17	1766.75	2015.41	8.35	7.67	7.48	7.59	7.36	7.28	0.066	0.044	0.033	0.021	0.018	0.0162	576.68	1641.02	7.407606	0.019294
Narrabri DDH02	Watermark	581.00	380.09	720.49	912.99	1195.03	1479.58	1543.87	18.04	17.67	17.35	17.58	17.64	17.39	1.40	1.051	1.19	1.13	1.05	1.05	581.00	1653.32	17.38811	1.003129
Narrabri DDH02	Watermark	586.08	520.05	716.03	1021.43	1396.82	1645.39	1974.88	12.92	12.91	12.51	12.05	11.81	11.78	0.083	0.055	0.045	0.035	0.033	0.031	586.08	1664.93	11.90429	0.033329
Narrabri DDH02	Watermark	592.22	542.71	760.36	992.09	1539.92	1780.24	2035.69	13.45	12.89	12.37	11.26	10.80	10.31	0.066	0.036	0.026	0.017	0.015	0.013	592.22	1685.25	10.96322	0.015195
Narrabri DDH02	Watermark	595.19	538.46	790.33	1030.65	1532.70	2012.95	ND	14.97	14.10	12.41	9.72	7.56	ND	0.10	0.041	0.024	0.012	0.0083	ND	595.19	1693.70	9.015589	0.0106
Narrabri DDH02	Watermark	599.21	534.51	783.74	1036.59	1528.78	2042.12	ND	7.20	5.47	4.11	2.57	2.11	ND	0.015	0.0051	0.002	0.0010	0.00063	ND	599.21	1705.14	2.407359	0.000876
Narrabri DDH02	Watermark	609.25	527.98	789.23	1037.48	1537.18	2036.97	ND	8.67	7.67	6.65	4.98	4.21	ND	0.020	0.0086	0.0053	0.0028	0.0018	ND	609.25	1733.71	4.703639	0.002343
Narrabri DDH02	Watermark	609.91	552.84	768.07	1027.41	1526.23	1795.11	2068.14	7.39	5.44	3.87	2.70	2.37	2.30	0.019	0.0055	0.0025	0.0010	0.00076	0.00064	609.91	1735.58	3.948882	0.000915
Narrabri DDH02	Watermark	615.40	528.61	784.35	1031.91	1524.03	1790.01	2071.54	6.81	6.26	5.43	4.04	3.41	3.02	0.024	0.0077	0.0038	0.0014	0.00098	0.00072	615.40	1751.21	3.594266	0.001078
Narrabri DDH02	Watermark	624.24	532.72	740.44	989.12	1546.13	1796.15	2031.14	2.57	2.27	1.85	1.47	1.46	1.29	0.0066	0.0029	0.0015	0.00059	0.00047	0.00039	624.24	1776.36	1.398558	0.000763
Narrabri DDH02	Watermark	627.51	544.93	733.61	1078.44	1319.18	1573.03	1803.68	1.12	1.50	1.48	1.46	1.43	1.22	0.0020	0.0013	0.00059	0.00041	0.00031	0.00024	627.51	1785.67	1.418	0.00027
Narrabri DDH02	Watermark	632.74	528.96	783.58	1034.23	1529.89	2041.14	2668.10	8.09	7.10	5.07	3.93	1.99	2.35	0.051	0.012	0.0029	0.00092	0.00039	0.00026	632.74	1800.55	3.04644	0.00049

2.3.2. DERIVATION OF CONFINING PRESSURE DEPENDENCY

When all data for all confining pressures are combined into pooled data sets, one for porosity and one for permeability, an exponential decrease of porosity and permeability with increasing confining pressure is evident from Figure 9. The confining pressure dependencies were modelled by fitting an exponential relationship to the data for each of the 59 core samples using:

$$\phi = a_\phi + b_\phi e^{-c_\phi P} \tag{3}$$

$$k = a_k + b_k e^{-c_k P} \tag{4}$$

where *Φ* (%) and *k* (mD) are the laboratory measurements of the porosity and Klinkenberg-corrected permeability, respectively, for a given confining pressure *P* (psi). The constants *a*, *b* and *c* are the fitting coefficients determined using a least squares fitting algorithm from pairs of {*Φ*, *P*} and {*k*, *P*} values available for each plug. This resulted in 59 sets of the constants {*a*, *b*, *c*}, one set for each plug. The red and blue curves on Figure 9 show the measured values and fitted exponential curves, respectively. The green star markers show the predicted in-situ values of porosity and permeability calculated using equations (3) and (4) and *P* values predetermined from the hydrostatic pressure $z \times \rho \times g$, where *z* is the sampling depth in meters (m), ρ_b is density in kg.m^{-3} and g = 9.81 m.sec^{-2} is the gravitational constant.

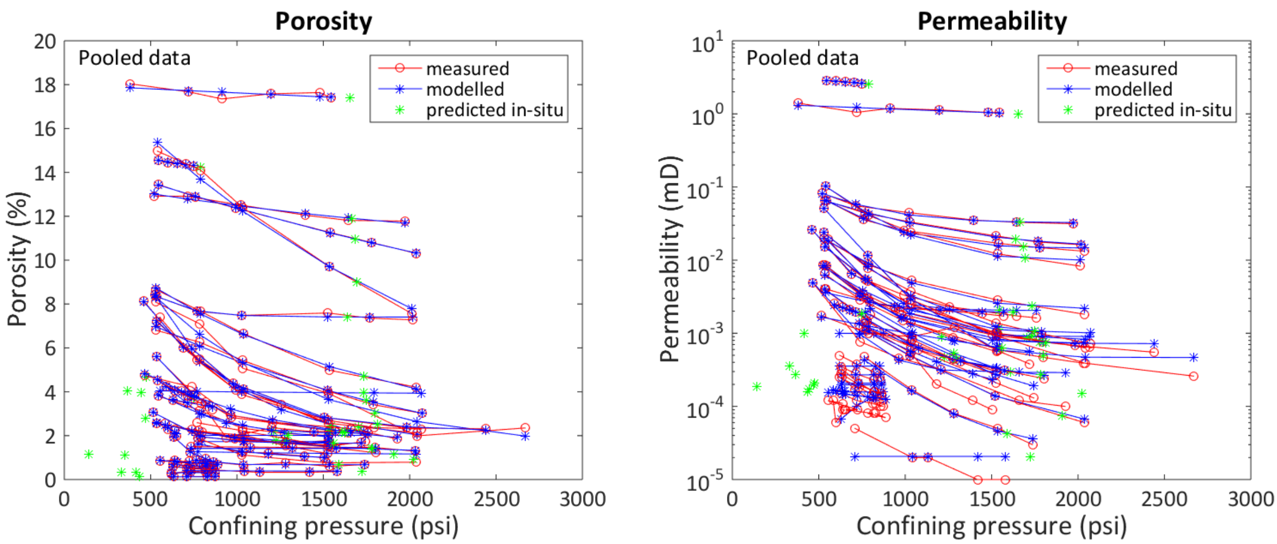

Figure 9 Porosity–confining pressure (left) and permeability-confining pressure (right) relationships for pooled data. Exponential model (blue) fitted to data (red). Green circles show the predicted in-situ values of porosity and permeability using the exponential models.

The confining pressure dependency of porosity and permeability is displayed for each of the formations separately in Figure 10 till Figure 13. In addition to the measured data, the fitted model is also shown. For most plugs there is a good agreement between data and model fit; there are some poor fits for Watermark (Figure 12) and Porcupine (Figure 13) formation porosities and permeabilities.

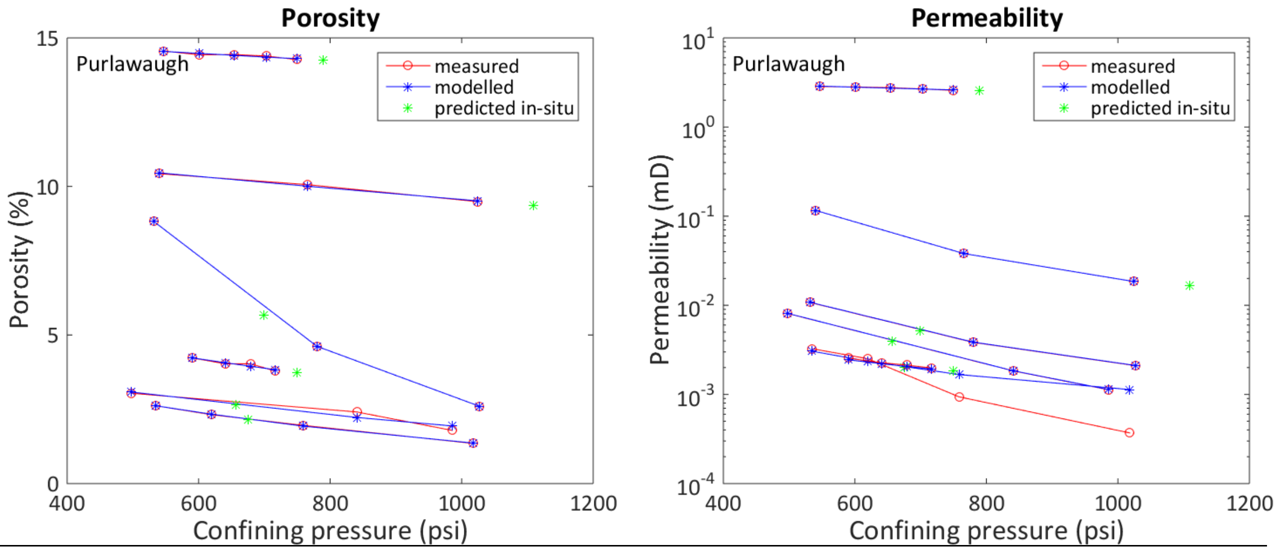

Figure 10 Porosity–confining pressure (left) and permeability-confining pressure (right) relationships for Purlawaugh Formation. Exponential model (blue) fitted to data (red). Green circles show the predicted in-situ values of porosity and permeability using the exponential models.

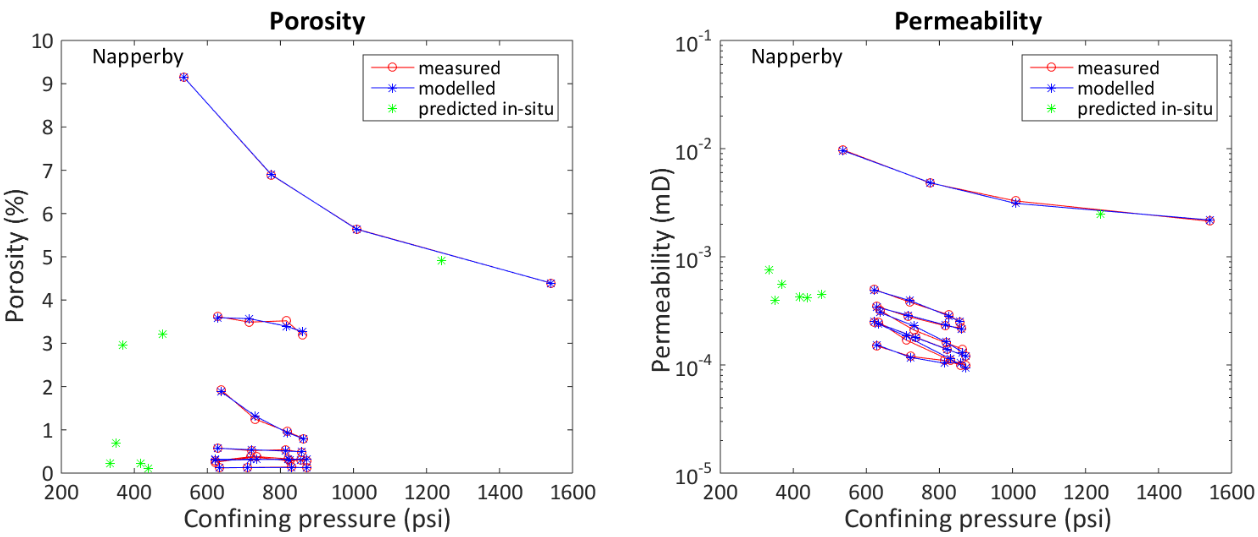

Figure 11 Porosity–confining pressure (left) and permeability-confining pressure (right) relationships for Napperby Formation. Exponential model (blue) fitted to data (red). Green circles show the predicted in-situ values of porosity and permeability using the exponential models.

Figure 11 shows the confining pressure – porosity and confining pressure – permeability relationships for the Napperby Formation which were fitted by second-order polynomial regression equations:

$$\phi = a_\phi + b_\phi P + c_\phi P^2 \tag{5}$$

$$k = a_k + b_k P + c_k P^2 \tag{6}$$

where P is confining pressure (psi). Equations (5) and (6) were selected for the Napperby Formation as they provided a higher correlation (R^2 = 0.61) between the measured and modelled values of porosity and permeability compared with the exponential models (3) and (4). The in-situ porosity and permeability values calculated using the established second-order polynomial regression models are indicated by green star-markers. Fitted parameters for Equations 5 and 6 are listed in Appendix 1.

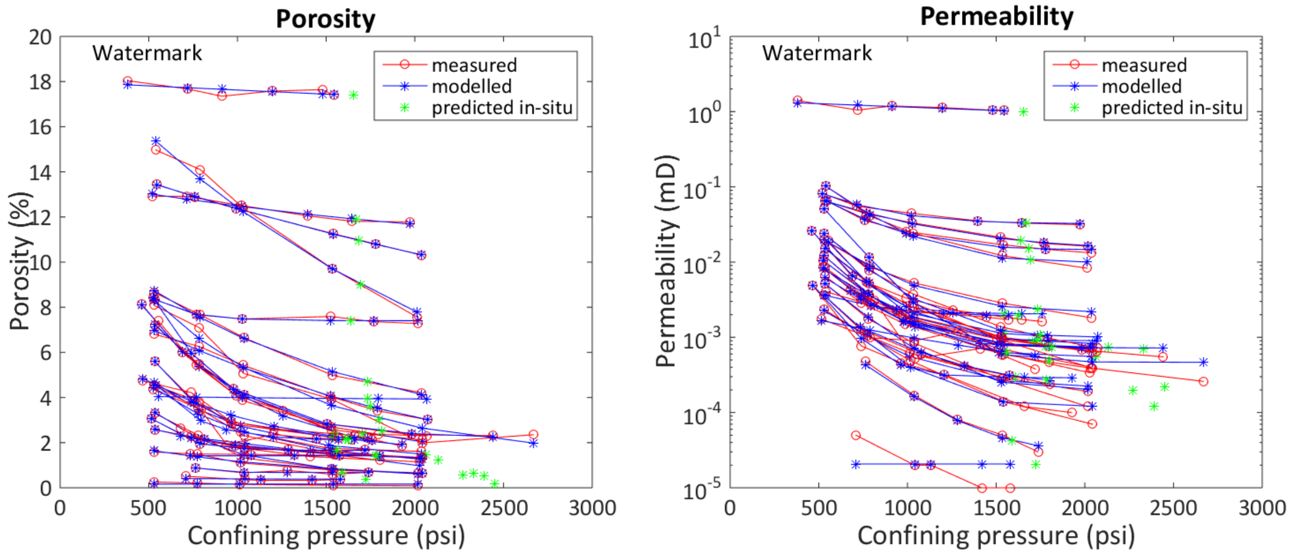

Figure 12 Porosity–confining pressure (left) and permeability-confining pressure (right) relationships for Watermark Formation. Exponential model (blue) fitted to data (red). Green circles show the predicted in-situ values of porosity and permeability using the exponential models.

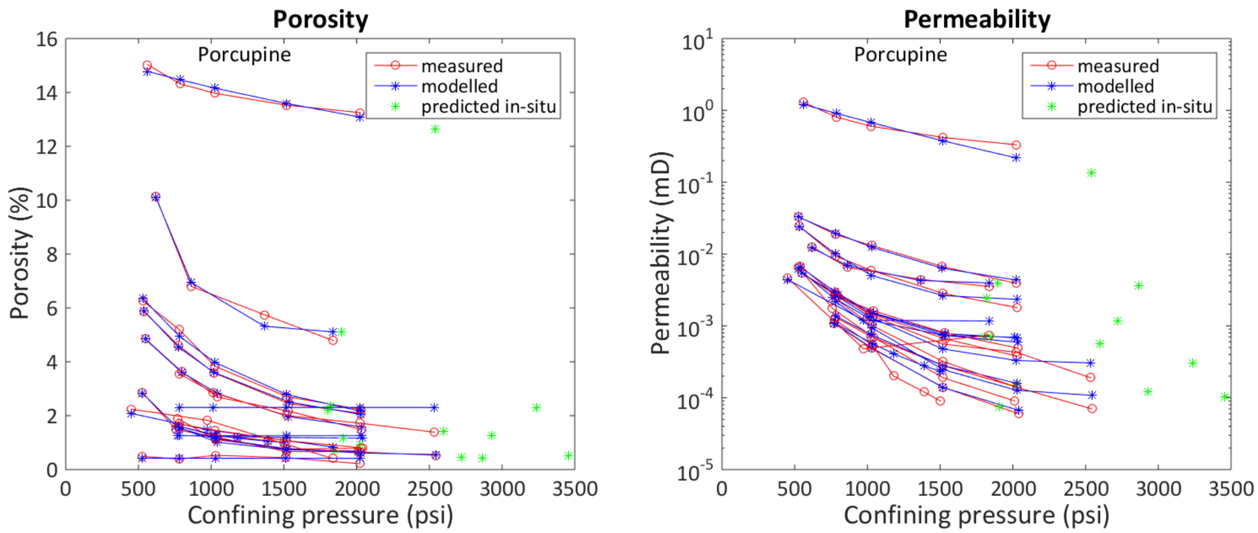

Figure 13 Porosity–confining pressure (left) and permeability-confining pressure (right) relationships for Porcupine Formation. Exponential model (blue) fitted to data (red). Green circles show the predicted in-situ values of porosity and permeability using the exponential models.

2.4. Porosity-permeability models in individual formations

2.4.1. DERIVATION OF POROSITY-PERMEABILITY MODELS

The previous laboratory measurements of porosity and permeability for up to six confining pressures from the 59 core plugs were used to estimate porosity-permeability models. Figure 8 presents the porosity and permeability values measured at the sampling depths of the 59 plugs, i.e. based on the in-situ pressure. First, the laboratory measurements of porosity and permeability shown in Figure 8 were considered as a pooled data set and used for modelling a linear porosity-permeability relationship across all four formations. Next, the pooled data set was expanded with porosity and permeability values measured on plugs at different confining pressure from the in-situ pressure; this larger data set was used to derive porosity-permeability relationships for each formation separately.

In order to characterise relationships between rock porosity and permeability, three analytical functions were developed for each aquitard unit: (1) a single linear model; (2) multiple linear models; and (3) a single non-linear model. Comparisons between these three approaches provide a means to explore the sensitivity of modelled results to structural model uncertainty.

2.4.2. SINGLE LINEAR MODELS

The in-situ porosity and permeability values were used for modelling the porosity-permeability relationship by fitting a single linear regression equation to the {Φ, $\log_{10}k$} pairs:

$$\log_{10} k = a_1\phi + a_0 \tag{7}$$

where a_0 and a_1 are the regression coefficients. First, the pooled data was used with 59 {Φ, $\log_{10}k$} pairs. Figure 14 presents a cross plot of the in-situ porosity and permeability values and the regression line fitted to the data indicating strong correlation with the determination coefficient R^2 = 0.79. Note the large variability in permeability for porosities less than 5%; the inability of a single model to describe the pooled data in the lower porosity range is addressed by developing regression models for each formation separately.

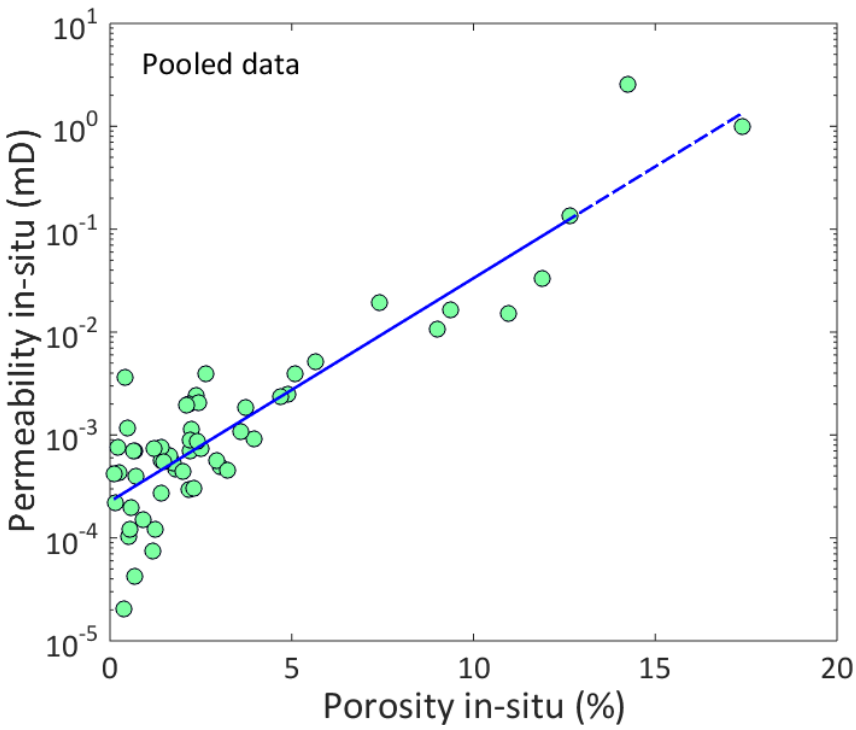

Figure 14 Cross plot of in-situ porosity and $\log_{10}$ permeability and linear regression model equation (5) using pooled data.

To investigate porosity-permeability relationships in the individual formations, similar models were built for Purlawaugh, Napperby, Watermark and Porcupine formations. To ensure statistical representativeness of the individual formation datasets for modelling porosity-permeability relationships in individual formations, porosity and permeability values measured on plugs at different confining pressure from the in-situ pressure were added to the 59 calculated in-situ porosity and permeability samples (shown in Figure 14). This significantly increases the size of the porosity-permeability data sets for each formation; the size of the combined data sets are as follows: Purlawaugh (23), Napperby (69), Watermark (146), and Porcupine (66). These pooled datasets were then each fitted by a linear regression model (Equation 7). Figure 15 shows cross plots of the porosity versus permeability $\{\Phi, \log_{10}k\}$ pairs. Table 5 presents best-fit coefficients of the porosity-permeability models established for individual formations and their coefficients of determination R^2. The additional advantage of having the porosity-permeability data across the full range of confining pressures is that the derived models implicitly account for depth-dependency of porosity and permeability.

Table 5 Fitted parameters and goodness-of-fit (R^2) for porosity-permeability models (4) in individual formations.

	Formation			
Parameter	Purlawaugh	Napperby	Watermark	Porcupine
a_1	0.26	0.17	0.20	0.22
a_0	-3.57	-3.73	-3.60	-3.40
R^2	0.91	0.62	0.81	0.66

Comparison of the porosity-permeability relationships showed strong correlation for all formations. The R^2 varied from 0.91 and 0.81 for Purlawaugh and Watermark formations, respectively, to 0.66 and 0.61 for Porcupine and Napperby formations, respectively. The relatively low R^2 for the Napperby Formation is explained by lack of plugs at higher porosity (5-10% range) and permeability (-3 to -2 $\log_{10} k$ range). Moreover, the accuracy of the low porosity and permeability measurements in the available Napperby Formation plugs could be poor due to the laboratory equipment sensitivity limits (k > 1 µD).

Despite the relatively large goodness-of-fit parameter for Purlawaugh and Watermark Formation (for R^2 values see Table 5), the regression models are unable to describe the variability in permeability for very small porosity values. This variability may be due in part to natural heterogeneity and in part due to the measurement approach. Indeed, we remind here that gas porosity-permeability method uses only 200 psi pore pressure to inject nitrogen gas in the pore network. In tight formation, such pore pressure might not be enough to properly invade all the pore systems to override the strong capillary pore pressure despite the high diffusivity of the gas.

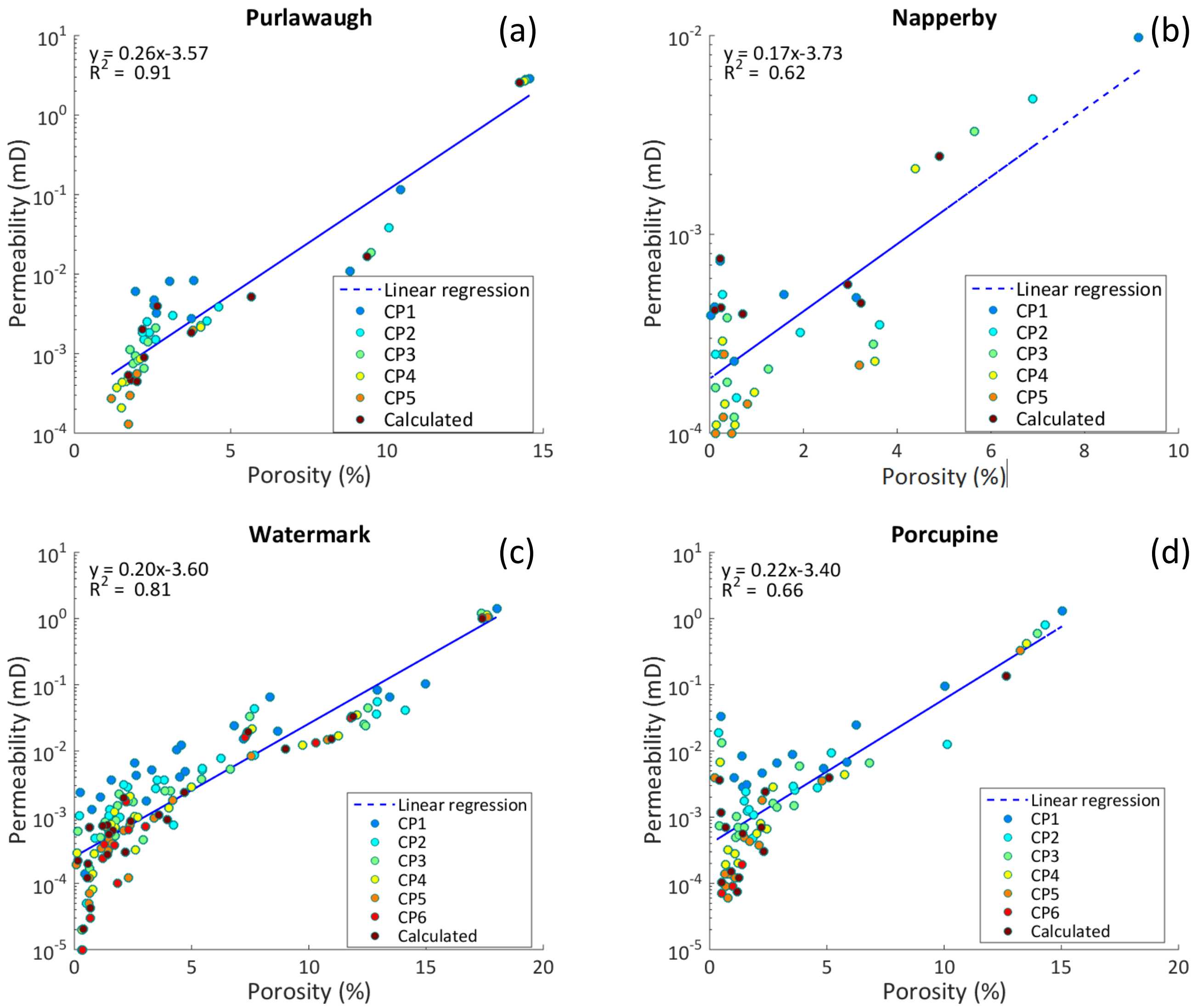

Figure 15 Porosity-log$_{10}$ permeability relationships in (a) Purlawaugh (b) Napperby, (c) Watemark, and (d) Porcupine formations. Labels CP1 to CP5 indicate laboratory measurements under varying confining pressure; 'Calculated' – stands for in-situ calculated porosity and permeability values.

2.4.3. MULTIPLE LINEAR MODELS

For each aquitard unit, a separate linear model identical to Equation 7 was developed for each confining pressure tested in the laboratory (Figure 16). The slope (a_1) and intercept (a_0) parameters were then combined into {a_1, z} and {a_0, z} data sets for each aquitards (symbols in Figure 17). Note that in Figure 16 the slope of the linear model for a given aquitard unit typically increases with increasing confining pressure from red (shallowest) to black or green (steepest).

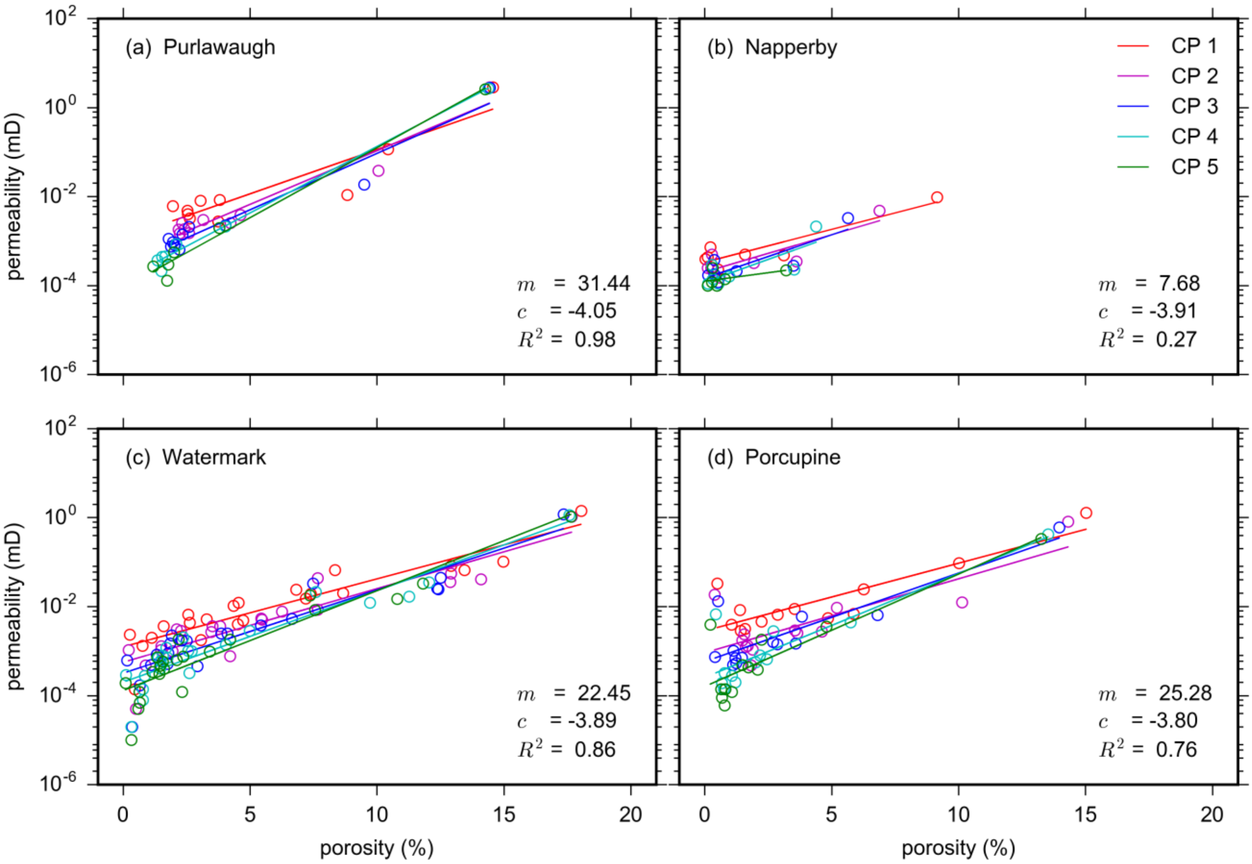

Figure 16 Linear porosity–$\log_{10}$ permeability models derived for each confining pressure (CP) tested in the laboratory for each of (a) Purlawaugh, (b) Napperby, (c) Watermark, and (d) Porcupine formations.

Based on these linear models, additional two-component linear models were then developed in order to calculate the depth-dependency of the slope and intercept values for each confining pressure (or its equivalent depth) tested. In this way, the permeability of the rock at a given depth is calculated as a function of both porosity and depth:

$$\log_{10} k = (m_1 z + c_1)\phi + (m_2 z + c_2) \tag{8}$$

where depth *z* (m) is considered to be interchangeable with an equivalent confining pressure, m_1, m_2, c_1 and c_2 are constants that will be fitted for each aquitard formation. The slope parameter ($m_1 z + c_1$) is plotted versus depth and for all aquitards in Figure 17a, whereas Figure 17b shows the intercept ($m_2 z + c_2$) values versus depth. Approaches that use a single linear model to calculate permeability as a function of porosity (see Section 2.4.2) do not consider depth explicitly. A potential advantage of the multiple linear model-based approach derived here is that depth is considered explicitly. This allows permeability to be estimated as function of a depth-dependent porosity through the slope parameter ($m_1 z + c_1$), while a second depth-dependency is introduced through the intercept ($m_2 z + c_2$).

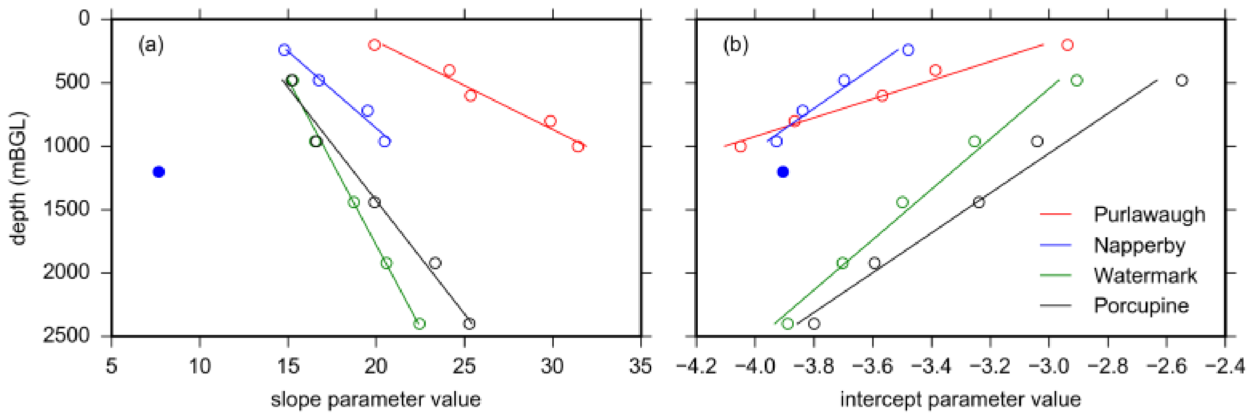

Figure 17 Multiple linear models of the (a) slope and (b) intercept of linear porosity-log$_{10}$permeability models at various confining pressures (confining pressure is converted to equivalent depth). Closed blue circles represent Napperby Formation data (relating to confining pressure #5) that were identified as outliers and excluded from analysis due to small sample size.

2.4.4. NON-LINEAR MODELS

As an alternative to the linear models presented previously, the relationship between rock porosity and permeability was characterised using a two-parameter exponential function:

$$\log_{10} k = Ae^{-B\phi} \tag{9}$$

where *A* and *B* are parameters calculated through calibration of the function to observed data. Unlike the linear models, the shape of such functions has a physical basis: starting from a porosity of near-zero (i.e. impermeable rock), permeability increases as increasing numbers of small pores conduct water flow. Once these relatively smaller pores are saturated, the rate of change in permeability decreases until the function reaches an asymptotic value. Similar models were previously developed by Aguilera (2006) for carbonate and siliclastic petroleum reservoirs.

Exponential functions were developed to describe each of the four aquitard units of interest (Figure 18). For each aquitard unit, the two model parameters (i.e. *A* and *B*) were estimated by calibrating the function to multiple observations of porosity and permeability. Calibration was undertaken using least squares-based linear regression, implemented using the Python language library SciPy (Jones et al. 2014). Derived *A* parameter values range from -4.444 (Purlawaugh Formation) to -3.863 (Napperby Formation) while *B* parameter values range from 6.737 (Napperby) to 17.777 (Purlawaugh Formation). The derived functions feature a coefficient of determination (i.e. R^2) value equal to or greater than 0.899. This implies that at least ~90% of the variability between porosity and permeability is accounted for by these functions.

Three types of analytical functions were used to characterise the relationship between porosity and permeability: (1) linear models, (2) multiple linear models, and (3) non-linear models. Although there are differences in predictive performance between the three models, with the single linear model performing less good than the other two models, this was not a reason to prefer one model over another. There are further differences in the physical basis of the models: only the non-linear model has a physical basis, but again this is not a reason for giving preference to this model. The purpose here was to capture the uncertainty about the porosity-permeability models by developing several alternative models that would have an equal likelihood when applied to generate K-profiles for use in modelling. This would then allow a multi-model approach where the groundwater flow model is run once with each porosity-permeability model. Comparisons between these three approaches provide a means to explore the sensitivity of model results to structural uncertainty in the porosity-permeability model. Depending on the magnitude of these predicted uncertainties, different courses of action can be taken, ranging from accepting the current models because they generate an acceptable uncertainty around e.g. predicted impacts to additional data collection to developing more reliable porosity-permeability relationships.

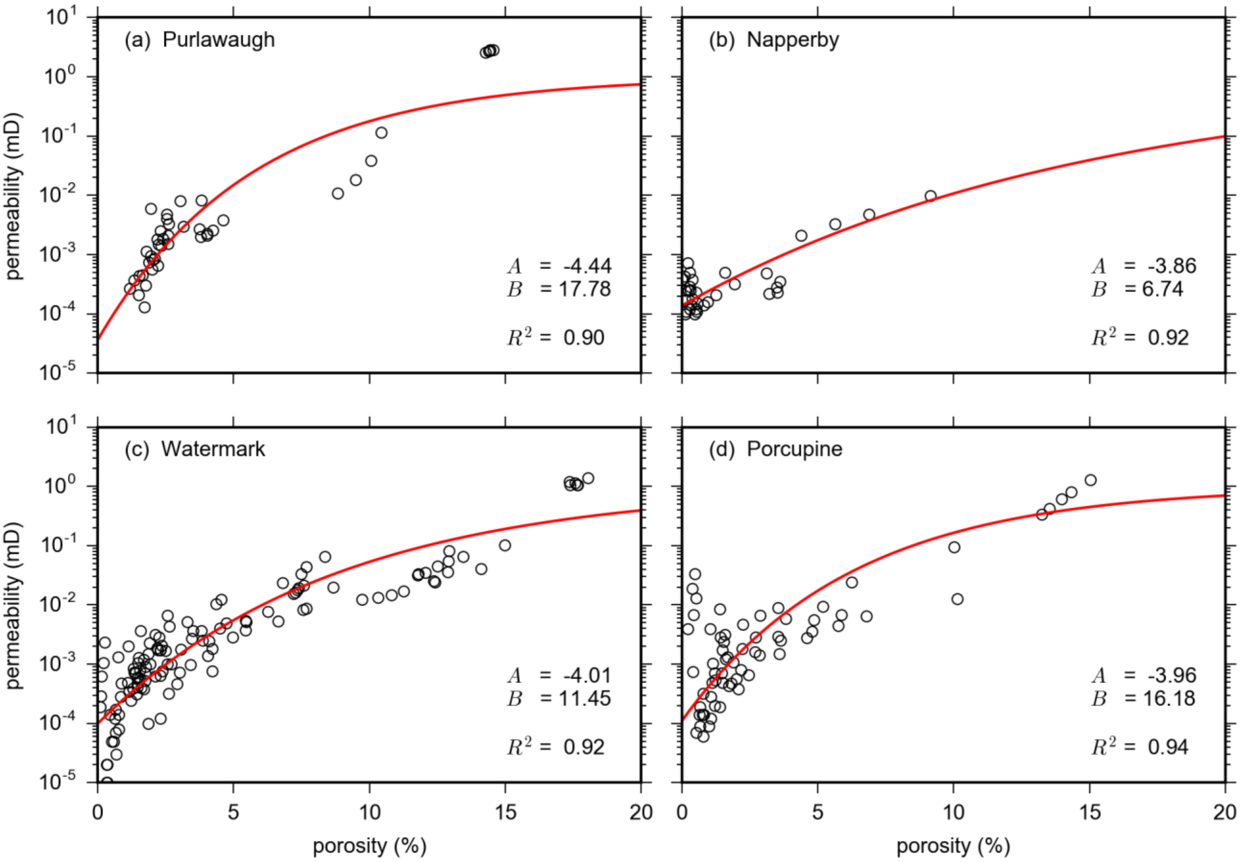

Figure 18 Non-linear two parameter exponential functions used to characterise porosity-log$_{10}$ permeability relationships in (a) Purlawaugh, (b) Napperby, (c) Watermark, and (d) Porcupine formations.

3. Predicted permeability profiles

3.1. Porosity profiles derived from down-hole bulk-density data

The porosity-permeability models (Section 2.4) derived for individual formations were used for predicting continuous profiles of permeability using porosity values inferred from wireline log measurements in boreholes, in this case the bulk density logs ρ_b:

$$\phi = \frac{\rho_g - \rho_b}{\rho_g - \rho_w} \tag{10}$$

where $\rho_g = 2.7$ g.cm^{-3} and $\rho_w = 1$ g.cm^{-3} are grain and freshwater density, respectively. Geophysical logs obtained from the DIGS database (NSW Department of Industry, 2015) were processed using the commercial software package Interactive Petrophysics (IP, 2015). To exclude coal layers, porosity values were calculated only for bulk densities ρ_b exceeding the 1.95 gram.cm^{-3} threshold that corresponds to the maximum maturity a coal can reach (Hollub and Schafer, 1992), while sandstones and other clastic materials always have bulk densities typically larger than 2 g/cm^3. The wire line log provides bulk density values at a spatial resolution of 0.01 m. High frequency noise in the calculated porosity profiles (Equation 10) is due to localized fractures and borehole quality variations (washouts and clay swelling by instance) affecting the bulk density reading log tool (a common issue in coal/clay rich formations). The noise was supressed while retaining sustained signal variations using a standard median filter applied prior to employing the porosity-permeability models from Section 2.4. The filtering was conducted over a 1-m-long moving-average window. The length was determined based on analysis of the aquitards' geological information from the well completion reports and serves to reduce noise and avoid missing signal components. Such filtering length has a much lower resolution than the centimetric resolution of the cracks/fractures/caving/washouts along the clay/coal rich intervals. All original bulk density logs and their calculated (using Equation 8) and filtered porosities are shown in Appendix 3; not filtering the porosity data would have resulted in unrealistically large small-scale variation in permeability with abnormally low bulk densities leading to abnormally high porosities and permeabilities at the sub-centimetre scale.

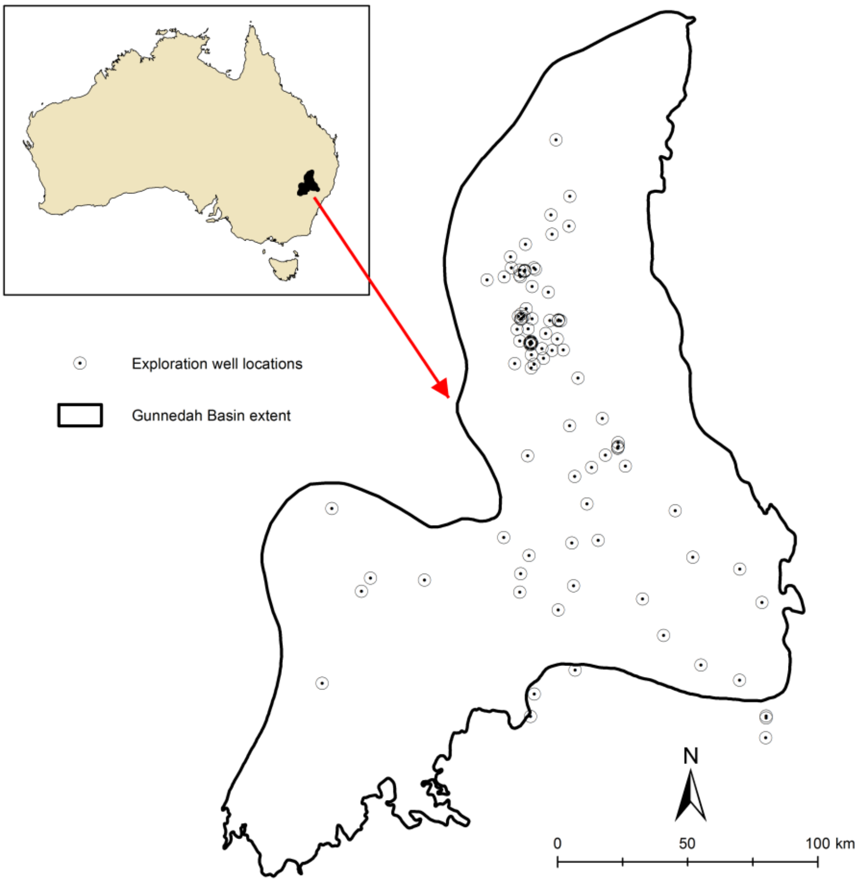

Figure 19 Gunnedah Basin study area and locations of 97 exploration wells featuring available geophysical wireline data (data source: DIGS database, NSW Department of Industry, 2015). Note that the spatial extent of the Gunnedah Basin (as shown) is considered an approximation.

A total of 97 exploration wells were identified within the Gunnedah Basin area (approximately 32 500 km^2 in size), which equates to a data density of one well per 335 km^2. Sixty-four of the 97 wells featured the presence of either the Purlawaugh or Napperby formations. These 64 wells were then used to upscale permeability and hydraulic conductivity values for the upper (i.e. Jurassic–Permian) aquitard sequence. Similarly, 78 of the 97 wells featured the presence of either the Watermark or Porcupine formations. These 78 wells were then used to upscale permeability and hydraulic conductivity values for the lower (i.e. Permian) aquitard sequence. Only wells with compensated bulk density logs and with formation tops and bottoms information provided were selected for analysis and permeability prediction. Using bulk density data from these wells, porosity values were calculated using equation 8 and subsequently filtered using a standard median filter (Section 3.1). A selection of 20 vertical profiles of porosity thus calculated are presented in Figure 20 (Jurassic-Permian aquitard units) and Figure 21 (Permian aquitard units). Permeability values were calculated using the models derived in Section 2.4 while accounting for the relevant depth intervals of the four aquitard formations (Figure 19).

Formation-specific porosity-permeability models were not available for interburden units overlying or underlying the Napperby Formation. These interburden units include the Garrawilla Volcanics; the Deriah, Digby, Trinkey, Wallala and Benelabri formations; and the Clare Sandstone. In order to derive a continuous permeability profile between the Pilliga Sandstone aquifer and the Hoskissons coal seam, the porosity-$\log_{10}$ permeability model for the Napperby Formation was applied to these interburden units. Similarly, formation-specific porosity-permeability models were not available for interburden units located above the Watermark Formation, such as the Brigalow, Arkarula and Pamboola formations. Instead, the porosity-$\log_{10}$ permeability model for the Watermark Formation was applied to the interburden units located above the Watermark Formation. Admittedly, all interburden permeability estimates are approximations, as they are not based on formation-specific core measurements. However they do provide an order of magnitude estimate for formations where there were previously few or no data (CDM Smith, 2014).

Even though a maximum number of exploration wells was used in the analysis to characterise aquitard permeability heterogeneity, including assessment of any significant discontinuity in sealing capacity, there remains a large uncertainty about this assessment. This uncertainty is introduced here as the permeability-porosity relationships are based on a relatively small rock sample set compared to the range of facies types for which we want to be able to estimate permeability. Understanding the degree of this uncertainty becomes important as this helps in undertaking sensitivity analysis and calibration of the dynamic model.

3.2. Permeability predictions

Twenty vertical profiles of permeability calculated from porosity data using linear models developed in Section 2.4.2 are presented in Figure 22 (upper aquitard sequence) and Figure 23 (lower aquitard sequence). A complete set of vertical porosity and permeability profiles along with gamma ray and density logs is provided in Appendix 3.

The twenty example vertical profiles of estimated permeability using multiple linear models developed in Section 2.4.3 and porosity calculated from bulk density measurements are presented in Figure 24 (upper aquitard sequence) and Figure 25 (lower aquitard sequence).

Finally, twenty vertical profiles of permeability calculated from porosity data using non-linear models developed in Section 2.4.4 are presented in Figure 26 (upper aquitard sequence) and Figure 27 (lower aquitard sequence).

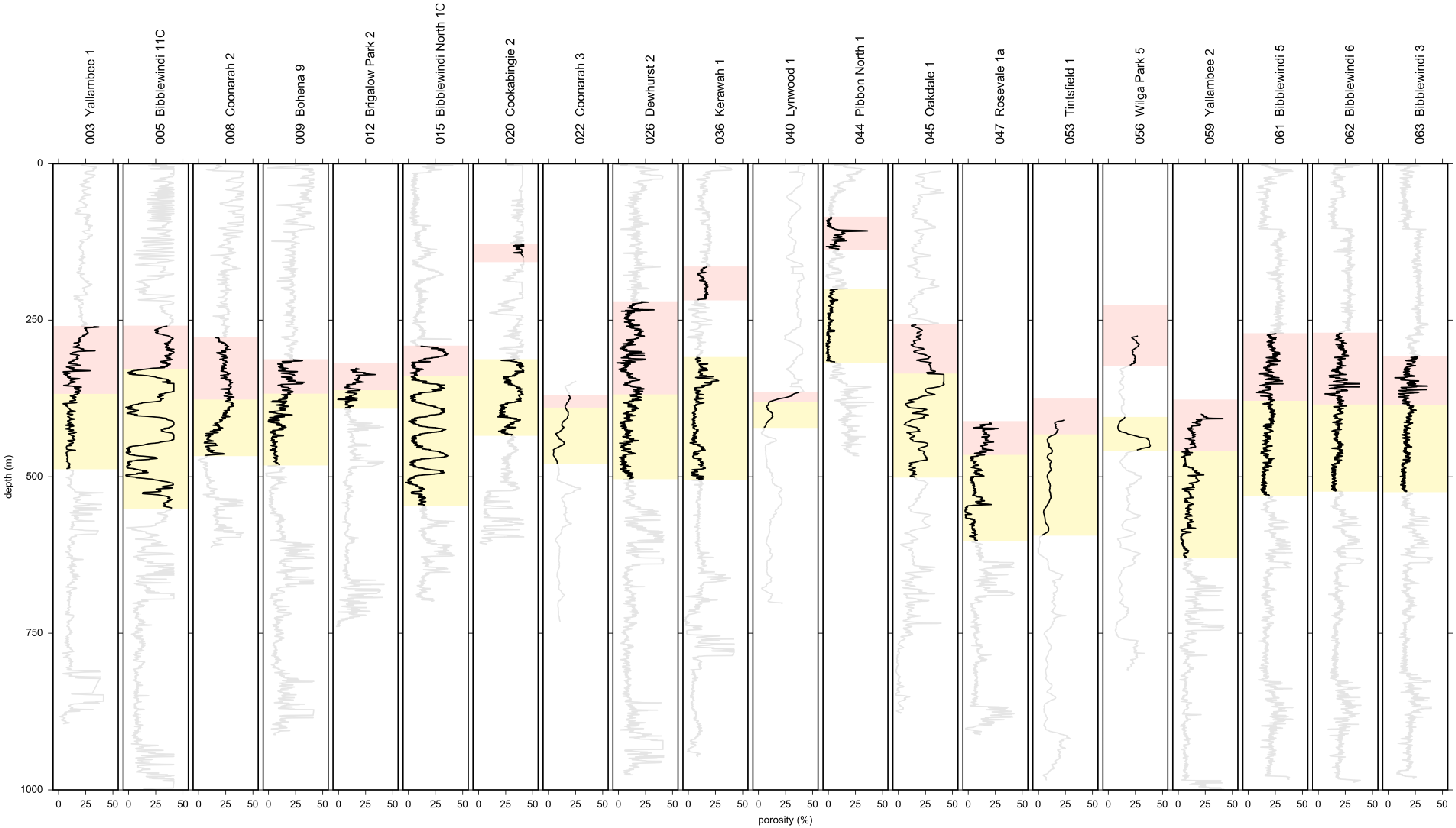

Figure 20 Selection of 20 vertical profiles of rock porosity (%) versus depth (mBGL) for the upper (Jurassic-Permian age) aquitard sequence derived from wireline bulk-density data. Shading indicates presence of key aquitard units: pink = Purlawaugh Formation; yellow = Napperby Formation.

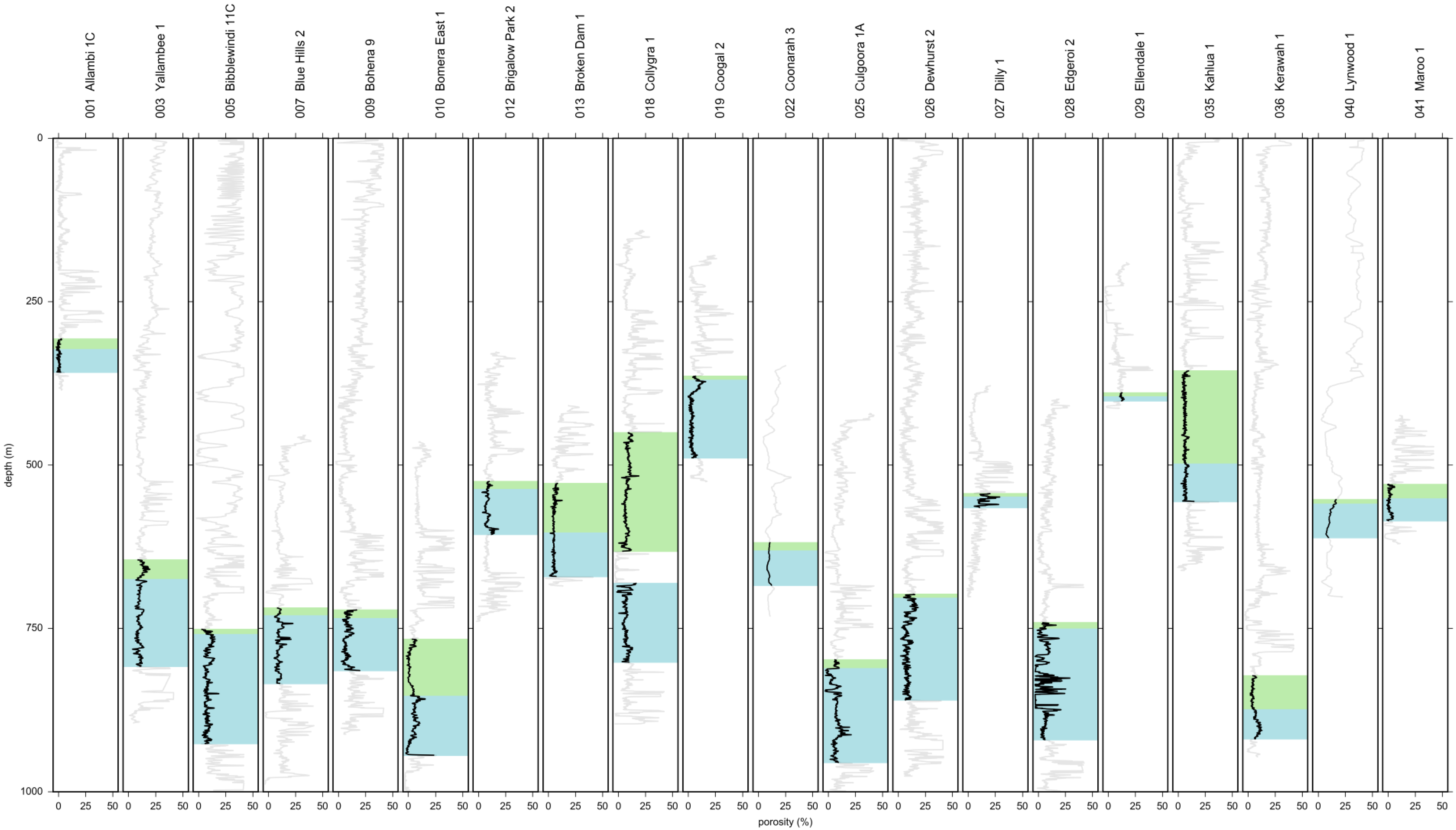

Figure 21 Selection of 20 vertical profiles of rock porosity (%) versus depth (mBGL) for the lower (Permian age) aquitard sequence derived from wireline bulk-density data. Shading indicates presence of key aquitard units: green = Watermark Formation; blue = Porcupine Formation.

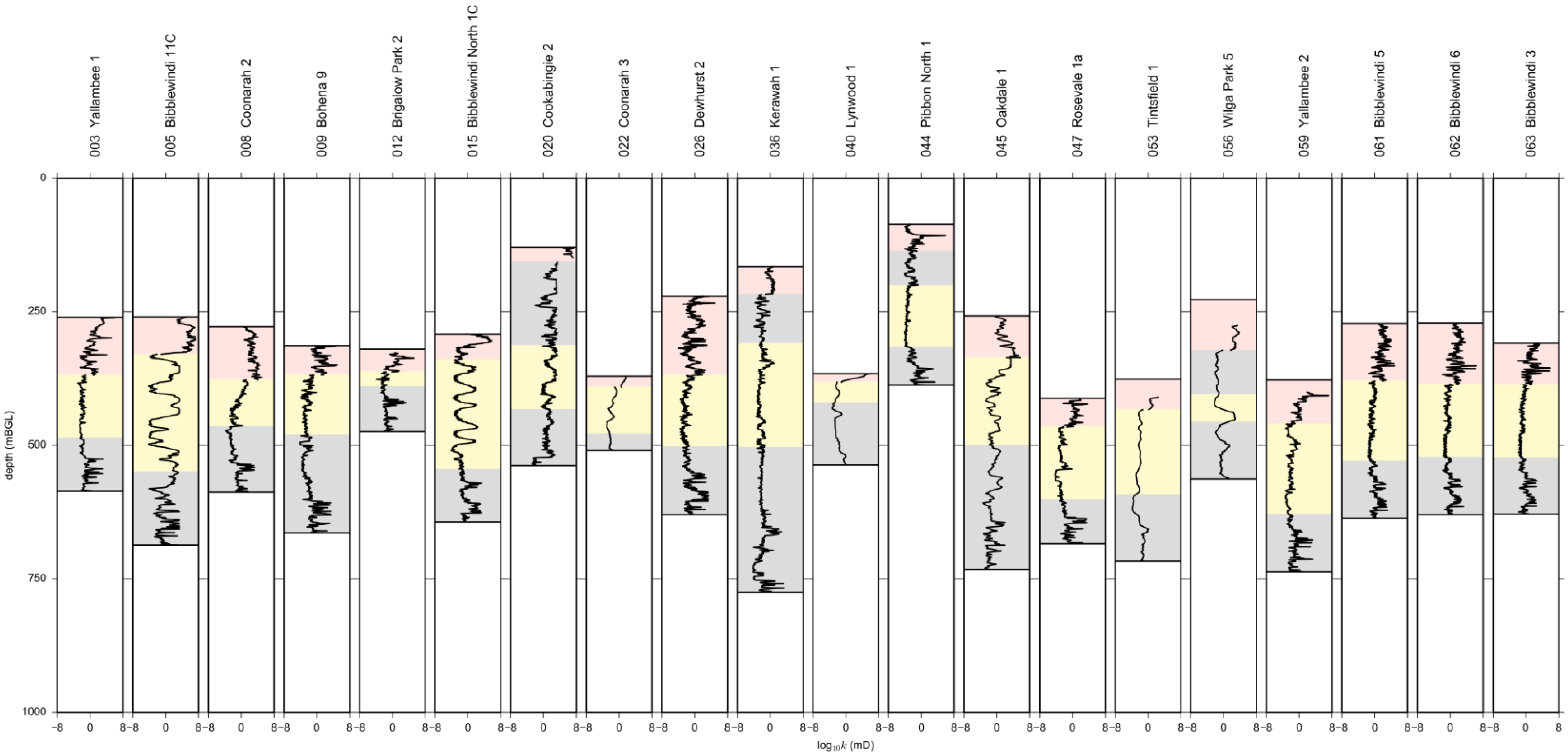

Figure 22 Selection of 20 vertical profiles of rock permeability (mD, log10 transformed) versus depth (mBGL) for the upper (Jurassic-Permian age) aquitard sequence derived from calculated porosity data using linear models. Shading indicates presence of key aquitard units: pink = Purlawaugh Formation; yellow = Napperby Formation; grey = other formations (i.e. interburden) to which the Napperby model has also been applied.

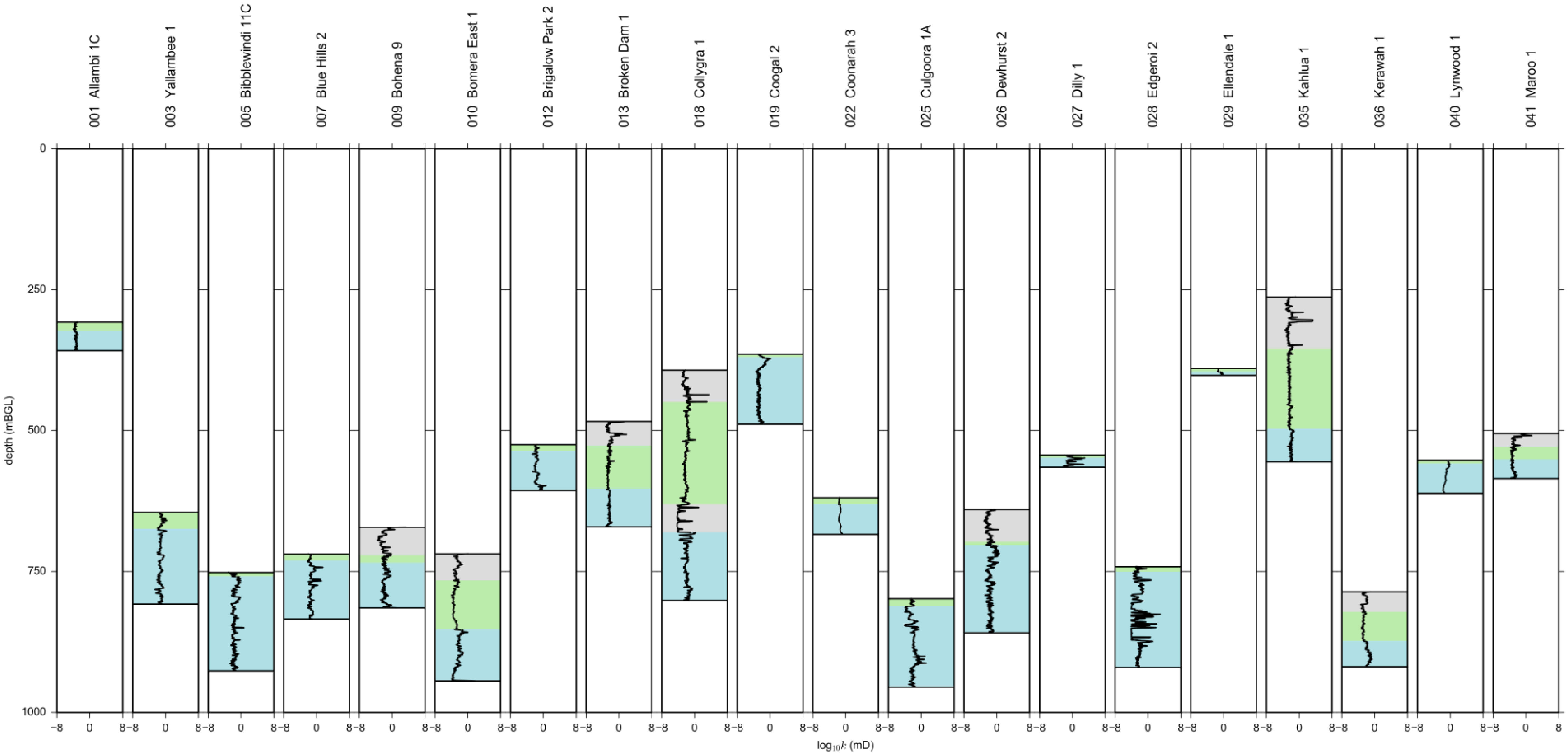

Figure 23 Selection of 20 vertical profiles of rock permeability (mD, log10 transformed) versus depth (mBGL) for the lower (Permian age) aquitard sequence derived from calculated porosity data using linear models. Shading indicates presence of key aquitard units: green = Watermark Formation; blue = Porcupine Formation; grey = other formations (i.e. interburden) to which the Watermark model has also been applied.

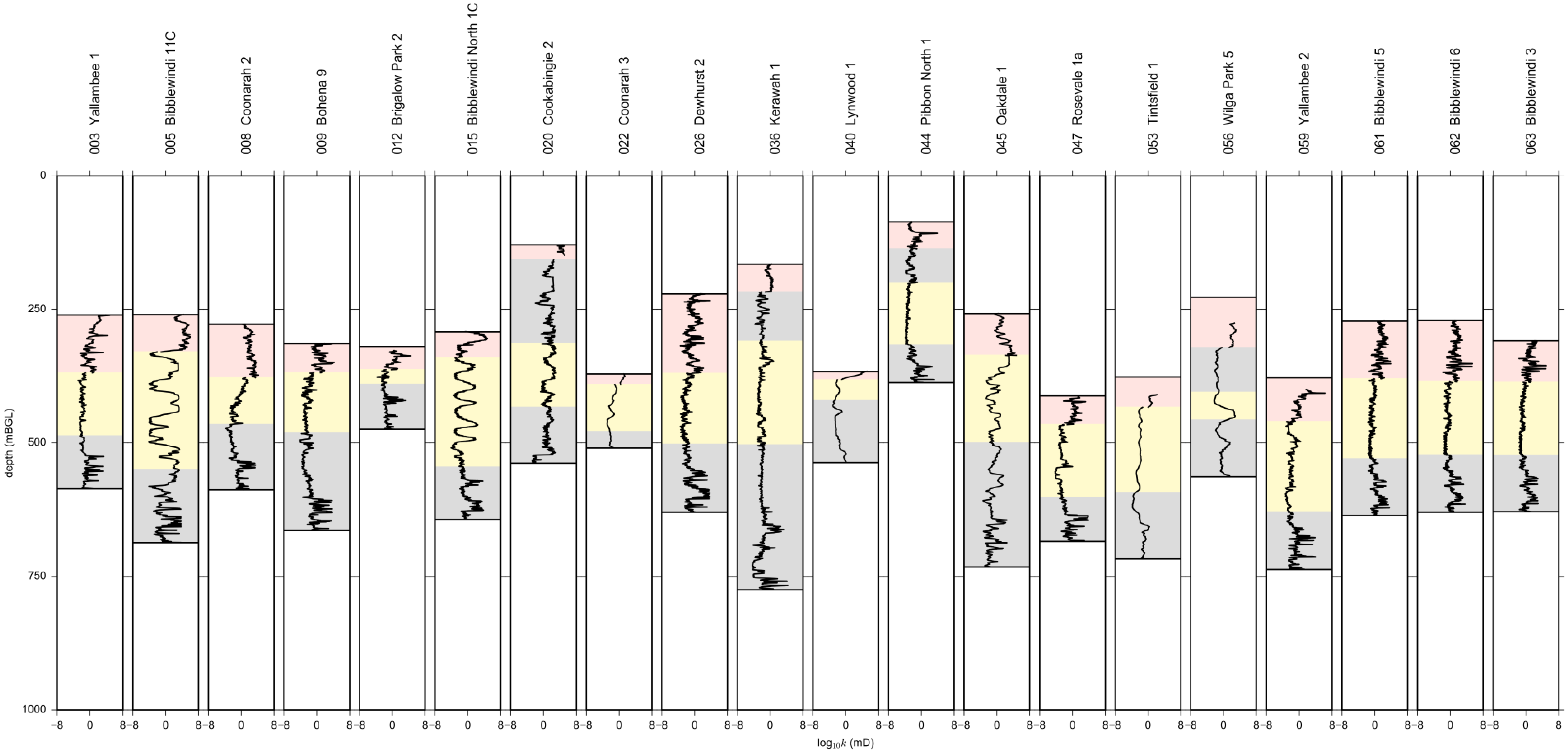

Figure 24 Selection of 20 vertical profiles of rock permeability (mD, log10 transformed) versus depth (mBGL) for the upper (Jurassic-Permian age) aquitard sequence derived from calculated porosity data using multiple linear models. Shading indicates presence of key aquitard units: pink = Purlawaugh Formation; yellow = Napperby Formation; green = Watermark Formation; blue = Porcupine Formation; grey = other formations (i.e. interburden) to which the Napperby model has also been applied.

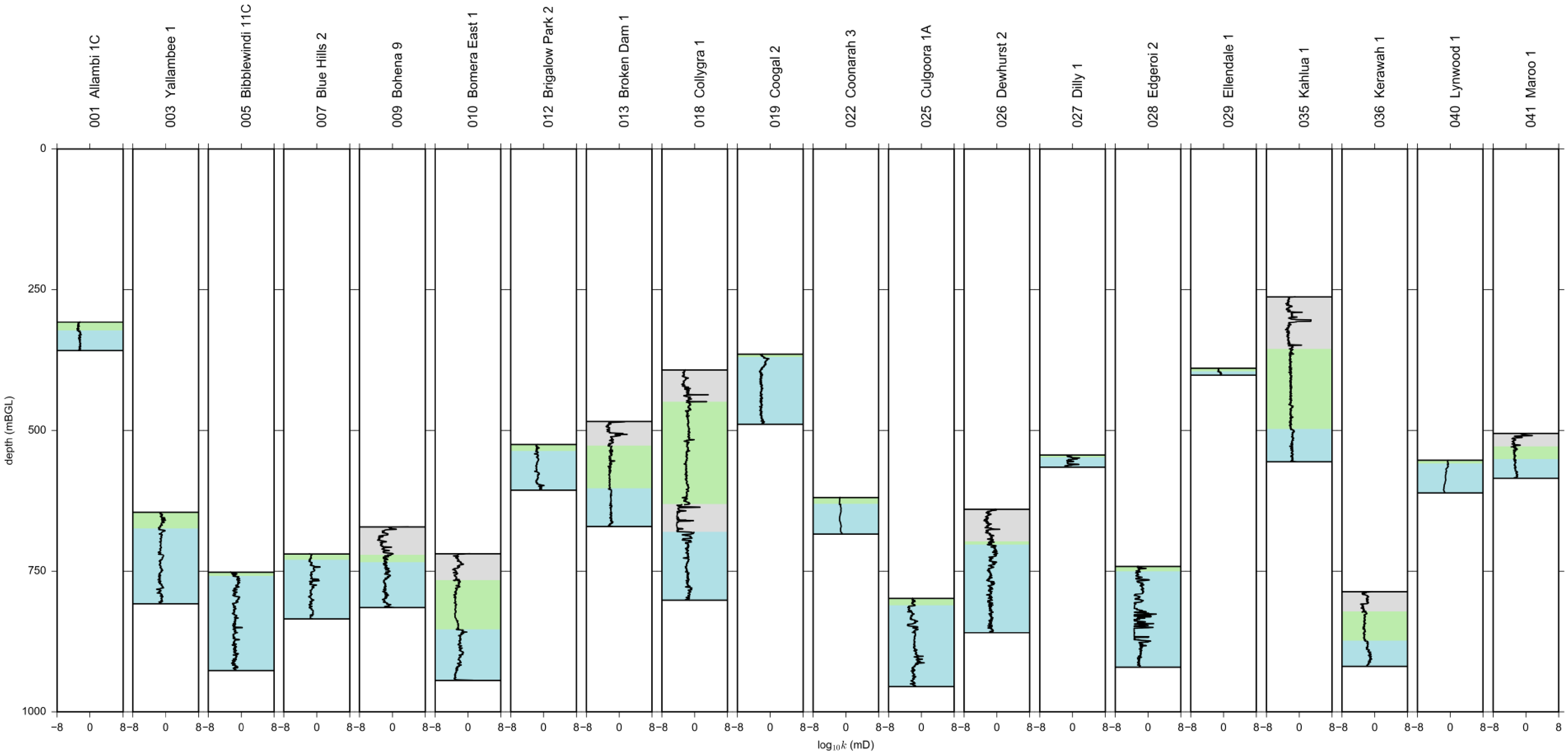

Figure 25 Selection of 20 vertical profiles of rock permeability (mD, log10 transformed) versus depth (mBGL) for the lower (Permian age) aquitard sequence derived from calculated porosity data using multiple linear models. Shading indicates presence of key aquitard units: pink = Purlawaugh Formation; yellow = Napperby Formation; green = Watermark Formation; and blue = Porcupine Formation; grey = other formations (i.e. interburden) to which the Watermark model has also been applied.

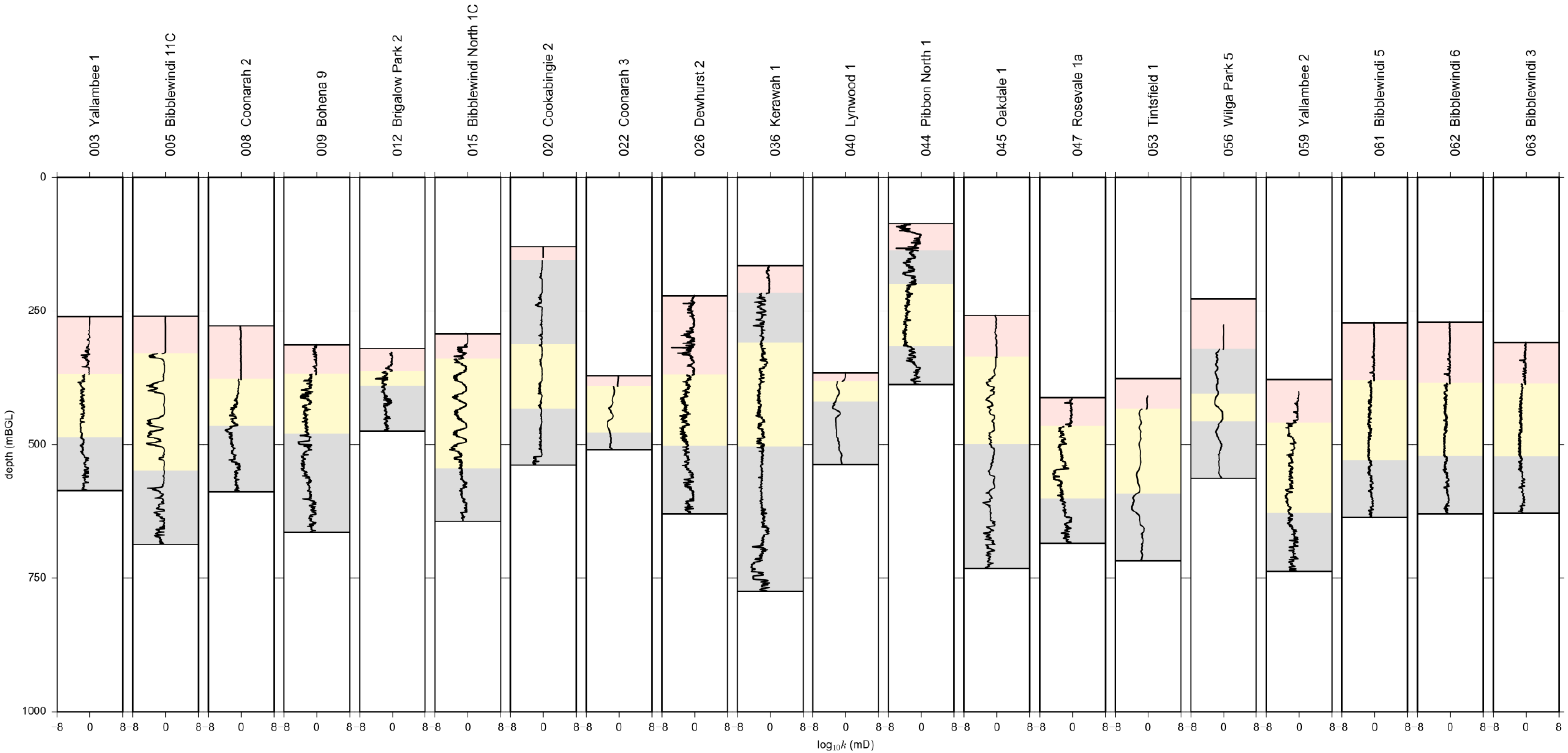

Figure 26 Selection of 20 vertical profiles of rock permeability (mD, log10 transformed) versus depth (mBGL) for the upper (Jurassic-Permian age) aquitard sequence derived from calculated porosity data using non-linear models. Shading indicates presence of key aquitard units: pink = Purlawaugh Formation; yellow = Napperby Formation; green = Watermark Formation; and blue = Porcupine Formation; grey = other formations (i.e. interburden) to which the Napperby model has also been applied.

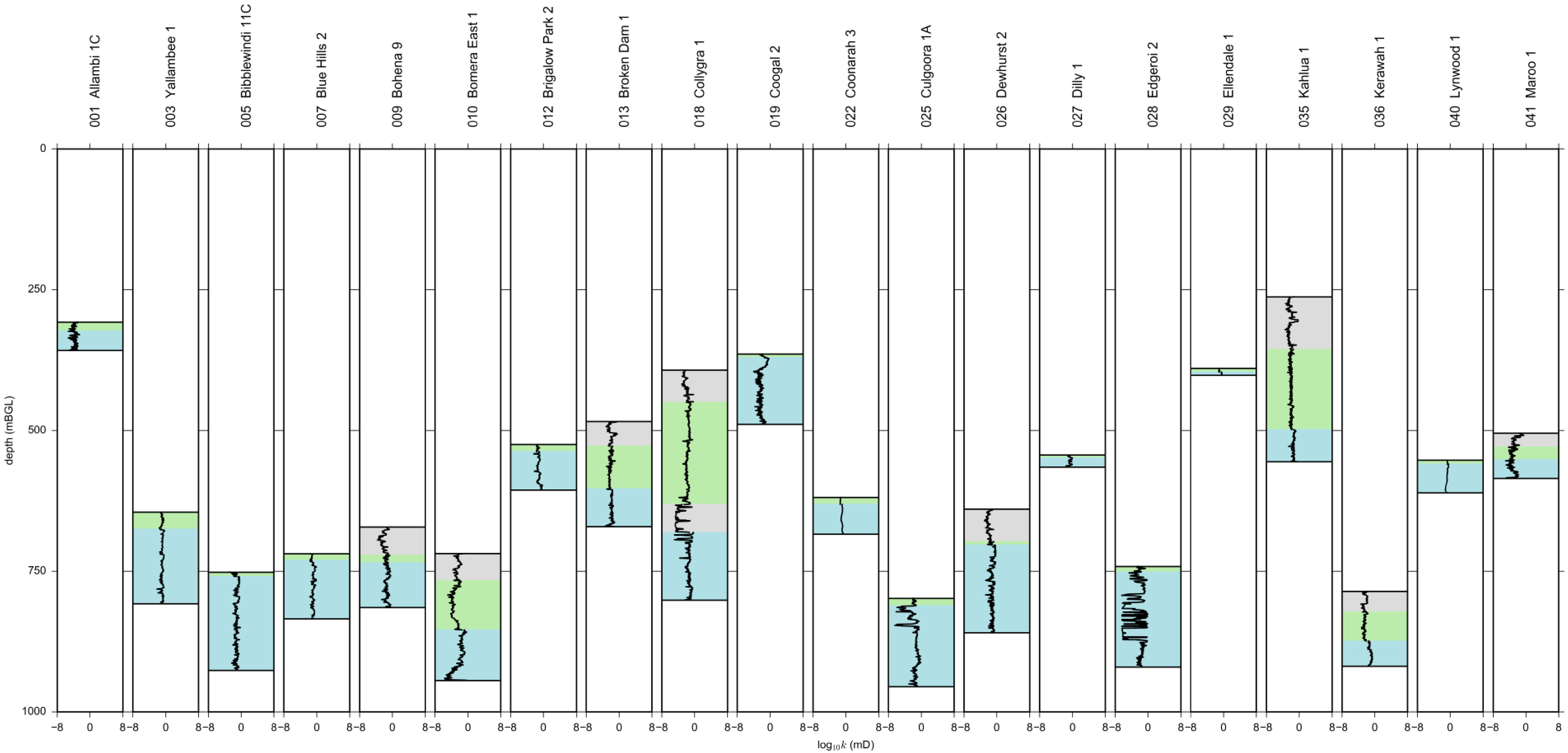

Figure 27 Selection of 20 vertical profiles of rock permeability for the lower (Permian age) aquitard sequence derived from calculated porosity data using non-linear models. Shading indicates presence of key aquitard units: pink = Purlawaugh Formation; yellow = Napperby Formation; green = Watermark Formation; and blue = Porcupine Formation; grey = other formations (i.e. interburden) to which the Watermark model has also been applied.

4. Upscaling of permeability and hydraulic conductivity values

4.1. Upscaling workflow

The workflow presented in Section 3 described the calculation of vertical profiles of aquitard permeability from downhole density logs and from pressure-permeability testing of core samples of the same aquitard units. Three types of analytical functions were used to characterise the relationship between porosity and permeability: (1) linear models, (2) multiple linear models, and (3) non-linear models. Comparisons between these three approaches provide a means to explore the sensitivity of model results to structural uncertainty. To incorporate the resulting vertical distributions of $\log_{10}$ permeability into a numerical model of groundwater flow, the following workflow was developed (Figure 27).

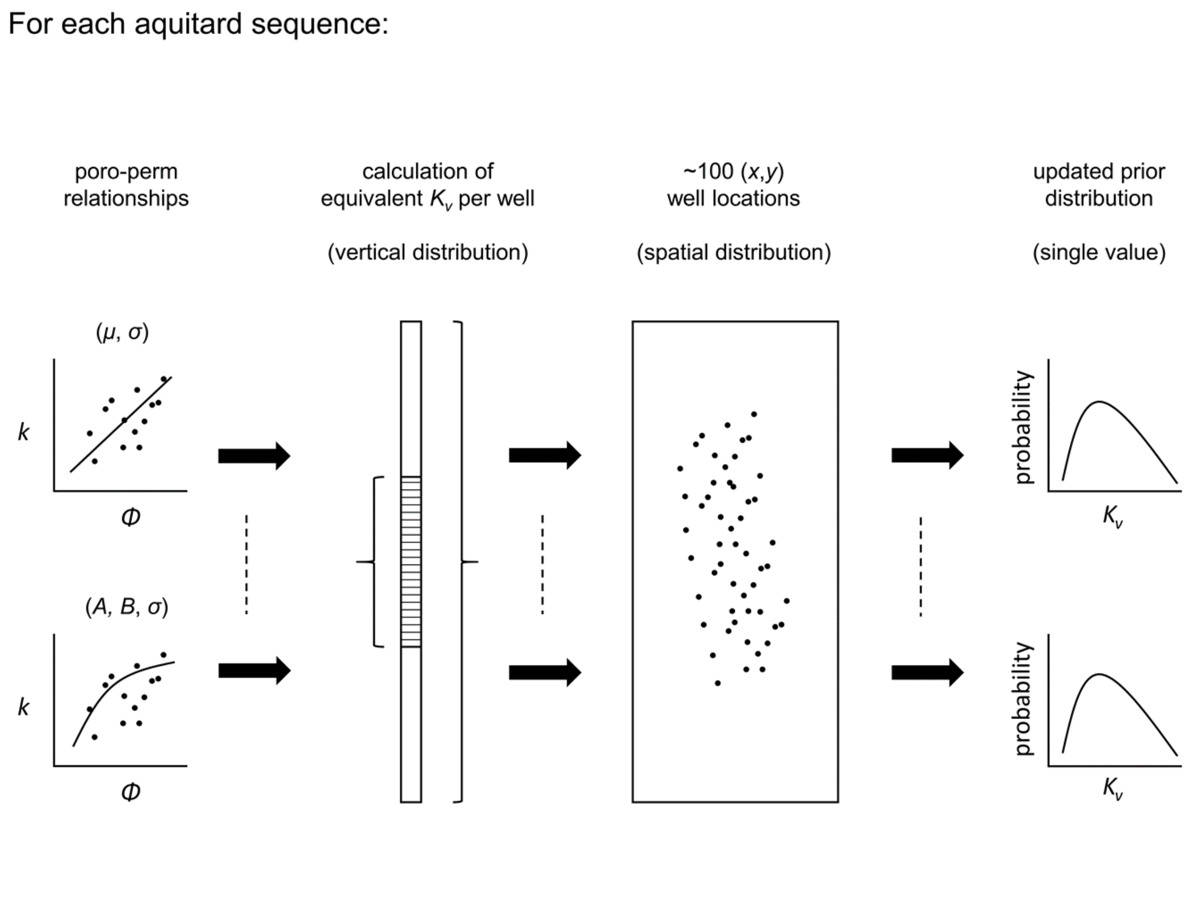

Figure 27 Aquitard vertical hydraulic conductivity (K_v) upscaling workflow: (a) characterisation of porosity-permeability relationships using linear and non-linear functions; (b) calculation of equivalent K_v values using one-dimensional Darcy flux models for each of the porosity-permeability relationships; (c) calculation of spatially averaged regional scale K_v values; (d) generation of an updated prior K_v statistical distribution for use in groundwater modelling.

The first step of the workflow involved the characterisation of the permeability of the two key aquitard sequences present at each exploration well location by single, 'equivalent' values (see Table 2). These values were calculated as the harmonic mean of all permeability values sampled within the aquitard sequence of interest. The subsequent step of the workflow required the upscaling of aquitard vertical hydraulic conductivity from the local scale to the regional scale. This involved computing the statistical properties, including the probability density function, of the equivalent aquitard hydraulic conductivity values across the model domain, based on vertically upscaled values obtained from 97 exploration wells. Harmonic mean permeability values from all exploration wells sampled were then aggregated by aquitard sequence (two in total) in order to produce a new sample distribution. Values were also aggregated by aquitard unit (up to four in total) for comparison purposes. Here, 'aquitard sequence' refers to an entire sequence of geological units located adjacent to an aquifer or coal seam. In the context of the Gunnedah Basin, the upper (Jurassic-Permian age) aquitard sequence refers to all units located between the Pilliga Sandstone and the Hoskissons Coal, including the Purlawaugh and Napperby Formations and any interburden units. The lower (Permian age) aquitard sequence refers to all units located between the Hoskissons Coal and the Maules Creek Formation coal seams, including the Watermark and Porcupine Formations and any interburden units (up to four in total). Permeability values for interburden units for which no cores were collected were based on the porosity- permeability models derived for the Napperby or Watermark formations.

4.2.Formation-scale permeability distributions

The statistical distribution of permeability for the entire upper (Jurassic-Permian age) aquitard sequence ('Combined') is presented in Figure 28. These are the regional-scale aquitard permeability or, after conversion, hydraulic conductivity values. Also shown are statistical distributions of permeability for all aquitard ('Purlawaugh', 'Napperby') and interburden units ('Interburden 1', 'Interburden 2') present in the sequence. For each sample group, three distributions (black boxes) are presented, corresponding to the results of analyses undertaken using (1) linear, (2) multi-linear, and (3) nonlinear models. Also shown for the 'Purlawaugh' and 'Napperby' sample groups are the statistical distributions of permeability summarised by CDM Smith (2014) in the reporting of the Gunnedah Basin groundwater flow model developed to predict the impacts of the Santos Narrabri Gas Project (blue boxes). [Note: CDM Smith (2014) reported distributions of hydraulic conductivity, which have been converted to permeability using equation (2) to facilitate comparisons to the results of the present study. Assumptions used in the conversion were: $\mu=1 \times 10^{-3}$ kg·(m·s)$^{-1}$, ρ=1000 kg.m^{-3}, g=9.8 m.s^{-2}].

For the Purlawaugh Formation, the probability distributions of linear and multi-linear upscaled K_v are very similar (based on interquartile range and median). The distribution based on the non-linear upscaled K_v displays a much smaller variability compared to the linear models; this is due to the assymptotic behaviour of the non-linear porosity-permeability model, which places an upper limit on permeability values with respect to increasing porosity values. Differences in probability distribution between models are much smaller for the Napperby Formation; in fact, median values and interquartile ranges are nearly identical. At these very low permeabilities, where median values are at least two orders of magnitude smaller than those of the Purlawaugh Formation, the effect of different porosity-permeability models seems practically unimportant.

Based on the interquartile range, the variability in upscaled K_v is approximately two and one orders of magnitude respectively for the Purlawaugh and Napperby formations. The variability of the combined interburden and aquitard data is similar to that of the Napperby, i.e. one order of magnitude based on the interquartile range.

It may be further observed that the median permeability values derived in the present study for the Purlawaugh Formation are approximately one magnitude larger than the value used in the CDM Smith groundwater flow model (i.e. 3.9×10^{-1} to 4.5×10^{-1} mD for the upscaled values and 1.0×10^{-2} mD, equivalent to 7.5×10^{-6} m.d^{-1} for the CDM Smith model). Conversely, median permeability values derived in the present study for the Napperby Formation are slightly smaller than the value used in the CDM Smith groundwater flow model (i.e. 2.6×10^{-3} to 3.3×10^{-3} mD for the updated values and 1.0×10^{-2} mD, equivalent to 7.5×10^{-6} m.d^{-1} for the CDM Smith model). The combined aquitard and interburden permeabilities are smaller than those of both Purlawaugh and Napperby CDM Smith estimates. The permeability ranges reported by CDM Smith are based on inverse modelling with a groundwater flow model for the Narrabri Coal Mine (Aquaterra, 2009); the use of different permeability zones in their groundwater model resulted in the permeability range shown in Figure 28. It should also be noted that, in comparison to the 'Purlawaugh', 'Napperby' and 'Interburden 2' distributions, the 'Interburden 1' distribution contained far fewer samples (9 of 97). The data represented in Figure 28 are also presented in tabular form in Appendix 2.

Based on the distribution of permeability data displayed in Figure 28, with median values of the "Combined" results consistently estimated at approximately 3.2×10^{-3} mD (equivalent to a hydraulic conductivity of 2.4×10^{-6} m/d), there is no evidence of discontinuity in the sealing capacity of the aquitard formations. Furthermore, an overall maximum hydraulic conductivity of 10^{-5} m/d (based on a maximum permeability of approximately 10^{-2} mD) is not indicative of a loss of sealing capacity.

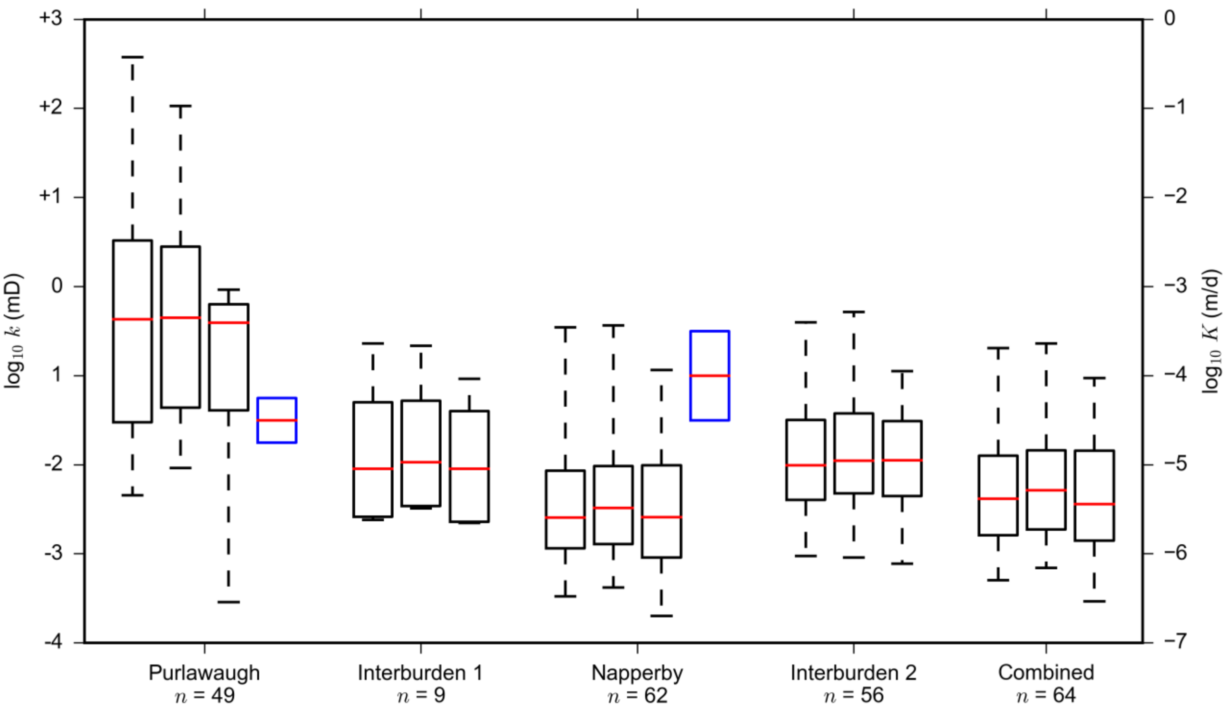

Figure 28 Statistical distributions of permeability (k) and hydraulic conductivity (K) for the entire upper (Jurassic-Permian age) aquitard sequence ('Combined'), as well as for all aquitard ('Purlawaugh', 'Napperby') and interburden ('Interburden 1', 'Interburden 2') units present within this sequence. For each sample group, three distributions (black boxes) are presented, corresponding to the results of analyses undertaken using (1) linear, (2) multi-linear, and (3) nonlinear models. Also shown for the 'Purlawaugh' and 'Napperby' sample groups are the statistical distributions of permeability summarised by CDM Smith (2014) (blue boxes). Boxes indicate interquartile ranges (i.e. between 25th and 75th percentiles), red lines indicate median values (i.e. 50th percentiles) and whiskers indicate 5th and 95th percentiles. Individual values are not shown.

The statistical distribution of permeability for the entire lower (Permian age) aquitard sequence ('Combined') is presented in Figure 29. Also shown are statistical distributions of permeability for all aquitard ('Watermark', 'Porcupine') and interburden units ('Interburden 1', 'Interburden 2') present in the sequence. For each sample group, three distributions (black boxes) are presented, corresponding to the results of analyses undertaken using (1) linear, (2) multi-linear, and (3) nonlinear models. It should also be noted that the 'Interburden 2' distribution contained only one sample. The data represented in Figure 29 are also presented in tabular form in Appendix 2. Permeability values of the Permian age aquitards used in the CDM Smith groundwater flow model had the same values as those for the Jurassic-Permian formations, with little or no measured data to support this choice.

Probability distributions derived for the permeability of the Watermark Formation are comparable in terms of interquartile ranges but vary in terms of median values, with exponential upscaling approach resulting in largest median values. Probability distributions derived for the permeability of the Porcupine Formation are considerably different in terms of differences in interquartile ranges and median values between linear, multi-linear, and non-linear upscaling approaches. Probability distributions based on the exponential approach feature the largest median values, for both Watermark and Porcupine formations. When the Watermark and Porcupine data are combined with interburden data, the exponential approach also results in the largest variability; i.e. more than two orders of magnitude. Conversely, the variability in results derived using the linear and multi-linear approaches is approximately 1.5 and 1.0 orders of magnitude, respectively.

Based on the distribution of permeability data displayed in Figure 29, with median values of the "Combined" results consistently estimated at 3.2×10^{-2} to $10^{-2.0}$ mD (or hydraulic conductivity around 2.4×10^{-5} to 7.6×10^{-6} m/d), there is no evidence of discontinuity in the sealing capacity of the aquitard formations. Although the overall maximum hydraulic conductivity of 0.7 mD is about two orders of magnitude larger than the median (Table 8), this is not indicative of a loss of sealing capacity.

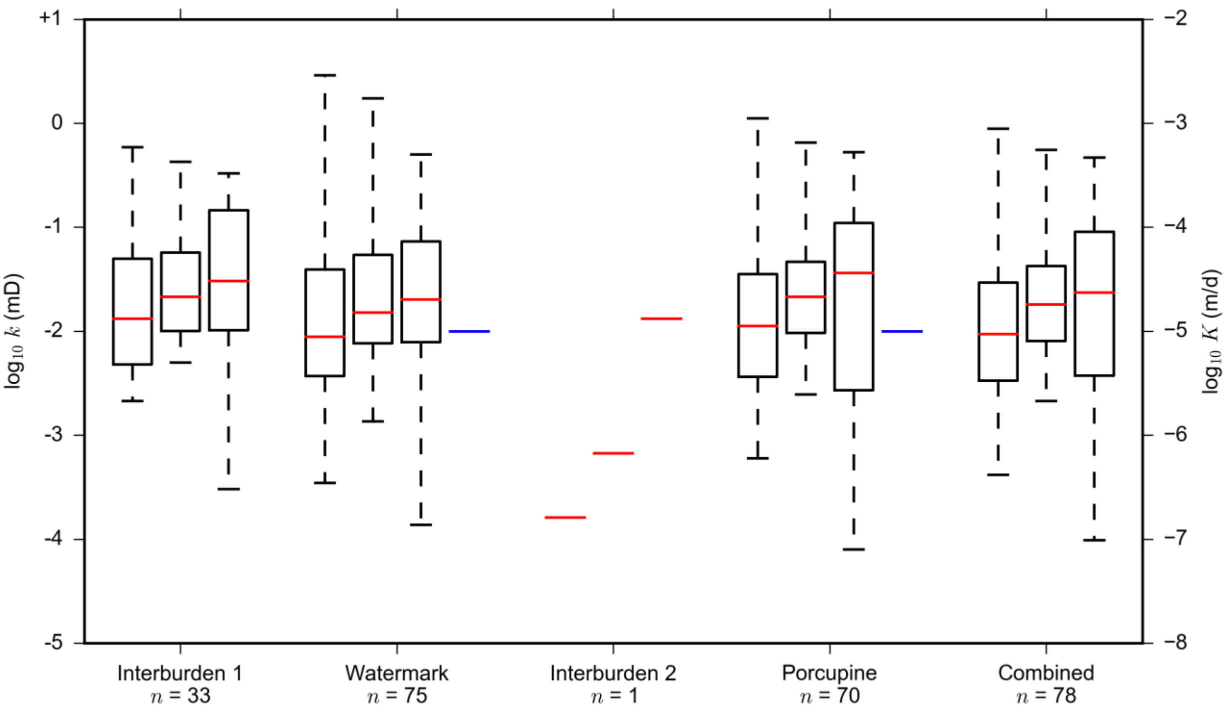

Figure 29 Statistical distributions of permeability (k) and hydraulic conductivity (K) for the entire lower (Permian age) aquitard sequence ('Combined'), as well as for all aquitard ('Watermark', 'Porcupine') and interburden ('Interburden 1', 'Interburden 2') units present within this sequence. For each sample group, three distributions (black boxes) are presented, corresponding to the results of analyses undertaken using (1) linear, (2) multi-linear, and (3) nonlinear models. Boxes indicate interquartile ranges (i.e. between 25th and 75th percentiles), red lines indicate median values (i.e. 50th percentile) and whiskers indicate 5th and 95th percentiles. Individual values are not shown.

Further research may involve the use of one-dimensional numerical groundwater flow models to also calculate equivalent hydraulic conductivity values. This approach has been previously implemented as Darcy- or Laplace equation-based fluxes (Warren and Price 1961; Li et al. 2011); similar approaches have been undertaken at regional scales and are known as 'numerical permeameter' models (OGIA 2015, pers. comm.). First, permeability values will be converted to hydraulic conductivity values using equation (2). These distributions, which were discretised at a sub-metre scale, will then be averaged to the metre scale; i.e., one value per one vertical metre of aquitard. These resampled distributions will be used to parameterise a one-dimensional numerical groundwater flow model. In addition to non-uniform distributions of hydraulic conductivity, these steady state models will feature Dirichlet (i.e. specified hydraulic head) boundary conditions applied on both upper and lower boundaries. This configuration will enable the imposition of a specific hydraulic gradient (i.e. 1 m / 1 m). The outflux through the upper boundary calculated by the model will be divided by the cross sectional area perpendicular to flow (i.e. 1 m^2) in order to compute an 'equivalent' hydraulic conductivity.

Following the upscaling of permeability and hydraulic conductivity values, the latter need to be spatially interpolated in order to generate three-dimensional parameter fields for use in groundwater flow modelling. One approach is to sample single upscaled K_v values directly from the previously derived distributions and apply this value uniformly across the model domain for inclusion in a numerical groundwater flow model. More complex approaches may be used to generate spatially heterogeneous distributions of K_v parameter fields; these may include spatially uniform or spatially heterogeneous fields. Spatial distributions of upscaled permeability values based on the linear model for both (a) upper and (b) lower aquitard sequences are presented in Figure 30. From these results it does not appear that significant spatial correlations are present. However, Figure 30b appears to suggest that the permeability of the lower aquitard sequence is lower in the south of the basin, in comparison to higher permeability values observed in the (relatively data rich) northern part of the basin.

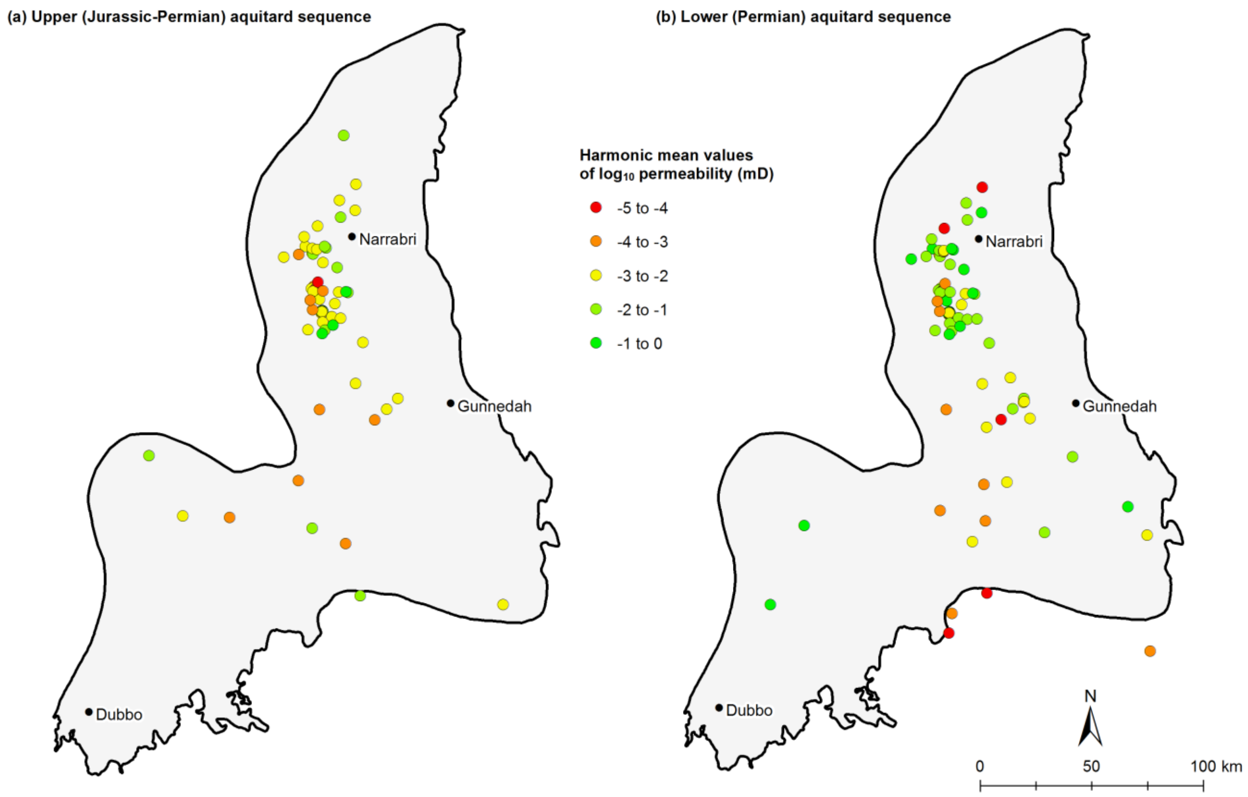

Figure 30 Spatial distributions of harmonic mean $\log_{10}$ permeability (mD) values derived from upscaling for (a) the upper (Jurassic-Permian) aquitard sequence and (b) the lower (Permian) aquitard sequence.model = linear

A range of approaches to the upscaling and interpolation of subsurface parameters was reviewed by Turnadge et al. (2018). However, the focus of the present research is to identify the degree to which an improved characterisation of aquitard K_v can constrain predictions produced by groundwater flow models. The existing CDM Smith groundwater flow model features the use of uniform values to describe hydraulic properties such as hydraulic conductivity. In this context, a change from uniform parameter values to spatially distributed parameter fields would represent a change in model structure. It is considered that changes to the structure of permeability may confound improvements resulting from improved characterisation of K_v. For this reason, spatial interpolation will be considered an update of the conceptual model, rather than an update of the parameterisation. Further work in this area could involve the application of the aquitard permeability upscaling workflow described here to a spatially distributed groundwater flow model.

While the focus of the present study is the characterisation of vertical hydraulic conductivity (K_v), these results will also be used to constrain horizontal hydraulic conductivity (K_h). The relationship between these two properties is typically specified as a ratio; for example, in data poor contexts K_v is often assumed to be one or two orders of magnitude smaller than K_h. For Gunnedah Basin geological units the CDM Smith groundwater flow model featured K_h:K_v ratios of 10:1 and 100:1. For Purlawaugh and Napperby formations, CDM Smith (2014) reported that K_h:K_v ratios of 10:1 and 100:1 had also been used in previous groundwater flow models of the Gunnedah Basin. Based on these relationships, K_h values will be calculated as two orders of magnitude larger than K_v values.

This workflow was designed to facilitate the propagation of the uncertainty associated with updated estimates of aquitard K_v (Figure 27). As such, this uncertainty will be propagated from variations in the functions used to describe the porosity-$\log_{10}$ permeability relationship for each aquitard unit. The parameters of each function will be resampled from prior uniform distributions defined by the calibrated parameter values (implemented as the mean values of the distributions) and using nominated upper and lower bounds. Using this stochastic approach, variations in upscaled hydraulic conductivity will be propagated from porosity-$\log_{10}$ permeability models, through analytical and/or numerical equivalent flux calculations and subsequent spatial averaging in order to produce single regional scale K_v values for inclusion in an updated version of the CDM Smith groundwater flow model.

4.3. Seal continuity discussion

The analysis of formation-scale permeability did not provide evidence (positive or negative) that the sealing capacity of the aquitard sequences was impaired by a lack of lateral continuity of the seal. On the basis of multiple wireline logs and permeability measurements the aquitard sequences are considered an effective seal that is laterally continuous and lithologically consistent, free of open faults/fractures, and has low permeability.

Our analysis of seal properties, however, is limited in being based largely on the core-scale properties of sealing sequences. The ultimate goal for any assessment of risk levels to seals is the definition of the three dimensional (3-D) architecture of the seal combined with a full description of the sealing properties in 3-D, in the context of past and present-day stress regimes. This includes a description of heterogeneities on any observable scale. The most vulnerable parts of a seal are, by definition, those that can act as fluid-migration pathways, i.e., the most permeable connected routes with the lowest capillary threshold pressures. A major challenge is to identify and predict these routes using a combination of geophysical (including 3-D seismic interpretation), petrophysical, and geological data.

Most of the techniques and methodologies used for studying hydrocarbon reservoirs or aquifers can be used for caprocks or seals. Major faults can be detected using seismic data, while small-scale fractures can be identified using well-bore imaging techniques. At large scales, seismic data calibrated to logging data and well-to-well correlation techniques can give an indication of the lateral continuity and thickness of the caprock or seal formation. An overview of various geological structures that may present a discontinuity of seal formations was provided by Cartwright et al. (2007). These authors present an interpretational framework for the analysis of a diverse set of geological structures that breach sealing sequences and allow fluids to flow vertically or subvertically across the seal. In their discussion, the term ‘‘sealing sequence’’ refers to an assemblage of generally low-permeability lithofacies that halt or retard the flow of petroleum or other hydrocarbons toward the basin surface.

In fluvial systems where there are base level changes one can encounter erosive features such a channels that downcut into older sealing strata and thus create bypass features (Hornung and Aigner, 2002).

Cartwright et al. (2007) in their discussion focus on seismic-scale permeability heterogeneities which is based on the recognition that some high-quality seals may be breached episodically or semi-permanently by a range of geological structures that they collectively term ‘‘seal bypass systems.’’ Seal bypass systems (SBS) are defined as ‘‘large-scale (seismically resolvable) geological features embedded within sealing sequences that promote cross-stratal fluid migration and allow fluids to bypass the pore network.’’

Cartwright et al. (2007) argue that if such bypass systems exist within a given sealing sequence, then predictions of sealing capacity based exclusively on rock physical properties such as capillary entry pressure, hydraulic conductivity, and wettability may be largely negated by the capacity of the bypass system to breach the microscale sealing framework of the grains and pore network. Cartwright et al. (2007) base their analysis mainly on 3-D seismic observations of sealing sequences in which geological discontinuities are embedded within the seal and breach it by acting as highly focused, vertical, or subvertical fluid-flow paths from the underlying reservoirs.

4.3.1. SEAL BYPASS SYSTEMS

Cartwright et al. (2007) identify three main groups of SBS, consisting of (1) faults, (2) intrusions, and (3) pipes. Of all the bypass systems discussed in the following sections, only faults and hydrothermal pipes (dykes) have been identified in the Narrabri Gas Project Area (CDM Smith 2014) and their relevance in regard to seal continuity has been briefly discussed.

4.3.1.1. FAULT BYPASS

This is the largest group of bypass systems, and their function of conduits across sealing sequences has been intensively studied. Because fault dimensions scale with fault displacement, seismically resolvable faults with throws greater than 10 m are commonly found to cross hundreds of meters of stratigraphic section, and fault conduits thus have great potential for long-range vertical fluid transmission (Hooper, 1991).

One of the major controls on the long-term behaviour of fault planes as flow conduits is the static permeability of the fault rocks. Faults whose damage zones are more permeable than their host sequences can be major flow routes irrespective of their specific history of rupture and displacement (Underschultz et al., 2018). However, most fault zone rocks are characterized by lower permeability than their host rocks, and steady-state leakage rates would be commensurately small.

The most recent study of faulting across the Narrabri Gas Project Area (CDM Smith 2014) concluded, based on interpretation of seismic data, that most faults in the Narrabri Gas Project area are Permian to Triassic in age and mainly displace Permian and (to a lesser extent) Triassic strata; with typical vertical displacements of less than 100 m. Note that Purlawaugh is of Middle Jurassic age, Napperby is of Middle Triassic age, while Watermark and Porcupic are of Middle Permian age. The study found no evidence of significant post-Jurassic age faulting extending into deeper Triassic and Permian age strata, or evidence of significant displacement of the Pilliga Sandstone. Where it is present, surface faulting in the Jurassic strata was assessed as minor. The study concluded that the faults present in the Project area are unlikely to provide preferential pathways for the leakage of water or hydrocarbons between strata.

4.3.1.2. INTRUSIVE BYPASS

Intrusive bypass systems are a group of intrusive structures that breach the integrity of a sealing sequence in one or another of the following three distinct ways:

- First, the intrusive event itself involves the puncturing of the seal, and the transmission of fluids through the seal along with the intrusive material. A good example of this behaviour is when mud volcanoes first form.
- Second, when the intruded material possesses a markedly higher permeability compared to the sealing sequence, fluid flow will be focused upward through the intrusion. Examples of this case are sandstone intrusions or highly fractured igneous intrusions.
- Third, when the intrusion process results in intense fracturing and deformation of the sealing sequence, fluid flow can exploit the increased permeability of the sealing sequence in the contact zone. Good examples of this can be found in the sheath zone around salt diapirs, or in metamorphic aureoles around igneous intrusions.

The magnitude of the permeability perturbation in each of these three cases depends on several factors related to the specific intrusion family.

Sandstone intrusions: This family is a potentially significant element in regional scale fluid flow in basins and a significant mode of seal failure; its existence at seismic scale has been recognized by Molyneux et al. (2002) and Hurst et al. (2003). Three-dimensional seismic data have revealed kilometer-scale sandstone dikes and sills in several petroleum systems in northwest Europe. The effect of a sandstone intrusion in this context is to insert a meters-wide conduit with Darcy permeability into a sequence with nano Darcy permeability.

Igneous Intrusions: In contrast to sandstone intrusions where it is the intrusive lithology (sand) that provides the permeable pathway to allow focused fluid migration along the intrusion, igneous intrusions have generally much lower permeability than the host medium typical sealing facies. However, the intrusion of hot magma at greater than 1000 °C into cold and wet sediments results in major changes in host rock properties, such as fracturing, for tens of meters away from the immediate contact zone (Einsele et al., 1980). These fractures provide a fracture permeability network at various scales surrounding the intrusion and occasionally within the body of the intrusion itself.

Mud Diapirs and Diatremes: Mud diapirs and diatremes are an important and widespread subgroup of SBS, most widely known from tectonically active settings such as convergent margins, foreland basins, and strike-slip provinces (Kopf, 2002; Dimitrov, 2002), but they are increasingly recognized in passive-margin settings (e.g., Hansen et al., 2005; Frey-Martinez et al., 2007). Mud diapirs or diatremes are commonly associated with mud volcanoes. Collectively, this group of intrusive and extrusive structures are increasingly being identified from producing regions on 3-D seismic data (Davies and Stewart, 2005). Mud volcanoes are also recognized as an extremely efficient mechanism for dewatering rapidly buried and overpressured clay-rich sedimentary sequences.

Salt Diapirs: Many hydrocarbon provinces are located in areas where salt tectonics is an integral part of the deformational regime and where diapirism is a common structural style. The growth of salt diapirs commonly involves forced folding and radial and concentric faulting, and this associated deformation can exert a major impact on fluid-flow regimes and seal integrity. Salt diapirs are widely associated with focused fluid flow.

4.3.1.3. PIPE BYPASS

Pipes are the least well documented of the SBS groups, and they have only relatively recently been described in detail with 3-D seismic data (Løseth et al., 2003; Berndt et al., 2003). They can best be defined seismically as columnar zones of disturbed reflections that may or may not be associated with subvertically stacked amplitude anomalies.

Dissolution Pipes: Dissolution pipes form by dissolution of rock units at depth to form subsurface cavities that promote instability in the overburden leading to collapse (Stanton, 1966; Cooper, 1986). They are thus likely to occur in areas of evaporite or carbonate karst.

Hydrothermal Pipes: Hydrothermal pipes form by the release of a high flux of hydrothermal fluids associated with certain kinds of igneous intrusions, particularly mafic sills or laccoliths (Svensen et al., 2004), and can therefore be expected to affect sealing sequences when they are breached by igneous intrusions. The hydrothermal fluids are derived from the magma by devolatilisation and from the host sediments by localized heating, metamorphism, or simply thermal pumping of pore fluids (Delaney, 1987; Einsele, 1992).

Blowout Pipes: Blowout pipes can have similar horizontal and vertical dimensions to the other types of pipe, and likewise as with other pipe families, they are typically seen on seismic data as a columnar zone of disturbed reflections or vertically stacked localized amplitude anomalies.

In the Narrabri Gas Project Area, both intrusive and extrusive rocks of the Garrawilla Volcanics are represented; these are underlying the Purlawaugh Formation. As a result, many dykes, sills and lava flows were formed, and small scale tensional normal faults may be associated with these events. The volcanics are not widely detected in exploration wells, suggesting they are present in only limited areal extend beneath the Narrabri Gas Project Area (CDM Smith, 2014).

4.3.2. RESEARCH GAPS

Cartwright et al. (2007) conclude there is abundant evidence on seismic data of focused fluid flow through low-permeability sedimentary units in many petroliferous sedimentary basins. The realisation that many sealing sequences are transected partly or entirely by features that facilitate cross-stratal fluid flow raises several fundamental questions that should be addressed. The recognition of seal bypass systems is also important in a wider context in basin analysis. For example, they are important to factor in to any modelling of basin fluid flow because the distribution and continuity of low-permeability units is a prime factor in flow routes and magnitudes (Bethke, 1985; Garven, 1995). At present, basin fluid-flow models do not implicitly incorporate SBS mainly because their importance is underappreciated and their function is poorly quantified.

Given that significant pathways for vertical fluid migration over distances greater than 1 km are widely developed in many sedimentary basins, future research relating to the wider significance of these pathways and reducing risk and uncertainty in sealing formation analysis should focus on quantifying the bulk permeability of specific families of bypass structures and defining scaling relationships of value in prediction. Current 3-D seismic data goes some way to enabling such an assessment to be conducted, but much work remains to be done on characterizing their permeability before assessment of seals containing bypass systems can be truly quantitative.

5. Conclusions

A key uncertainty in forecasting aquitard performance in regional groundwater models is the prediction of lateral continuity of sealing horizons and aquifers; another important uncertainty relates to the characterisation of the permeability of a given facies type or geobody. To determine uncertainty about lateral continuity, reservoir engineers construct multiple static geological models that consider a range of possible geometries for key aquifer and seal geobodies within the constraints of well and seismic data. Subsequently, a probability distribution of rock properties is imposed onto each of these multiple geometric realisations which are then tested in a sequence of dynamic simulations. In the current study the uncertainty about permeability of aquitards is investigated by using a combination of geophysical and hydrogeological data at a spatial resolution that also allows a qualitative assessment of lateral continuity of sealing horizons.

The combination of geophysical wireline logs obtained from exploration wells with laboratory measurements of rock porosity and permeability provides a cost-effective means of hydraulic characterisation of low-permeability formations such as aquitards over large spatial scales typical of regional-scale groundwater flow models. For the Gunnedah Basin in New South Wales a total of 97 exploration wells had high-resolution wireline data, including neutron density, for all of the four key aquitards that were selected to demonstrate the data generation methodology. Two of the four selected aquitards, i.e. the Purlawaugh Formation and the Napperby Formation, provided hydraulic isolation between the shallowest (i.e. Hoskissons Coal) of the two coal target formations and the alluvial and Pilliga Sandstone aquifers. Two further aquitards, the Watermark Formation and Porcupine Formation, provided additional isolation between the shallowest (Hoskissons Coal) and deepest (Maules Creek Formation) coal target formation. These aquitards were chosen on the basis of their lateral continuity within the study area, and because they are considered negligibly transmissive units.

The geophysical wireline logs (i.e. neutron density) were used to derive continuous (i.e. with a centimetre-scale spatial resolution) porosity profiles. The ability to convert such porosity profiles into continuous permeability profiles then depends on the availability of formation-specific porosity-permeability relationships. To this end, porosity-permeability relationships were established for the four key aquitard formations on the basis of laboratory measurements of both porosity and permeability on 59 core plugs obtained from drill cores. The gas porosity-permeability measurements were carried out under various confining pressures reflecting different overburden pressures at different depths within the aquitards. In this way the effect of increasing overburden pressure on rock porosity and permeability is accounted for.

Measurements show that all four aquitard formations display low permeability, i.e. from a few mD down to 10 nanoD in the case of the Porcupine Formation. Nearly all samples showed significant confining pressure dependency, illustrating a decreasing trend in porosity and permeability with greater depth. Both linear and non-linear regression models were developed to describe the relationship between porosity and permeability. While all regression models tested did provide a good description of the data, they were conceptually different and thus provide the opportunity to account for conceptual model uncertainty in regards to generating formation-scale hydraulic conductivities.

The wireline log-based porosity profiles were subsequently converted into continuous permeability profiles using formation-specific porosity-permeability relationships. These models were applied to the four aquitard units of interest at 77 well locations. Upscaling of the resulting high-resolution K_v profiles was then undertaken using harmonic averaging to derive a single equivalent K_v value for each hydrostratigraphic unit.

The degree to which the probability distributions for linear, multi-linear, and non-linear upscaled K_v differ from each other depends on the formations. For the shallowest aquitard (Purlawaugh), the distribution based on the non-linear upscaled K_v displays a much smaller variability compared to the linear models. For the underlying Napperby Formation differences in probability distribution between models are much smaller, with the median and interquartile range nearly identical. For the two deepest aquitards, i.e. Watermark and Porcupine Formations, the probability distributions of linear, multi-linear, and non-linear upscaled K_v are considerably different. The distribution based on the non-linear upscaled K_v displays the largest median and interquartile range, (more than two orders of magnitude variation) for both Watermark and Porcupine.

In a final step the aquitard hydraulic conductivities were defined at a regional scale. This involved computing the statistical properties, including the probability density function, of the equivalent aquitard hydraulic conductivity values across the model domain. The consistently low permeability values, with median values around 10^{-5} m/d, for the combined formations did not indicate discontinuities in the sealing capacity.

Our analysis of seal properties, however, is limited in being based largely on the core-scale properties of sealing sequences. Although so-called seal bypass systems have been described in the literature for other basins, typically involving faults, intrusions, and pipes, previous studies in the Narrabri Gas Project Area have identified only faults and hydrothermal pipes (dykes). These previous studies also concluded that the faults present in the Project area are unlikely to provide preferential pathways for the leakage of water or hydrocarbons between strata, while the volcanic rocks linked to dykes are not widely detected in exploration wells. Future research could involve detailed 3-D seismic data that would enable the assessment of seal bypass structures and their permeability.

Future work within this project will involve the use of 1-D numerical groundwater flow models as an alternative means of deriving equivalent values, and simulations of the propagation of depressurisation based on the derived hydraulic conductivity distributions.

6. References

Aguilera R (2006) Sandstone vs. carbonate reservoirs: A global perspective on porosity-depth and porosity-permeability relationships: Discussions. American Association of Petroleum Geologists Bulletin 90 (5): 807-810.

Aquaterra (2009) Narrabri Coal Mine Stage 2 Longwall Project Hydrogeological Assessment. Prepared for Whitehaven Coal Narrabri Coal Operations Pty Ltd by Aquaterra Consulting Pty Ltd.

Berndt C, Bunz S, Mienert J (2003) Fluid expulsion from polygonally faulted clays, Norwegian margin, in P van Rensbergen, R Hillis, A Maltman, and C Morley, eds., Subsurface sediment mobilisation: Geological Society (London) Special Publication 216, p. 223–243.

Bethke CM (1985) A numerical model of compaction-driven groundwater flow and heat transfer and its application to the paleohydrology of intracratonic sedimentary basins. Journal of Geophysical Research 90: 6817–6828.

Caers J, Zhang T (2004) Multiple-point geostatistics: A quantitative vehicle for integrating geologic analogs into multiple reservoir models. In: Grammer M, Harris PM, Eberli GP (eds.). Integration of outcrop and modern analogs in reservoir modelling. American Association of Petroleum Geologists Memoir 80, 383-394.

Cartwright J, Huuse M, Aplin A (2007) Seal bypass systems. American Association of Petroleum Geologists Bulletin 91 (8): 1141–1166.

CDM Smith (2014) Santos Narrabri Gas Project Groundwater Impact Assessment, Subiaco, Western Australia.

Comunian A, Jha SK, Giambastiani BMS, Mariethoz G, Kelly BFJ (2014) Training Images from Process-Imitating Methods An Application to the Lower Namoi Aquifer, Murray-Darling Basin, Australia. Mathematical Geosciences 46: 241-260.

Cooper AH (1986) Subsidence and foundering of strata caused by dissolution of Permian gypsum, North Yorkshire, in GM Harwood and DB Smith, eds., The English Zechstein and related topics: Geological Society (London) Special Publication 22, p. 127–139.

Corvi et al. (1992) Reservoir characterisation using expert knowledge, data and statistics. Oilfield Review, January: 25-39.

Davies RJ, Stewart SA (2005) Emplacement of giant mud volcanoes in the South Caspian Basin: 3D seismic reflection imaging of their root zones. Journal of the Geological Society (London) 162: 1– 4.

Delaney PT (1987) Heat transfer during the emplacement and cooling of dykes, in HC Halls and WH Fahrig, eds., Mafic dyke swarms: Geological Association of Canada Special Paper 34, p. 31 –46.

Deutsch CV, Journel AG (1998) GSLIB: Geostatistical Software Library and User's Guide, 2nd edition. New York, Oxford University Press, Applied Geostatistics Series, 350 pp.

Dewhurst DN, Clennell MB, Burgar I, Josh M, Sarout J, Delle Piane C, Esteban L, Pervukhina M, Raven MD (2012) A Multi-Disciplinary Workflow for Characterising Shale Seals. 3rd EAGE International Conference on Fault and Top Seals.

Department of Industry (NSW) (2015) DIGS (Digital Imaging Geological System), Department of Industry, Resources and Energy. Accessed on 30 July 2015.

DoE (Department of the Environment) (2014) Aquifer connectivity with the Great Artesian Basin, and the Surat, Bowen and Galilee Basins. Background Review, Office of Water Science, March 2014. Australian Government, Canberra.

Dimitrov LI (2002) Mud volcanoes— The most important pathway for degassing deeply buried sediments. Earth Science Reviews 59: 49–76.

Einsele G, Gieskes JM, Curray J, Moore DM (1980) Intrusion of basaltic sills into highly porous sediments, and resulting hydrothermal activity. Nature 283: 441– 445.

Einsele G (1992) Sedimentary basins, evolution, facies and sediment budget: Berlin, Springer-Verlag, 628 p.

Falivenne O, Cabrera L, Munoz JA, Arbues P, Fernandez O, Saez A (2007) Statistical grid-based facies reconstruction and modelling for sedimentary bodies. Alluvial-palustrine and turbiditic examples. Geologica Acta 5(3): 199-230.

Frey-Martinez JM, Cartwright J, Hall B, Huuse M (2007) Clastic intrusion at the base of deep-water sands: A trap-forming mechanism in the eastern Mediterranean, in A Hurst and JA Cartwright, eds., Sand injectites: Implications for hydrocarbon exploration and production: AAPG Memoir 87, p. 49–63.

Gautschi A (2001) Hydrogeology of a fractured shale (Opalinus Clay): Implications for deep geological disposal of radioactive wastes. Hydrogeology Journal 9: 97-107.

Garven G (1995) Continental-scale groundwater flow and geologic processes. Annual Reviews in Earth and Planetary Sciences 24: 89–117.

Gibson-Poole CM, Svendsen L, Underschultz J, Watson MN, Ennis-King J, van Ruth PJ, Nelson EJ, Daniel RF, Cinar Y (2008) Site characterisation of a basin-scale CO2 geological storage system: Gippsland Basin, southeast Australia. Environmental Geology 54: 1583–1606.

Giger SB, Clennell MB, Çiftçi NB, Harbers C, Clark P, Ricchetti M (2013) Fault transmissibility in clastic-argillaceous sequences controlled by clay smear evolution. American Association of Petroleum Geologists Bulletin 97 (5): 705-731.

Gómez-Hernández J, Srivastava RM (1990) ISIM 3D: an ANSI-C three-dimensional and multiple indicator conditional simulation program. Computers and Geosciences 16: 355-410.

Green CP, Ennis-King J (2010) Effect of Vertical Heterogeneity on Long-Term Migration of CO2 in Saline Formations. Transport in Porous Media 82: 31–47.

Hansen JPV, Cartwright JA, Huuse M, Clausen OR (2005) 3D seismic expression of fluid migration and mud remobilization on the Gjallar Ridge, offshore mid-Norway. Basin Research 17:123–140.

Hollub V, Schafer P (1992) A guide to coalbed methane operations. Chicago: Gas Research Institute, p. 376.

Hooper ECD (1991) Fluid migration along growth faults in compacting sediments. Journal of Petroleum Geology 14:161–180.

Hornung J, Aigner T (2002) Reservoir architecture in a terminal alluvial plain: an outcrop analogue study (upper Triassic, Southern Germany) Part II: Cyclicity, controls and models. Journal of Petroleum Geology 25 (2): 151-178.

Hurst A, Cartwright JA, Huuse M, Jonk R, Schwab A, Duranti D, B Cronin (2003) Significance of large scale sand injectites as long-term fluid conduits: Evidence from seismic data. Geofluids 3: 263–274.

IP (Interactive Petrophysics) (2015) IP Release 4.3.2015.49. LR Senergy Software Ltd, a member of the Lloyd's Register group.

Jones SC (1972) A rapid accurate unsteady-state Klinkenberg permeameter. SPE 3535: 383-397.

Jones E, Oliphant T, Peterson P (2014) SciPy: Open Source Scientific Tools for Python, http://www.scipy.org.

Klinkenberg LJ (1941) The permeability of porous media to liquid and gases. API Drill. Prod. Pract. 41: 200–213.

Kolterman CE, Gorelick SM (1996) Heterogeneity in sedimentary deposits: A review of structure-imitating, process-imitating, and descriptive approaches. Water Resources Research 32(9): 2617-2658.

Kopf A (2002) Significance of mud volcanism. Reviews of Geophysics 40: 1005, doi:10.1029/2000RG000093.

Løseth H, Wensaas L, Arntsen B, Hovland M (2003) Gas and fluid injection triggering shallow mud mobilization in the Hordaland Group, North Sea, in P van Rensbergen, R Hillis, A Maltman, and C Morley, eds., Subsurface sediment mobilisation: Geological Society (London) Special Publication 216, p. 139–157.

Li L, Zhou H, Gomez-Hernandez J (2011) A comparative study of three-dimensional hydraulic conductivity upscaling at the macro-dispersion experiment (MADE) site, Columbus Air Force Base, Mississippi (USA). Journal of Hydrology 404(3-4): 278-293.

Mahmud K, Mariethoz G, Baker A, Sharma A (2015) Integrating multiple scales of hydraulic conductivity measurements in training image-based stochastic models. Water Resources Research 51(1): 465-480.

Mallants D, Jacques D, Perko J (2007) Modelling multi-phase flow phenomena in concrete barriers used for geological disposal of radioactive waste. In: The 11th International Conference on Environmental Remediation and Radioactive Waste Management, Bruges, Belgium, 2-6 September 2007 / ASME, Fairfield, NJ, USA, United States, American Society of Mechanical Engineers, 2008, ICEM07-7202, p. 1-8.

Marithoz G, Lefebre S (2014) Bridges between multiple-point geostatistics and texture synthesis: Review and guidelines for future research. Computers and Geosciences 66: 66-80.

Molyneux S, Cartwright JA, Lonergan L (2002) Conical amplitude anomalies as evidence for large scale sediment intrusions. First Break 20: 123–129.

Moore C, Doherty J, Howell S, Erriah L (2014) Some Challenges Posed by Coal Bed Methane Regional Assessment Modeling. Groundwater (in press).

Pervukhina M, Gurevich B, Dewhurst DN, Siggins AF (2010) Experimental verification of the physical nature of velocity-stress relationship for isotropic porous rocks. Geophysical Journal International 181: 1473–1479.

Renard P, de Marsily G (1997) Calculating equivalent permeability: a review. Advances in Water Resources 20(5-6): 253-278.

Ricard L, Godel B, Smerdon B, Esteban L (2014) Aquitard hydraulic properties estimation from wireline logs analysis: An application to the Surat Basin, Queensland, Australian Earth Science Convention.

Rubel AP, Sonntag C, Lippmann J, Pearson FJ, Gautschi A (2002) Solute transport in formations of very low permeability: Profiles of stable isotope and dissolved noble gas contents of pore water in the Opalinus Clay, Mont Terri, Switzerland. Geochimica et Cosmochimica Acta 66(8): 1311–1321.

Sanchez-villa Z, Carrera J, Girardi JP (1996) Scale effects in transmissivity. Journal of Hydrology 183: 1-22.

Shapiro SA (2003) Elastic piezosensitivity of porous and fractured rocks. Geophysics, 68(2): 482-486.

Smerdon BD, S. L., Harrington GA, Gardner WP, Delle Piane C, Sarout J (2014) Estimating the hydraulic properties of an aquitard from in situ pore pressure measurements. Hydrogeology Journal (available online: DOI 10.1007/s10040-014-1161-x).

Smith SD, Solomon DK, Gardner WP (2013). Testing helium equilibrium between quartz and pore water as a method to determine pore water helium concentrations. Applied Geochemistry 35: 187-195.

Smith S, Mathouchanh E, Mallants D (2018) Characterisation of fluid flow in aquitards using helium concentrations in quartz, Gunnedah Basin, NSW, prepared by the Commonwealth Scientific and Industrial Research Organisation (CSIRO), Canberra.

Stanton RJ (1966) The solution brecciation process: Geological Society of America Bulletin 77: 843–848.

Svensen H, Planke S, Malthe-Sorensen A, Jamtveit B, Myklebust R, Rey S (2004) Release of methane from a volcanic basin as a mechanism for initial Eocene global warming. Nature 429: 542– 545.

TerHeege JH, Wassing BBT, Orlic B, Giger SB, Clennell MB (2013) Constraints on the Sealing Capacity of Faults with Clay Smears from Discrete Element Models Validated by Laboratory Experiments. Rock Mechanics Rock Engineering 46: 465–478.

Tran T (1996) The ‘missing scale’ and direct simulation of block effective properties. Journal of Hydrology 183: 37-56.

Turnadge C, Mallants D, Peeters L (2018) Overview of aquitard and geological fault simulation approaches in regional scale assessments of coal seam gas extraction impacts, prepared by the Commonwealth Scientific and Industrial Research Organisation (CSIRO), Canberra.

Underschultz J, Esterle J, Strand J, Hayes S (2018) Conceptual representation of fluid flow conditions associated with faults in sedimentary basins. Prepared for the Department of the Environment by The University of Queensland Centre for Coal Seam Gas, Queensland.

Varma S, Underschultz J, Giger SB, Field B, Roncaglia L, Hodgkinson J, Hilditch D (2013) CO2 geosequestration potential in the Northern Perth Basin, Western Australia. Australian Journal of Earth Sciences 60: 23–44.

Vistrand P (2001) Comparison of upscaling methods to estimate hydraulic conductivity. Groundwater 39(3): 401-407.

Warren J, Price H (1961) Flow in heterogeneous porous media. Society of Petroleum Engineers Journal 1(3): 153-169.

Wen Z-H, Gomez-Hernandez JJ (1996) Upscaling hydraulic conductivities in heterogeneous media: An overview. Journal of Hydrology 183: ix-xxxii.

Wu Y-S, Pruess K, Persoff P (1998) Gas flow in porous media with Klinkenberg effects. Transport in Porous Media 32: 117-137.

Yu L, Rogiers B, Gedeon M, Marivoet J, De Craen M, Mallants D (2013) A critical review of laboratory and in-situ hydraulic conductivity measurements for the Boom Clay in Belgium. Applied Clay Science 75-76: 1-12.

Appendix 1 Parameters for porosity-confining pressure and permeability-confining pressure models

Table 6 Fitted parameters for porosity-confining pressure and permeability-confining pressure models (highlighted cells were removed from the data set due to poor performance.

			Porosity-confining pressure model			Permeability-confining pressure model		
Well	Formation	Depth (m)	A_Poros	B_Poros	C_Poros	A_Perm	B_Perm	C_Perm
Narrabri	Black Jack	541.3	2.1277	21.1486	0.0034	0.0010	0.0562	0.0039
Narrabri	Black Jack	543.3	1.1309	14.1474	0.0015	0.0021	0.6898	0.0073
Narrabri	Maules Creek	632.74	1.3138	12.5182	0.0011	0.0005	1.2164	0.0060
Narrabri	Maules Creek	638.08	2.1909	20.9460	0.0023	0.0007	0.0916	0.0047
Coonarah 3	Napperby	435.99	3.8858	18.3078	0.0023	0.0021	0.0704	0.0042
NC283C	Napperby	117.03	0.3125	0.2877	0.0253	0.0004	0.0646	0.0573
NC283C	Napperby	123.19	0.4820	7.1772	0.0069	0.0007	-0.0010	0.0006
NC283C	Napperby	129.22	0.0000	4.6591	0.0004	0.0003	0.4502	0.7284
NC283C	Napperby	146.65	0.3125	0.2876	0.0245	0.0010	0.0009	0.0127
NC283C	Napperby	153.64	0.1276	-0.4521	0.0125	0.0002	0.8541	1.0798
NC283C	Napperby	167.78	0.5182	106.6726	0.0068	0.0002	0.2977	0.3096
NC303C	Napperby	156.36	1.0006	27.1809	0.0050	0.0008	-0.0006	-0.0001
NC303C	Napperby	165.72	0.6172	40962.7770	0.0209	0.0002	1.1620	1.7980
ROS053C	Napperby	49.18	0.0003	1.2690	0.0007	0.0008	-0.0006	-0.0001
Coonarah 3	Porcupine	632.43	1.6692	10.0721	0.0016	0.0007	0.0495	0.0039
Coonarah 3	Porcupine	640.28	1.5535	9.9404	0.0014	0.0023	0.2034	0.0042
Coonarah 3	Porcupine	649.99	0.6768	14.3444	0.0036	0.0007	0.0660	0.0047
Coonarah 3	Porcupine	665.84	5.0754	61.7260	0.0040	0.0039	0.1027	0.0041
DH Bando	Porcupine	670.38	1.1391	0.3484	0.0013	0.0001	0.0133	0.0033
DH Bando	Porcupine	711.45	0.8824	4.5105	0.0024	0.0001	0.0105	0.0031
Kerawah 1	Porcupine	893.18	10.0000	5.6549	0.0003	0.0500	2.4236	0.0013
Kerawah 1	Porcupine	912.83	1.3014	8.9547	0.0017	0.0006	0.0308	0.0034
Slacksmith 1	Porcupine	955.35	0.0000	2.8039	0.0007	0.0012	0.1845	0.0089
Slacksmith 1	Porcupine	1007.12	0.4129	0.0198	0.0009	0.0035	0.1015	0.0024
Slacksmith 1	Porcupine	1029.11	1.2575	-0.3125	0.0336	0.0001	0.0109	0.0028
Slacksmith 1	Porcupine	1137.07	2.3060	-1.3418	0.0941	0.0003	0.0371	0.0035
Slacksmith 1	Porcupine	1213.65	0.5230	4.4690	0.0019	0.0001	0.0353	0.0036
Coonarah 3	Purlawaugh	389.88	0.0003	11.6185	0.0002	0.0138	3.1970	0.0064
Dewhurst 19	Purlawaugh	230.75	0.0000	4.9391	0.0009	0.0005	0.0926	0.0050
Dewhurst 19	Purlawaugh	237.31	0.0000	5.3977	0.0014	0.0009	0.0252	0.0046
Dewhurst 19	Purlawaugh	245.88	0.7119	38.7335	0.0029	0.0015	0.1781	0.0056
Narrabri	Purlawaugh	263.4	0.0335	6.6842	0.0008	0.0010	0.0117	0.0036
Narrabri	Purlawaugh	277.55	0.5154	14.7177	0.0001	-0.0806	3.8073	0.0005
Narrabri	Purlawaugh	425.35	1.6431	6.6647	0.0020	0.0006	0.1047	0.0048
Narrabri	Purlawaugh	430.78	1.5803	3.2666	0.0022	0.0003	0.0394	0.0044
Narrabri	Purlawaugh	450.25	1.7275	-1.5684	0.0426	0.0002	0.0388	0.0037
Narrabri	Purlawaugh	455.7	2.0125	-1.4823	0.0807	0.0001	0.0215	0.0032
DH Bando	Watermark	558.92	0.6802	13065.6882	0.0146	0.0000	0.0086	0.0040
DH Bando	Watermark	604.94	0.3777	0.1104	0.0019	0.0000	2.3683	2.6385
Kerawah 1	Watermark	861.25	0.1640	-0.2622	0.1083	0.0002	0.0145	0.0037
Narrabri	Watermark	548.25	1.6520	24.1368	0.0055	0.0003	0.0027	0.0013
Narrabri	Watermark	565.47	1.3734	6.2835	0.0013	0.0003	0.1271	0.0071
Narrabri	Watermark	570.64	2.0893	22.2852	0.0041	0.0019	0.0096	0.0032
Narrabri	Watermark	576.68	7.4044	14.4848	0.0051	0.0143	0.1558	0.0021
Narrabri	Watermark	581	9.9685	8.0319	0.0000	0.0499	1.3698	0.0002
Narrabri	Watermark	585.08	9.9999	3.7071	0.0004	0.0322	0.2803	0.0033
Narrabri	Watermark	592.22	2.7150	12.1358	0.0002	0.0145	0.3793	0.0037
Narrabri	Watermark	595.19	0.0000	19.7062	0.0005	0.0098	0.8500	0.0041
Narrabri	Watermark	599.21	1.4918	13.3073	0.0016	0.0008	0.1776	0.0047
Narrabri	Watermark	609.25	1.7854	10.1834	0.0007	0.0021	0.1213	0.0036
Narrabri	Watermark	609.91	3.8968	0.2353	0.0009	0.0009	0.5213	0.0061
Narrabri	Watermark	615.4	0.0000	9.3105	0.0005	0.0010	0.2547	0.0046
Narrabri	Watermark	624.24	1.1685	3.0950	0.0015	0.0007	0.0446	0.0039
Narrabri	Watermark	627.51	1.4180	-0.8958	0.0190	0.0002	0.0101	0.0030
Slacksmith 1	Watermark	725.02	1.2293	8.4374	0.0017	0.0006	0.1731	0.0051
Slacksmith 1	Watermark	749.78	0.9600	8.1641	0.0016	0.0007	0.1127	0.0047
Slacksmith 1	Watermark	798.62	0.5012	8.9664	0.0022	0.0002	0.0554	0.0045
Slacksmith 1	Watermark	818.69	9.9992	-7.1176	-0.0001	0.0007	0.0660	0.0044
Slacksmith 1	Watermark	840.03	0.2998	2.1900	0.0009	0.0001	0.0541	0.0052

Appendix 2 Statistical summaries of upscaled permeability distributions using harmonic averaging

Table 7 Summary statistics of log_{10} permeability harmonic mean values (mD) derived from porosity data using linear, multi-linear and non-linear (exponential) models for the upper (Triassic-Permian age) aquitard sequence (also depicted in Figure 28). *Note: the 'Interburden 1' set contains only nine samples.

Formation	Model	min	5th	50th	95th	max
Purlawaugh	linear	-3.116	-2.728	-0.369	2.836	5.819
	multi-linear	-2.805	-2.223	-0.350	2.368	4.173
	exponential	-4.606	-3.553	-0.406	-0.022	-0.006
Interburden 1*	linear	-3.169	-2.949	-2.047	-0.246	0.015
	multi-linear	-2.938	-2.758	-1.974	-0.316	-0.085
	exponential	-3.311	-3.049	-2.043	-0.787	-0.623
Napperby	linear	-3.922	-3.479	-2.591	0.439	2.431
	multi-linear	-3.703	-3.393	-2.484	0.379	2.318
	exponential	-4.214	-3.704	-2.590	-0.641	-0.317
Interburden 2	linear	-3.473	-3.026	-2.008	-0.278	2.604
	multi-linear	-3.344	-3.061	-1.954	-0.170	2.758
	exponential	-3.649	-3.158	-1.949	-0.877	-0.295
Combined	linear	-3.519	-3.299	-2.382	-0.662	2.571
	multi-linear	-3.333	-3.214	-2.285	-0.608	2.452
	exponential	-3.981	-3.624	-2.444	-1.018	-0.246

Table 8 Summary statistics of log_{10} permeability harmonic mean values values (mD) derived from porosity data using linear, multi-linear and non-linear (exponential) models for the lower (Permian age) aquitard sequence (also depicted in Figure 29). *Note: the 'Interburden 2' set contains only one sample.

Formation	Model	min	5th	50th	95th	max
Interburden 1	linear	-2.842	-2.736	-1.878	-0.200	-0.019
	multi-linear	-2.430	-2.323	-1.669	-0.351	-0.132
	exponential	-4.291	-3.570	-1.518	-0.433	-0.299
Watermark	linear	-3.667	-3.478	-2.053	0.581	3.780
	multi-linear	-3.173	-2.868	-1.820	0.314	2.797
	exponential	-4.350	-3.932	-1.693	-0.298	-0.052
Interburden 2*	linear	-3.789	-3.789	-3.789	-3.789	-3.789
	multi-linear	-3.174	-3.174	-3.174	-3.174	-3.174
	exponential	-1.880	-1.880	-1.880	-1.880	-1.880
Porcupine	linear	-3.551	-3.247	-1.948	0.061	0.685
	multi-linear	-2.908	-2.628	-1.666	-0.177	0.390
	exponential	-4.804	-4.111	-1.440	-0.274	-0.118
Combined	linear	-3.545	-3.383	-2.026	-0.047	0.700
	multi-linear	-3.014	-2.673	-1.741	-0.252	0.399
	exponential	-4.489	-4.021	-1.627	-0.329	-0.114

Appendix 3 Geophysical logs and predicted porosity-permeability profiles

CONTACT US

t 1300 363 400
+61 3 9545 2176
e enquiries@csiro.au
w www.csiro.au

YOUR CSIRO

Australia is founding its future on science and innovation. Its national science agency, CSIRO, is a powerhouse of ideas, technologies and skills for building prosperity, growth, health and sustainability. It serves governments, industries, business and communities across the nation.

FOR FURTHER INFORMATION

CSIRO
Lionel ESTEBAN
t +61 8 6436 8927
e lionel.esteban@csiro.au
w www.csiro.au/